REGULATION OF DOPAMINE TRANSPORTER SUBCELLULAR LOCALIZATION AND TRAFFICKING

by

Shiqi Ma

B.S., Peking University, 2011

Submitted to the Graduate Faculty of

School of Medicine in partial fulfillment of the requirements for the

degree of

Doctor of Philosophy

University of Pittsburgh

2017

UNIVERSITY OF PITTSBURGH

SCHOOL OF MEDICINE

This dissertation was presented

by

Shiqi Ma

It was defended on

September 12, 2017

and approved by

Edda Thiels, Ph.D., Department of Neurobiology

Susan G. Amara, Ph.D., National Institute of Mental Health

Yan Dong, Ph.D., Department of Neuroscience

Adam Kwiatkowski, Ph.D., Department of Cell Biology

Manojkumar A. Puthenveedu, Ph. D., Department of Neurobiology

Dissertation Advisor: Alexander D. Sorkin, Ph.D., Department of Cell Biology

REGULATION OF DOPAMINE TRANSPORTER SUBCELLULAR LOCALIZATION AND TRAFFICKING

Shiqi Ma, PhD

University of Pittsburgh, 2017

Dopamine transporter (DAT) controls dopamine (DA) neurotransmission by clearing synaptically released DA. The substrate uptake function of DAT is regulated by its subcellular localization. We propose that DAT localization and trafficking are regulated by its molecular conformation and interactions of the transporter with lipids and membrane-associated proteins. We used several experimental approaches and two DAT mutants to demonstrate that accumulation of DAT in plasma membrane protrusions, such as myosin X-dependent filopodia, requires an outward facing (OF) conformation of the DAT molecule. Furthermore, using targeted plasma membrane depletion of phosphatidylinositol 4,5-bisphosphate (PIP_2), a lipid that is highly enriched in the plasma membrane and proposed to bind DAT, we demonstrated that PIP_2 is necessary for protein kinase C (PKC)-stimulated DAT endocytosis but not essential for maintaining steady-state levels of DAT at the cell surface. Therefore, these results suggest that PIP_2 is essential for clathrin-mediated PKC-stimulated DAT endocytosis and PIP_2 is not involved in the retention of DAT at the cell surface. In search of DAT interactors regulating its plasma membrane retention, distribution, subcellular localization, and function, we used quantitative mass spectrometry analysis to identify proteins that are co-precipitated with DAT isolated from the mouse striatum. A novel interaction of DAT with Gαo, the α subunit of Go proteins that are coupled to dopamine D2 receptor and other receptors, was confirmed by reciprocal co-immunoprecipitation and western blotting in mouse striatum and a heterologous expression

system. While structure-functional analysis of this interaction will be performed in the future studies, our biochemical and morphological analyses led to the hypothesis that DAT-Gαo interaction may mediate the regulatory effects of D2 auto-receptors on DAT localization and activity. In summary, our data suggest that the localization of DAT in filopodia, which is regulated by DAT conformation and possibly DAT-Gαo interaction but not DAT interaction with PIP_2, is the primary mechanisms of the retention of functional DAT at the cell surface.

TABLE OF CONTENTS

LIST OF FIGURES

PREFACE

I would like to thank my advisor Dr. Alexander D. Sorkin who has been an absolutely wonderful mentor and teacher. Thank you to my committee members Drs. Edda Thiels, Manojkumar A. Puthenveedu, Yan Dong and Adam Kwiatkowski for so much helpful discussion and support of my career. Also, thanks to former and current Sorkin lab members for making such a wonderful lab environment for learning and experiments. I would like to thank all the members of the Cell Biology Department and the CNUP program. Especially, I thank Mary H. Cheng in Dr. Ivet Bahar's lab for the contribution of molecular dynamics and docking simulations; I thank Amy H. Newman for the contribution of significant cocaine analog JHC1-64 for the relevant experiments; I thank John Caltagarone and Ethan R. Block for tuition in primary dopaminergic neuron culture and striatal synaptosome preparation; I thank Dr. Gerry Hammond for providing DNA constructs for the approach of rapamycin-induced membrane PIP_2 depletion; I thank Xuemei Zeng from Dr. Nathan Yates's lab in the Biomedical Mass Spectrometry Center for assisting with mass spectrometry analysis. Finally, thank you to my family for their unyielding support and love.

1.0 INTRODUCTION

1.1 THE DOPAMINE SYSTEM

Dopamine (DA) is an essential neurotransmitter in the mammalian central nervous system (CNS); it is involved in reward-motivated behavior, motor control, cognitive capacities development, and attention regulation (Nieoullon 2002, Schultz 2002). Dysfunction of the dopaminergic system is involved in neuronal pathologies such as Parkinson's disease, schizophrenia, bipolar disorder, attention deficit hyperactivity disorder (ADHD), and psychostimulant drug abuse (Volkow et al 2009).

The somas of dopaminergic neurons are mainly located in the midbrain. There are four predominant dopaminergic pathways (Figure 1.1). In the nigro-striatal pathway, dopaminergic neurons in the substantia nigra pars compacta (SNc) project to the dorsal striatum (composed of caudate nucleus and putamen). The nigro-striatal pathway plays an important role in motor control. Degeneration of nigro-striatal dopaminergic neurons results in Parkinson's disease (Christine & Aminoff 2004). Dopaminergic neurons in both the mesolimbic pathway and the mesocortical pathway originate from the ventral tegmental area (VTA). Mesolimbic dopaminergic neurons project mainly to the nucleus accumbens (NAc). In the mesocortical pathway, dopaminergic neurons project to the olfactory bulb, the amygdala, the hippocampus, the orbital and medial prefrontal cortex, and the cingulate gyrus. The mesolimbic pathway

mediates pleasure in the brain, and functions in emotion and reward systems (Björklund & Dunnett 2007). The mesolimbic pathway can be plastically changed by drugs of abuse, and plays an important role in the development of drug addiction. Dysfunction in the mesolimbic pathway is also associated with schizophrenia, bipolar depression, and learning deficits. The mesocortical pathway regulates cognitive functions including motivation, reward, emotion, and impulse control, and is involved in cognitive and emotional diseases such as schizophrenia and ADHD (Björklund & Dunnett 2007). In the tuberoinfundibular pathway, dopaminergic neurons in the arcuate nucleus of the hypothalamus project to the pituitary gland. The function of DA released in the tuberoinfundibular pathway is to inhibit prolactin release (Ben-Jonathan & Hnasko 2001).

There are interactions between DA and other neurotransmitters such as γ-aminobutyric acid (GABA). For example, the VTA-to-NAc pathway contains parallel dopaminergic and GABAergic projections that are often co-activated by reward stimulation (Steffensen et al 1998). DA released in the synapse induces inhibition of presynaptic GABA release via dopamine receptors in the presynaptic GABAergic neurons (Ishikawa et al 2013). Extra DA released in the mesolimbic pathway also causes the generation of silent glutamatergic synapses in which the N-methyl-D-aspartic acid receptor (NMDAR)-mediated excitatory postsynaptic currents (EPSCs) are relatively stable and α-amino-3-hydroxymethyl-4-isoxazolepropionic acid receptor (AMPAR) currents are minimal. In the NAc shell, exposure to cocaine generates silent glutamatergic synapses that are formed by membrane insertion of new NMDARs (Huang et al 2009).

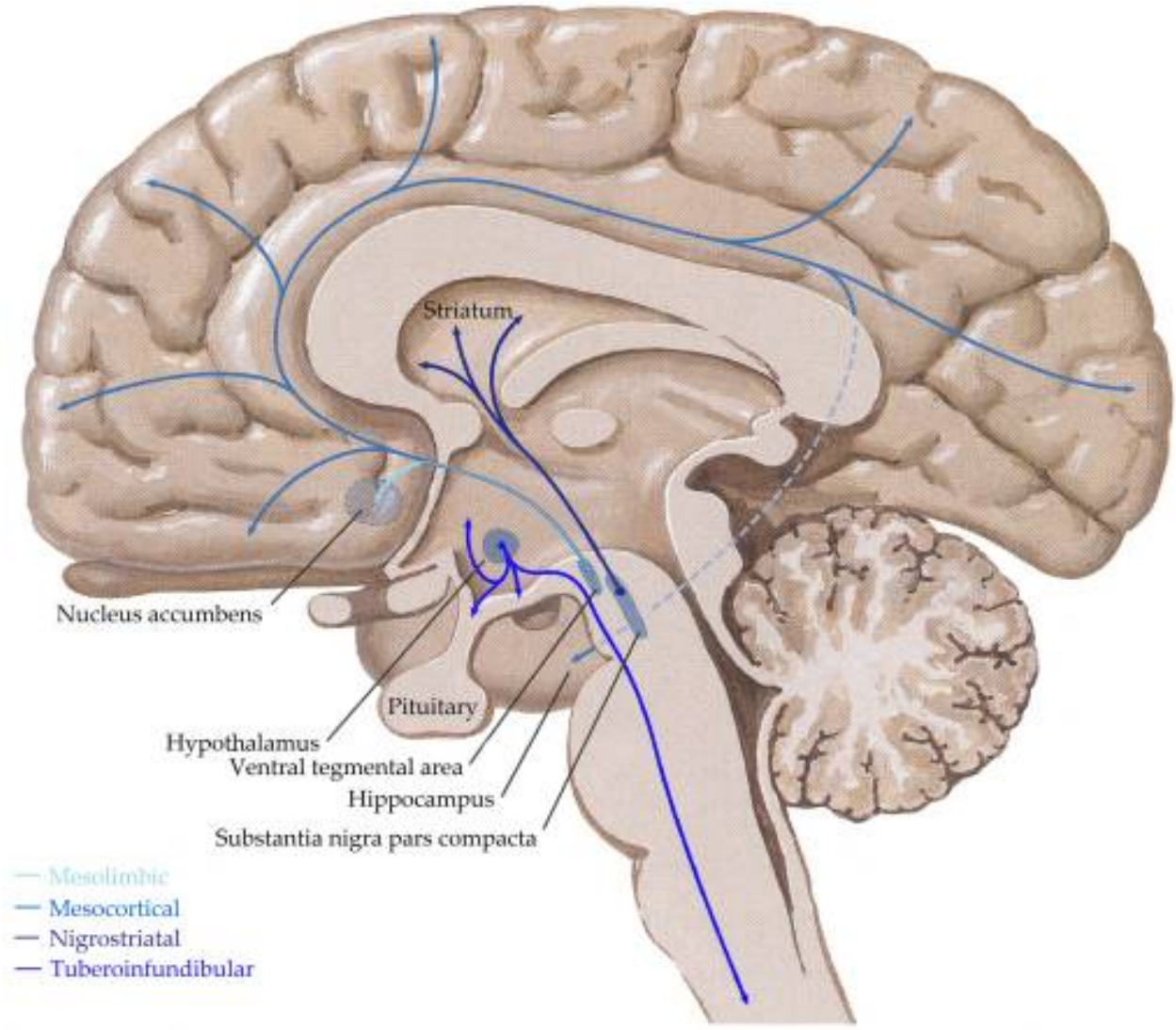

Figure 1.1. Major dopaminergic pathways in the CNS (Scarr et al 2013).

DA is synthesized from tyrosine in the cytoplasm of dopaminergic neurons. Tyrosine hydroxylase (TH) converts tyrosine to L-DOPA, which is the rate-limiting step in DA synthesis. L-DOPA is rapidly converted to DA by aromatic amino acid decarboxylase. DA is released into the synaptic cleft through vesicle exocytosis upon dopaminergic neuron activation. Extracellular DA is cleared by the dopamine transporter (DAT) expressed in dopaminergic neurons (Amara & Kuhar 1993, Giros et al 1996) and can also be metabolized by the catechol-O-methyl transferase (Diego et al 2012).

The five subtypes of DA receptors (D1-D5) are members of the G-protein-coupled receptor (GPCR) superfamily. They are divided into two major subclasses. The D1-like receptors (D1 and D5) are coupled to Gs proteins and stimulate signal transduction through activating cyclic adenosine monophosphate (cAMP) formation. D2-like receptors (D2, D3 and D4) are coupled to Gi/o proteins and exert the opposite effect on cAMP level (Seeman 2010). Both D1 and D2 receptors are located in the NAc and dorsal striatum (Girault & Greengard 2004). D1 and D2 receptors are the most abundant DA receptors in human CNS, while the other three receptors are expressed at significantly lower levels. D1 and D5 receptors are mostly involved in postsynaptic signal transduction, whereas D2, D3 and D4 receptors are involved in both pre- and postsynaptic signal transduction (Seeman 2010). There are two forms of D2 receptors, short form (D2SR) and long form (D2LR). D2SR is predominantly located on the presynaptic membrane and functions as an auto-receptor (Khan et al 1998). The D2 auto-receptor senses DA level in the synaptic cleft and regulates extracellular DA by modulating DA synthesis, DA vesicle exocytosis, and the function of DAT (Bello et al 2011, Dickinson et al 1999, Ford 2014).

1.2 DOPAMINE TRANSPORTER (DAT) – STRUCTURE, FUNCTION AND LOCALIZATION

Synaptically-released DA is primarily cleared from extraneuronal space by DAT (Amara & Kuhar 1993, Giros et al 1996). The rate of DA clearance by DAT controls the duration and amplitude of post-synaptic DA signaling. DAT is exclusively expressed in dopaminergic neurons. The highest density of DAT is observed in the presynaptic surface of axons in the dorsal striatum and the NAc (Block et al 2015, Ciliax et al 1999).

DAT belongs to the high-affinity, sodium- and chloride- dependent SLC6 transporter gene family, which also includes serotonin, norepinephrine, glycine, and GABA neurotransmitter transporters (Gether et al 2006). Like other members of the family, DAT consists of intracellular amino- (N-) and carboxyl- (C-) termini, and 12 transmembrane helical segments (TM), with TM1-5 and TM6-10 forming pseudo-symmetrically inverted repeats (Penmatsa et al 2013). A centrally located high-affinity primary substrate-binding site (S1) lined by TM1, 3, 6 and 8 binds the substrate (DA) and ions, before their translocation and release to the cytoplasm. Helices TM1 and TM6 are broken into two segments each, TM1a, TM1b, TM6a, and TM6b, near the DA/ions binding site. Another substrate-binding site (S2) is located closer to the extracellular (EC) vestibule of DAT and formed by residues from TM1, 3, 10, and extracellular loops (EL) 2 and 4 (Shan et al 2011). DA uptake by DAT requires the co-transport of two sodium ions and one chloride ion driven by the electrochemical gradients of these ions (Sonders et al 1997).

A multitude of substrates and inhibitors have been shown to bind DAT. Besides DA, norepinephrine and amphetamines (AMPHs) can be transported by DAT (Sulzer 2011). Conversely, DA is the substrate of the norepinephrine transporter. Cocaine and its derivatives are the best-studied competitive inhibitors of DAT. Cocaine binds with high affinity to the S1 site in the extracellular vestibule of DAT, thus blocking the binding and transport of DA.

It has been proposed that DAT conformation dynamically shifts between outward-facing (OF) and inward-facing (IF) states during the transport cycle (Figure 1.2) (Shan et al 2011, Yamashita et al 2005). Substrate binding in the OF conformation of DAT (*red*) promotes the formation of an occluded conformation (*orange*). The binding of a second substrate (doubly occupied state in *green*) induces conformational changes in the S1 site and the intracellular side through conserved interaction networks (colored lozenges) positioned between the S2 and S1

sites, which reorganize the interaction network at the intracellular end, eventually leading to the release of substrate in the S1 site from the IF conformation (*cyan*). Inhibitors that bind the substrate binding sites block the transition of DAT from OF state to IF state.

An intracellular (IC) interaction network involving TM1a, TM5, TM6b, TM8, and the N-terminal segment (amino acids, a.a. 1-65) has been found to play a role in regulating the conformational transitions in DAT (Cheng & Bahar 2015, Khelashvili et al 2015, Loland et al 2004). In particular, the closure of the IC vestibule in the OF state of DAT is stabilized by the salt bridge between R60 (N-terminus) and D436 (TM8) and the tri-aromatic interaction of W63 (N-terminus), F332 (TM6b) and Y335 (TM6b) (Cheng & Bahar 2015, Khelashvili et al 2015, Loland et al 2004). Disruption of this IC interaction network was observed to facilitate the structural transition from OF state to IF state in DAT (Cheng & Bahar 2015) and in its structural homolog, the leucine transporter (LeuT) (Cheng & Bahar 2014). Mutations of IC networking residues have been predicted to shift the conformational equilibrium toward the IF state (Kniazeff et al 2008), in which the EC vestibule becomes less accessible (to the EC environment) than does the IC vestibule (to the cytoplasmic environment).

It has been demonstrated that binding substrates such as DA and AMPH drives a structural transition toward the IF state of DAT (Cheng & Bahar 2015, Cheng et al 2015, Khelashvili et al 2015, Shan et al 2011), while inhibitors such as cocaine stabilize DAT in the OF state (Chen et al 2000, Dehnes et al 2014) through competitive binding to the S1 site (Beuming et al 2008, Cheng et al 2015, Wang et al 2015). During the binding of DA or other substrates, it is necessary for DAT to be in the OF state, and then transit to the IF state when the substrates are taken up (Figure 1.2). Similarly, the serotonin transporter (SERT) is proposed to exhibit the same alteration between outward- and inward-facing states, driven by substrates and

inhibitors (Zhang et al 2016). The OF conformation of SERT can be stabilized by cocaine, and the IF state of SERT can be induced by its substrates such as serotonin.

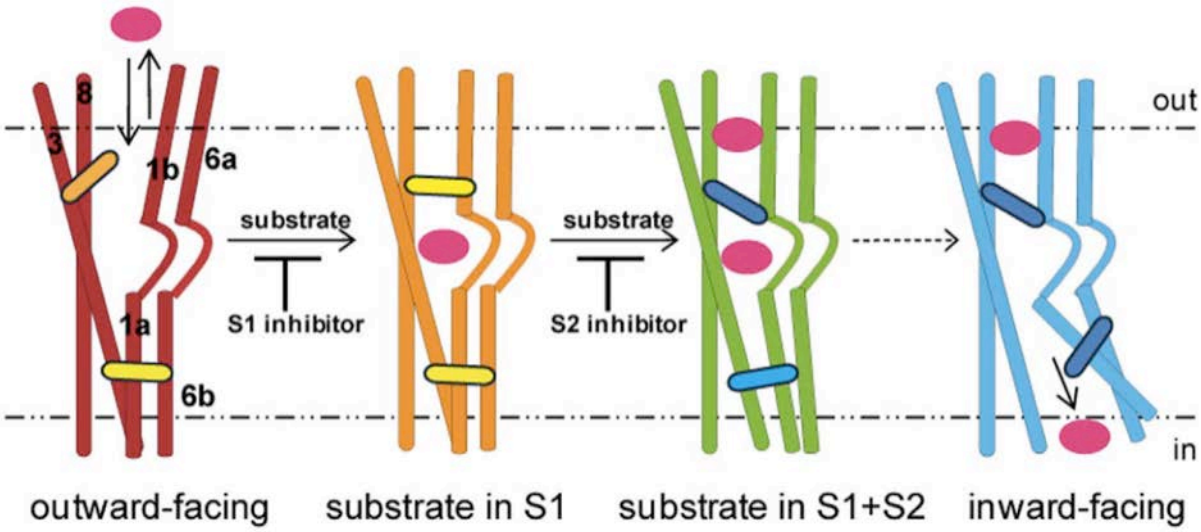

Figure 1.2. Cartoon model of substrate-induced transition of DAT conformation (Shan et al 2011).

Palmitoylation and lipids/ions binding may stabilize the structure of DAT. DAT has also been shown to be palmitylated via a thioester bond connected to a cysteine residue (C580) at the plasma membrane. Inhibition of DAT palmitoylation results in decreased DA uptake activity of DAT (Rastedt et al 2017). The X-ray structure of DAT reveals a cholesterol molecule that is located in a groove between TM5 and TM7 (Penmatsa et al 2013). It has been suggested that the binding of cholesterol helps to stabilize the OF conformation of DAT (Hong & Amara 2010). Besides, zinc ion binds four extracellular residues of DAT and stabilizes its OF conformation (Stockner et al 2013).

Another DAT substrate, AMPH, activates calcium/calmodulin-dependent protein kinase II (CaMKII) through the mechanisms independent of the transport through DAT. CaMKII is proposed to phosphorylate the N-terminus of DAT. The phosphorylation of the N-terminus results in the reverse substrate transport activity of DAT (efflux) and has been attributed to a

shift in the equilibrium distribution of DAT conformation towards its IF state (Cheng et al 2015, Fog et al 2006, Guptaroy et al 2011). Phosphorylated DAT in cells treated with AMPH, functions as a channel and mediates constitutive DA release from the cytoplasm without the coupling to sodium or chloride ions (Sonders et al 1997).

1.3 DAT SUBCELLULAR LOCALIZATION, TRAFFICKING AND ENDOCYTOSIS

1.3.1 DAT synthesis and trafficking

DAT is synthesized at the endoplasmic reticulum (ER) membrane of dopaminergic neurons that is localized in the neuronal soma (Hoffman et al 1998, Turiault et al 2007). Vesicles containing newly synthesized DAT molecules leave the rough ER membrane and fuse with the *cis* face of the Golgi apparatus. DAT undergoes N-linked glycosylation in the ER and the Golgi apparatus. DAT then traffics in vesicles from the trans-Golgi network (TGN) to the plasma membrane (Hersch et al 1997). N-glycosylation is critical for the efficient trafficking of newly synthesized DAT to the plasma membrane as well as for the proper DA uptake activity of DAT (Li et al 2004). The DAT C-terminus is important for the ER export of DAT. Mutation of DAT C-terminal residues such as Lys-590, Asp-600 or Gly-585 to alanine results in the retention of DAT in the ER (Miranda et al 2004). Deletion of the last three residues (PDZ binding motif) in the DAT C-terminus (LKV) also results in insufficient plasma membrane delivery of newly synthesized DAT (Bjerggaard et al 2004). DAT oligomers are formed in the ER and maintained in the trafficking system and the plasma membrane (Sorkina et al 2003). The oligomerization of

DAT is necessary for proper DAT trafficking from the ER to the plasma membrane (Sorkina et al 2003, Torres et al 2003).

1.3.2 DAT at the cell surface: subdomain distribution

DAT is found in the plasma membrane of the soma, dendrites, and axons of dopaminergic neurons, and DAT is especially enriched in the membrane of the axons in the striatum (Block et al 2015, Nirenberg et al 1996). However, mechanisms controlling this distribution are unknown. Besides, DAT is found to accumulate in the filopodia-like membrane protrusions in cultured postnatal dopaminergic neurons and brain striatum slices. DAT displays normal (characteristic of a typical membrane protein) distribution in the plasma membrane of cultured dopaminergic neurons, although DAT is significantly less mobile in the filopodia (Eriksen et al 2009, Rao et al 2012). The mechanisms underlying high fraction of immobile DAT in filopodia are unclear, and the mechanisms of DAT targeting to filopodia are unknown.

Membrane lipids also regulate the distribution of DAT in the plasma membrane. DAT was shown to partially localize to cholesterol-rich membrane rafts in the plasma membrane (Foster et al 2008). Furthermore, the uptake activity of DAT is decreased by methyl-β-cyclodextrin (mβCD), which extracts cholesterol from membranes and disrups lipid rafts (Kabouridis et al 2000). A membrane raft protein flotillin-1 (Flot1) has been shown to regulate DAT membrane mobility and facilitate AMPH-induced DAT-dependent drosophila hyperlocomotion (Pizzo et al 2013, Sorkina et al 2013). The N-terminus of DAT interacts with Phosphatidylinositol (4,5)-bisphosphate (PIP_2), an important membrane lipids that regulates the function of many ion channels, receptors, and transporters (Hamilton et al 2014). It has been demonstrated that the mutation of PIP_2 binding sites in DAT (K3/K5) to alanine (K3A/K5A)

reduces the effect of AMPH-induced DAT-mediated psychomotor behaviors in drosophila. It has been proposed that the DAT-PIP_2 interaction may serve as part of the mechanism for the retention of DAT from endocytosis in the plasma membrane (Fagan et al 2015).

1.3.3 Endocytosis

Endocytosis is the process by which cells internalize membrane molecules by engulfing them with the cell membrane. Endocytosis and post-endocytic trafficking regulate the surface expression of many plasma membrane receptors, transporters, and ion channels. The best-understood endocytosis pathway is clathrin-mediated endocytosis (CME) (Kirchhausen et al 2014). CME begins with the assembly of clathrin, cargo molecules, the adaptor complex AP-2, and other clathrin-associated proteins into clathrin-coated pits (CCPs) on the inner surface of the plasma membrane. CCPs bud into the cell and form clathrin-coated vesicles (CCVs). The scission of newly formed CCVs from the plasma membrane requires the GTPase dynamin.

There are other endocytic pathways that occur in the absence of clathrin. The small-scale (<200 nm vesicle) clathrin-independent endocytosis (CIE) pathways can be classified as dynamin-dependent and dynamin-independent pathways (Mayor et al 2014). Dynamin-dependent CIE pathways include caveolin-dependent endocytosis, RhoA-dependent endocytosis, and endophilin-mediated endocytosis (Boucrot et al 2015). Dynamin-independent CIE pathways include the endocytosis of GPI-AP enriched early endosomal compartments (GEECs) mediated by clathrin-independent carriers (CLICs) (CG pathway), Arf6-dependent endocytosis, and flotillin-dependent endocytosis. Overall, mechanisms of clathrin-independent endocytosis are poorly understood.

The endocytic trafficking itinerary is schematically shown in Figure 1.3. Membrane cargos can be endocytosed by clathrin-dependent, caveolin-dependent, or other mechanisms that are dependent or independent of dynamin. Both CCVs and non-clathrin coated vesicles that bud from the plasma membrane are fused with early endosomes (EEs), tubular-vesicular compartments with heterologous morphology (Sorkin & Puthenveedu 2013). The vacuolar domain of an EE is often termed a sorting endosome (SE), in which endocytosed cargos are sorted for recycling or degradation. The extending tubule of an EE is a recycling endosome (RE) that can detach from a SE, forming peripherally a RE or a peri-centriolar endosomal recycling compartment (ERC). Cargos destined for recycling to the plasma membrane are packaged into recycling carriers (typically tubules) that budded from the SE-attached REs (fast-recycling pathway) or vesicles budded from the ERCs or peripheral REs (slow-recycling pathway) (Klumperman & Raposo 2014). SEs undergo fusion and maturation after cargo destined for recycling is left, leading to formation of late endosomes (LEs). SE and LE often display a morphology of multivesicular bodies (MVBs), endosomes containing intraluminal vesicles (ILVs). Cargos destined for degradation are accumulated in ILVs and thus sequestered from recycling. LEs fuse with primary lysosomes (LYSs), where enzymes degrade ILVs and their cargos (Seaman 2008). The pH level decreases from EE (6.2-6.3) to LE (5.2-5.8) (Yamashiro & Maxfield 1987).

Small monomeric Ras-like GTPases of the Rab family play a crucial role in regulating endosome tethering and fusion, maturation and sorting processes (Grosshans et al 2006). Because of the specificity of individual Rab GTPases for various types of endosomes and other membrane compartments, Rabs have been widely used as markers of these compartments. For

example, Rab5 is predominantly localized to EEs, Rab11 to ERCs and peripheral REs, and Rab7 to LEs.

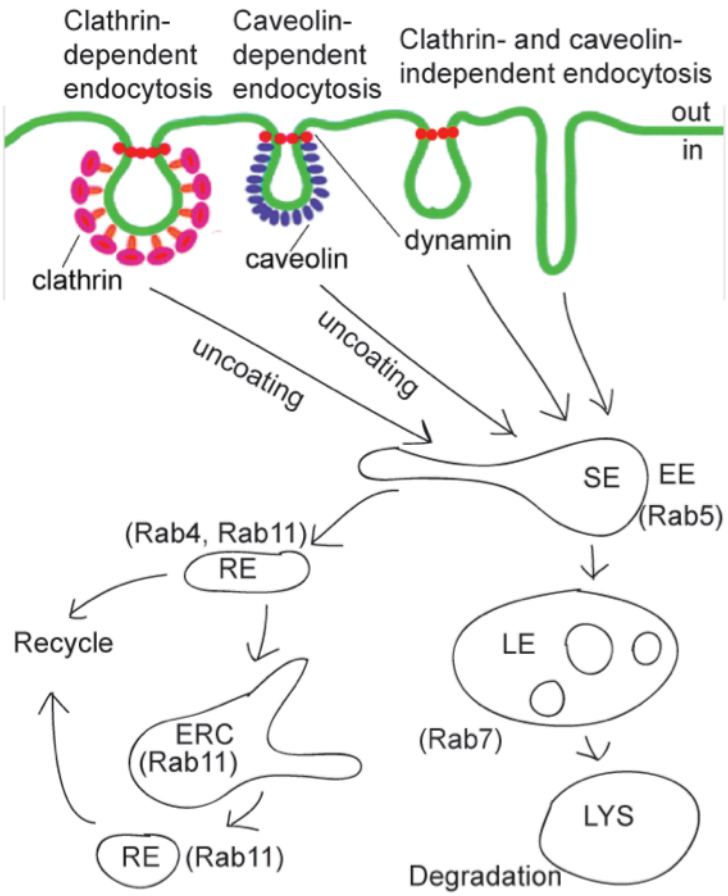

Figure 1.3. Pathways of endocytic trafficking.

1.3.4 Constitutive and stimulated DAT endocytosis

Endocytosis may regulate the surface expression level of DAT, and therefore regulates the Vmax of DA uptake activity. DAT is proposed to constitutively internalize from the plasma membrane. DAT endocytosis is stimulated by protein kinase C (PKC), substrates such as DA and AMPH, glial cell-derived neurotrophic factor (GDNF), and the inhibition of activated by cdc42 kinase 1

(Ack1) (Chi & Reith 2003, Richardson et al 2016, Wu et al 2015, Zahniser & Sorkin 2009, Zhu et al 2015). PKC- and AMPH-stimulated DAT endocytosis are the best studied.

Constitutive endocytosis of DAT has been observed in the soma and synaptic varicosity of cultured dopaminergic neurons using fluorescent cocaine analog JHC1-64 that binds to DAT with high affinity (Eriksen et al 2009). A pool of DAT has been found in EEs, REs and LEs (Eriksen et al 2010). Using knock-in mice expressing HA-DAT, it has been demonstrated that a small pool of HA-DAT is internalized into EEs and REs in the varicosities of cultured dopaminergic neurons that also contain synaptic markers (Rao et al 2012). By contrast, in acute sagittal brain slices and intact animals, endosomes containing DAT are virtually absent in axons and synapses of dopaminergic neurons in the striatum, while DAT is presented in EEs, REs and a small fraction of LEs and LYSs in the somatodendritic regions of dopaminergic neurons (Block et al 2015). The latter study proposes that constitutive DAT endocytosis is negligible in the axonal domain. Other groups have used biochemical techniques, such as biotinylation, to demonstrate DAT endocytosis in striatum (Gabriel et al 2013). Unfortunately, up to date, significant concentration of DAT in endosomes has not been directly demonstrated by optical methods.

It has been demonstrated that constitutive DAT endocytosis is dynamin-dependent in dopaminergic neurons (Eriksen et al 2009). Our laboratory has also shown that constitutive DAT endocytosis is both clathrin- and dynamin- dependent in PAE cells using siRNA knockdown of clathrin/dynamin and biotinylation (Sorkina et al 2005). However, other research groups have reported that constitutive DAT endocytosis is dynamin-independent in brain slices and the heterologous SK-N-MC cells using biotinylation, whereas the recycling of DAT to the plasma

membrane requires dynamin (Gabriel et al 2013). Additional experiments using more sensitive methods and more effective ways of depleting clathrin are necessary to reconcile these results.

Based on current findings, we propose that most constitutive DAT endocytosis occurs in the cell body and axon varicosities of dopaminergic neurons, and there is limited DAT cycling between surface and RE in synapses (Figure 1.4). DAT is synthesized in the cytoplasm of dopaminergic neurons and transported to the plasma membrane through the endoplasmic reticulum (ER) and Golgi apparatus. In the somatodendritic region of a dopaminergic neuron, DAT is constitutively internalized through conventional CME or dynamin-dependent CIE pathways. DAT-containing endocytic vesicles (EVs) fuse with EEs, where DAT is sorted for recycling (to recycling endosomes, REs) or degradation (to late endosomes, LEs, and then to lysosomes, LYSs). DAT travels from the soma to the dendrites and axons of dopaminergic neuron through either vesicular transport or lateral membrane diffusion. Axons contain numerous synaptic areas (varicosities) where DA in synaptic vesicles (SVs) is released. DAT endocytosis in a varicosity probably involves rapid cycling between the plasma membrane and EE/RE. DA released in the synaptic cleft binds postsynaptic dopamine receptors such as D1 receptor (D1R) and the long form of D2 receptor (D2LR), and is mainly cleared by DAT in the presynaptic membrane.

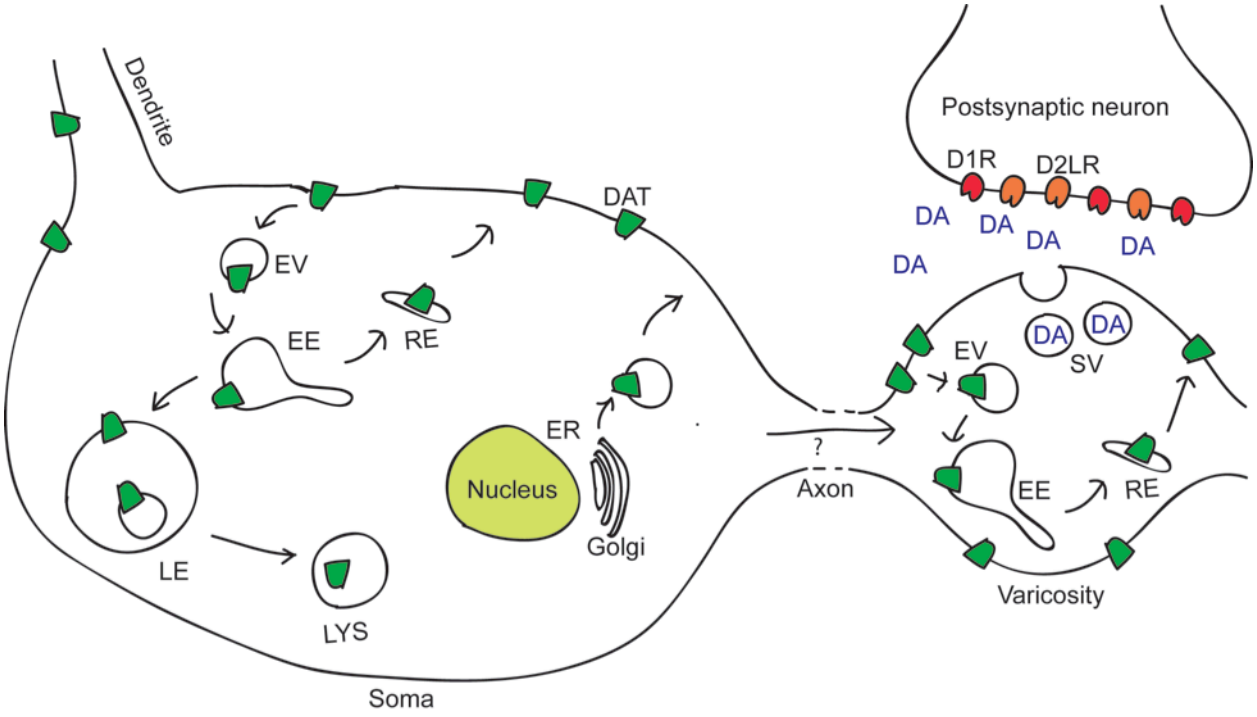

Figure 1.4. Hypothetical model of DAT trafficking in dopaminergic neurons.

PKC activation induced by phorbol 12-myristate 13-acetate (PMA) acutely down-regulates surface DAT by rapidly increasing basal endocytic rates and slowing surface delivery, which is widely demonstrated in heterologously expressing cells (Daniels & Amara 1999, Loder & Melikian 2003, Miranda et al 2005, Rao et al 2012). PKC-stimulated DAT endocytosis is dependent on the ubiquitination of DAT. PKC activation induces DAT ubiquitination through the mediation of an E3 ubiquitin ligase neural precursor cell expressed, developmentally down regulated 4-2 (NEDD4-2) (Sorkina et al 2006). A single four-ubiquitin Lys63-linked chain that can be conjugated to various N-terminal DAT lysine residues modifies each ubiquitinated DAT molecule (Vina-Vilaseca & Sorkin 2010). Ubiquitinated DATs are proposed to be recruited to CCPs through ubiquitin adaptor proteins epsin, epidermal growth factor pathway substrate clone 15 (Eps15), and Eps15-related protein (Eps15R) (Sorkina et al 2006). Ubiquitinated DATs are then endocytosed through CME and targeted for degradation through the MVB mechanism (Miranda et al 2005). Our laboratory and other research group have not observed PMA-

stimulated endocytosis in dopaminergic neurons (Eriksen et al 2009, Rao et al 2012). So that it is still controversial if it happens in neurons. The model for the mechanism of PKC-stimulated DAT endocytosis mediated by ubiquitination is shown in Figure 1.5.

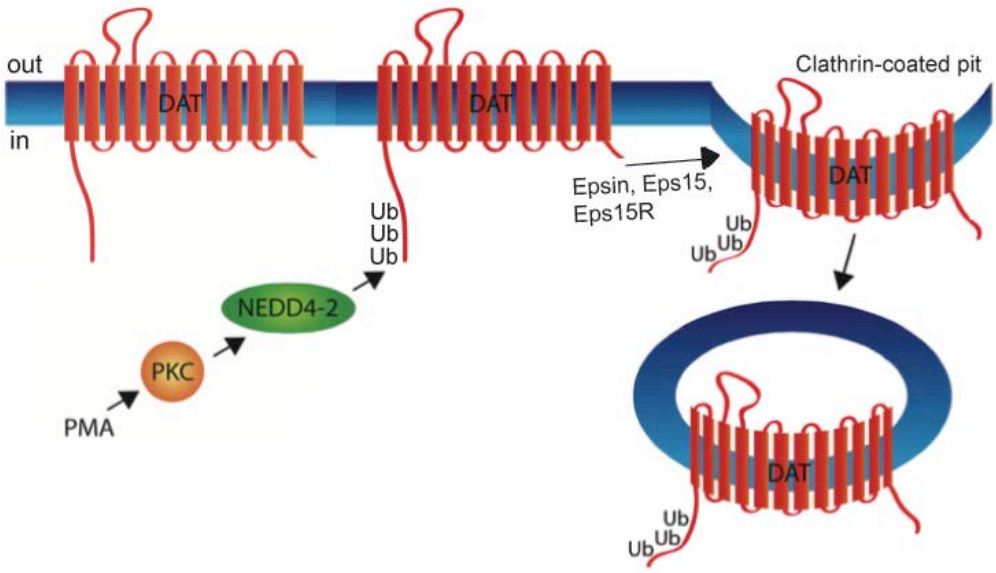

Figure 1.5. Schematic hypothesis of ubiquitination-mediated PKC-stimulated DAT endocytosis, modified from (Eriksen et al 2010).

AMPH treatment (5 min-30 min) triggers DAT endocytosis through the activation of the small GTPase RhoA in a dynamin-dependent, clathrin-independent manner (Saunders et al 2000, Wheeler et al 2015). AMPH-stimulated DAT endocytosis can be blocked by cocaine, indicating that the uptake of AMPH into the cytoplasm by DAT or the DAT conformational change from OF to IF state (which can be blocked by cocaine) is required (Johnson et al 2005). AMPH-stimulated DAT endocytosis is observed in heterologously expressing cells, cultured dopaminergic neurons, and midbrain slices (Wheeler et al 2015). Internalized DAT is found mostly in EEs and REs under AMPH treatment, in contrast to its efficient targeting to LEs and LYSs upon PKC activation (Hong & Amara 2013). It means that during AMPH treatment, internalized DAT mostly enter the recycling pathway. The elevated level of cytosol DA that is

induced by AMPH treatment may activate RhoA-mediated DAT endocytosis, during which the clathrin-light chain does not colocalize with DAT (Wheeler et al 2015).

In summary, constitutive endocytosed DAT can be sorted to EEs, REs, or LEs in the somatodendritic region of dopaminergic neurons, although there are controversies between Melikian group and Gether group. The former suggests that internalized DAT recycles back to the plasma membrane through the slow-recycling pathway via ERCs (Melikian & Buckley 1999), while the later suggests that internalized DAT recycles through the fast-recycling pathway (Eriksen et al 2010). PKC-stimulated DAT endocytosis in heterologous expression system is clathrin-dependent and requires ubiquitination at least in PAE and HeLa cells (Hong & Amara 2013, Miranda et al 2005), while AMPH-stimulated DAT endocytosis is dynamin-dependent and clathrin-independent (Wheeler et al 2015).

1.4 REGULATION OF DAT FUNCTION BY PROTEIN-PROTEIN INTERACTIONS

A multitude of proteins that interact with DAT have been found. Protein-protein interactions regulate DAT localization, trafficking, activity and degradation. Studies on these interactions contribute to revealing mechanisms for the regulation of DAT function.

The interaction between DAT and scaffolding proteins may regulate DAT localization in the presynaptic membrane. DAT binds the PDZ domain-containing protein interacting with C kinase 1 (PICK1) through the last three C-terminal residues (LKV) in a heterologous expression system (Torres et al 2001). The mutation of LKV to AAA impairs the localization of DAT to the presynaptic membrane. However, it is possible that this effect is due to the important role of the DAT C-terminus in regulating the trafficking of DAT from the ER to the plasma membrane but

not the disruption of the DAT-PICK1 interaction, since the DAT LKV-AAA mutant maintains normal expression in the plasma membrane of HEK293 cells (Bjerggaard et al 2004).

Several DAT interacting proteins are involved in AMPH-stimulated DAT endocytosis and conformational changes. CaMKII binds the C-terminus of DAT and phosphorylates the N-terminus of DAT (Fog et al 2006). DAT interacts with SNARE protein syntaxin1A, which is localized to the presynaptic membrane (Lee et al 2004). The interaction between DAT and syntaxin1A is dependent on the phosphorylation of the DAT N-terminus by CaMKII, which can be activated by AMPH treatment. The overexpression of syntaxin1A in turn facilitates AMPH-induced DA efflux (Binda et al 2008). However, the mechanisms for this interaction (e.g., the binding motifs of DAT) are not known.

DAT interacts with the β subunit of PKC (PKCβ) (Chen et al 2009). Mice with PKCβ knockout exhibit decreased surface DAT levels and DA uptake activity, and reduced AMPH-induced DAT endocytosis and DA efflux, suggesting that PKCβ maintains normal DAT function and plays an important role in AMPH-stimulated DAT endocytosis (Chen et al 2009, Johnson et al 2005). However, this is not in agreement with the general observation that PKC is not involved in AMPH-stimulated DAT endocytosis.

Several DAT interacting proteins down regulate the surface level of DAT. The orphan G protein-coupled receptor 37 (GPR37) has also been reported to interact with DAT and regulate DAT trafficking and endocytosis. Mice with GPR37 knockout exhibit enhanced surface DAT levels and elevated DA uptake activity (Marazziti et al 2007). Surface DAT level is also down regulated by the interaction between DAT and the focal adhesion protein Hic-5. Overexpression of Hic-5 results in the reduction of surface DAT and DA uptake activity (Carneiro et al 2002).

DAT also interacts with α-synuclein, although the effect of down-regulation of α-synuclein on DAT function remains controversial (Lee et al 2001, Wersinger & Sidhu 2003).

DAT activity can be regulated by protein-protein interaction directly. The DA uptake activity of DAT is increased by its interaction with synaptogyrin-3, a protein that resides in the membrane of synaptic vesicles. The effects of synaptogyrin-3 on DAT activity is dependent on the vesicular monoamine transporter 2 (VMAT2), suggesting that DAT activity is regulated by synaptic vesicles (Egaña et al 2009). It has been shown that D2SR interacts with the N-terminus of DAT and stabilizes DAT surface expression and DA uptake activity (Lee et al 2007). G protein βγ subunits interact with DAT and inhibit DA uptake activity or increase DA efflux through DAT (Garcia-Olivares et al 2013).

Several DAT interacting proteins are involved in DAT ubiquitination. DAT is constitutively uniquitinated and degraded (Miranda et al 2005). As described in **1.3.4**, the uniquitination of DAT is enhanced upon PKC activation. DAT ubiquitination is specifically regulated by the ubiquitin ligase NEDD4-2, which directly interacts with DAT. Ubiquitinated DAT also interacts with ubiquitin adaptor proteins epsin, Eps15, and Eps15R, which are important for the recruitment of ubiquitinated proteins to CCPs (Sorkina et al 2006).

In summary, DAT function is regulated by protein-protein interactions. However, most interactions of DAT have been demonstrated in a single study and have not been reproduced (Torres 2006). None of the interactions (except through ubiquitin) have shown clear molecular mechanisms for the interaction and mapped interacting motifs (Eriksen et al 2010). Most interactions have unknown function. Therefore, it is important to perform new screens of DAT-interacting proteins.

1.5 FILOPODIA

Filopodia are highly dynamic finger-like protrusions of the plasma membrane containing a uniform bundle of 15-20 linear actin filaments (Pacheco & Gallo 2016). Filopodia extend from the plasma membrane and move rapidly as the cell seeks biological cues. An example of EM image of filopodia is shown in Figure 1.6, which is the tomogram of 3D reconstructed of filopodia images from cryo-electron tomography. In the filopodia, actin filaments are bundled tightly and periodically (*left*). Cross-section from bottom view shows that actin filaments are bundled hexagonally, and the thickness of filopodia is around 200 nm (*right*). The width of mammalian filopodia is about 0.1-0.3 μm (Pertz 2011).

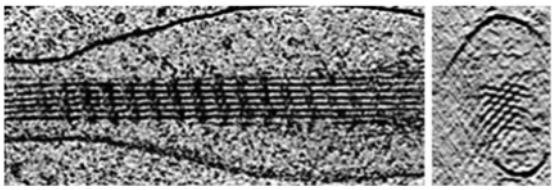

Figure 1.6. The structure of filopodia (Aramaki et al 2014).

The mechanisms of filopodia formation and maintenance are not fully understood. It is suggested that there might be several distinct mechanisms of filopodia formation. One of the mechanisms for filopodia formation involving the recruitment of I-BAR (inverse Bin-Amphiphysin-Rvs) protein IRSp53 to the plasma membrane is the best studied so far (Figure 1.7). IRSp53 (or other inverse I-BAR domain-containing proteins) facilitate plasma membrane protrusion by directly deforming the membrane (from a to b in Figure 1.7). I-BAR domain proteins form convex (away from the cytoplasm) dimers and induce the curvature of membrane that they bind to (Mattila et al 2007). The activation of active cell division control protein 42 (Cdc42, a small GTPase of the Rho family) or Rac-related C3 botulinum toxin substrate 1 (Rac1)

recruits IRSp53 to the plasma membrane (Scita et al 2008). IRSp53 dimers deform the plasma membrane and generate membrane protrusions. The I-BAR domain of IRSp53 also has an actin-binding site, which may induce the binding of actin filaments.

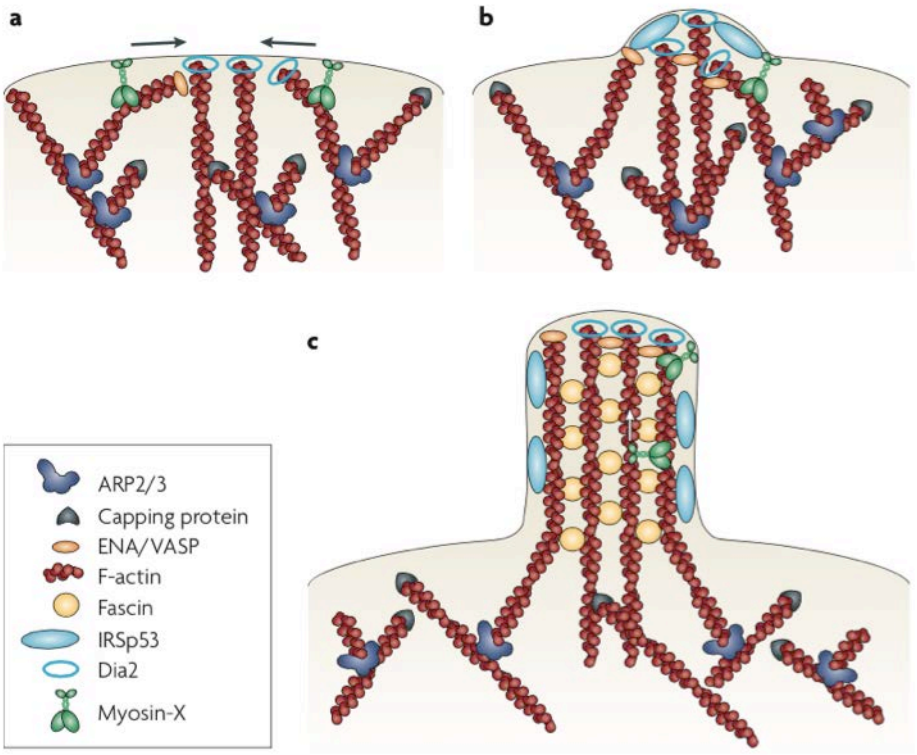

Figure 1.7. A model for filopodia formation (Mattila & Lappalainen 2008).

IRSp53 binding partners such as Enabled/vasodilator-stimulated phosphoprotein (Ena/VASP) and diaphanous 2 (Dia2) facilitate the barbed end growth of actin filaments by protecting them from capping proteins (Scita et al 2008).As the filopodia generate (from b to c in Figure 1.7), Dia2 and Ena/VASP are localized to the tip to regulate the elongation of barbed-end actin filaments, and the actin crosslinking protein fascin crosslinks actin filaments into semi-ordered array. However, a number of studies demonstrated that Rho-family GTPases are not necessary for filopodia formation. Ena/VASP and Dia2 bind profilin, an actin-binding protein enhancing the growth of actin filaments (Romero et al 2004). Therefore, actin filaments are recruited to the deformed (bended) membrane and bundle together as they elongate to shape

membrane protrusions. A subset of uncapped actin filaments of the actin-related protein-2/3 (ARP2/3)-nucleated dendritic network is targeted for continued elongation by Dia2 and/or by Ena/VASP via preventing the binding of capping proteins.

Another I-BAR domain protein, missing in metastasis (MIM), which does not bind actin filaments, Ena/VASP, or Dia2, is also able to deform the plasma membrane and induce the formation of filopodia, suggesting that it may regulate filopodia formation through a different mechanism. Several other members of the Rho family small GTPases also regulate filopodia formation. For example, Rho in filopodia (Rif) binds Dia2 (Ahmed et al 2010). IRSp53, MIM, and profilin bind PIP_2, and Ena/VASP binds membrane rafts that are enriched in PIP_2, suggesting that the protein complex for actin binding may form a staging area with PIP_2 during filopodia initiation (Lai et al 2008, Mattila et al 2007, Skare & Karlsson 2002).

A motor protein myosin X (MyoX) also plays an important role in filopodia formation (Figure 1.7). MyoX moves up along actin filament barbed ends and then slides down with the retrograde actin flow in an ATP-dependent manner. It has been suggested that MyoX carries Ena/VASP and a number of focal contact components such as integrins as cargos to the tips of filopodia (Heckman & Plummer 2013). It has also been demonstrated that overexpression of MyoX induces filopodia formation, as the motor activity of MyoX promotes actin filaments convergence (Tokuo et al 2007). MyoX may act downstream of Cdc42, and it can initiate filopodia formation without Ena/VASP (Bohil et al 2006)

Filopodia are involved in many cellular and developmental processes, as reviewed in (Mattila & Lappalainen 2008). In particular, in the nervous system, it is thought that filopodia are involved in formation of dendritic spines. Filopodia plays an important role in axon branching/pathfinding, also called axon guidance, during neuronal growth (Gallo 2011). The

function of filopodia as growth cone sensors has been well studied in the dorsal closure in embryonic development. When growth cone filopodia of a neuron are contacting the surface of another neuron that is destined to interact with it (attractive target), the filopodia will tightly attach to the target. When growth cone filopodia of a neuron are contacting the surface of another neuron that is not related to it (repulsive target), the filopodia movement in the contact place is stopped, while the other filopodia on the growth cone continue to move forward and seek other targets (Heckman & Plummer 2013).

There are no dendritic spines in dopaminergic neurons, and our lab has observed the localization of DAT in the filopodia of axons and growth cones of cultured dopaminergic neurons (Rao et al 2012). Besides, DAT is accumulated in the membrane protrusions that contain filamentous actin and a filopodia actin motor MyoX (Caltagarone et al 2015). DAT has also been demonstrated to interact with PIP_2 (Hamilton et al 2014), which is essential for the formation of filopodia as described above. So far, the role of DAT in filopodia and the mechanism for DAT accumulation in filopodia have not been demonstrated.

1.6 THESIS GOALS AND HYPOTHESES

The subcellular localization and trafficking of DAT is critical for its proper function. How DAT is transported from the soma to the dendrites and axons of dopaminergic neurons is not understood. Our laboratory has found that DAT is enriched in filopodia and may induce filopodia formation when overexpressed. The capacity of DAT to concentrate in filopodia may facilitate synaptogenesis processes during development, or be part of the mechanism by which DAT concentrates in striatal axonal processes. In contrast to wild-type DAT, R60A and W63A

DAT mutants with disrupted intramolecular interaction and substrate transport function are not enriched in filopodia compared to wild-type DAT, suggesting that DAT conformation is important for DAT filopodia targeting. Therefore, we hypothesize that filopodia targeting of DAT is regulated by DAT conformation.

On the other hand, our laboratory proposed the existence of plasma membrane retention mechanisms that prevent constitutive endocytosis of DAT, maintaining the bulk of the transporter at the cell surface. We also found that this retention is mediated by N-terminus. Since it has been demonstrated that PIP_2 a critical phosphoinositide enriched in the plasma membrane and interacts with the N-terminus of DAT (Khelashvili et al 2015), it can be proposed that this is the retention mechanism. It has indeed been proposed that the interaction with PIP_2 may retain DAT in the plasma membrane (Fagan et al 2015). However, PIP_2 regulates the function of many proteins involved in endocytosis, the actin cytoskeleton and cell adhesion, by recruiting them to the plasma membrane. It is also known to bind and modify the function of potassium channels. At the same time, PIP_2 is involved in clathrin-mediated endocytosis through recruitment of various proteins associated with the clathrin-coated pits. Therefore, the role of PIP_2 in regulating DAT retention in the plasma membrane and its endocytosis is important to elucidate. We hypothesize that PIP_2 regulates DAT levels at the plasma membrane by preventing constitutive endocytosis but also is necessary for endocytosis. It is possible that the retention of DAT in the plasma membrane by PIP_2 prevents constitutive DAT endocytosis. At the same time, PIP_2 is necessary for all kinds of endocytosis, because PIP_2 is highly associated with cytoskeleton.

While the role of conformation and lipid binding of PIP_2 to DAT are to be tested as proposed above, DAT function is likely regulated by protein interactions. As we described above, virtually no interactions of DAT with other proteins are understood on the molecular and

functional levels. Therefore, it is still important to perform rigorous screening for DAT interactors in the brain.

The overall goal of the dissertation is to study the mechanisms determining subcellular localization and trafficking of DAT. We will study the role of DAT conformation and PIP_2, in DAT targeting to filopodia and subcellular distribution, as well as search for new DAT interactors that control DAT localization and function in the cell.

2.0 TARGETING OF DAT TO FILOPODIA

2.1 ABSTRACT

Dopamine transporter (DAT) has been shown to accumulate in filopodia in neurons and non-neuronal cells. High levels of DAT expression in non-neuronal cells induce filopodia formation. To examine the mechanisms of DAT filopodial targeting, we used quantitative live-cell fluorescence microscopy, and compared the effects of the DAT inhibitor cocaine and its fluorescent analog JHC1-64 on the plasma membrane distribution of wild-type DAT and two non-functional DAT mutants, R60A and W63A, that do not accumulate in filopodia. W63A did not bind JHC1-64, whereas R60A did, although less efficiently compared to the wild-type DAT. Molecular dynamics simulations predicted that R60A preferentially assumes an outward-facing (OF) conformation through compensatory intracellular salt bridge formation, which in turn favors binding of cocaine. Imaging analysis showed that JHC1-64-bound R60A mutant predominantly localized in filopodia, whereas free R60A molecules were evenly distributed within the plasma membrane. Cocaine binding significantly increased the density of R60A, but not that of W63A, in filopodia. Further, zinc binding, known to stabilize the OF state, also increased R60A concentration in filopodia. Finally, amphetamine, which is thought to disrupt the DAT OF conformation, reduced the concentration of wild-type DAT in filopodia. Altogether,

these data indicate that the OF conformation is required for the effective targeting of DAT to, and accumulation in, filopodia.

2.2 INTRODUCTION

DAT conformation dynamically shifts between outward-facing (OF) and inward-facing (IF) states during the transport cycle. Maintaining the OF conformation and the OF-IF transition leading to the substrate release are critical for the substrate uptake function of DAT. However, whether such conformation states (or their transitions) affect subcellular localization of DAT has not been elucidated.

We have previously demonstrated that DAT is accumulated in filopodia-like membrane protrusions in dopaminergic neurons and non-neuronal cells (Rao et al 2012, Sorkina et al 2009). In our previous studies, we also showed that filopodia tip motor protein myosin X (MyoX) was concentrated on the tips of many DAT-labeled membrane protrusions that extended from the cell edge, dorsal membrane and large ruffle-like structures (Caltagarone et al 2015). MyoX transports cargo proteins towards the tip of filopodia along actin filaments (Sato et al 2017). We proposed that the ability to accumulate in the highly curved membranes of filopodia might be enabled by the same mechanism that is also responsible for DAT accumulation in dopaminergic axons whose dimensions (~200 nm in diameter) and membrane curvature are similar to those of filopodia, especially during axonal branching. Based on the observation that DAT mutants with disrupted intramolecular interactions and diminished substrate transport activity were not enriched in filopodia (Caltagarone et al 2015), we hypothesized that a proper functional conformation of the DAT molecule is necessary for its targeting to filopodia, and that DAT can

promote filopodia formation when expressed at high levels. Therefore, we directly examine the filopodia-promoting ability of DAT and analyze the relationship between DAT filopodia targeting and DAT conformational states. We use molecular dynamics (MD) simulations to determine the conformational state of two DAT mutants, and define the effects of cocaine and its fluorescent analog JHC1-64 on the conformation of these mutants. We then used several independent experimental approaches to control the conformational state of DAT and its mutants to demonstrate that the OF state of DAT is required for its enrichment in filopodia.

2.3 MATERIALS AND METHODS

2.3.1 Reagents

Cocaine hydrochloride, D-amphetamine hemisulfate salt and $ZnCl_2$ were from Sigma-Aldrich (St. Louis, MO). JHC1-64 was synthesized in the Medicinal Chemistry Section, NIDA-IRP as described (Cha et al 2005). Restriction enzymes are from New England Biolabs (Ipswich, MA). All other chemicals were from Thermo Fisher Scientific (Pittsburgh, PA) or Sigma-Aldrich.

2.3.2 Plasmids

Yellow fluorescent protein (YFP)- and hemagglutinin epitope (HA)-tagged human DAT (YFP-HA-DAT, Addgene plasmid # 90244) and mutant versions of YFP-HA-DAT (R60A and W63A, Addgene plasmids # 90245 and #90246, respectively) were described previously (Sorkina et al 2006, Sorkina et al 2009). RFP-HA-DAT (Addgene plasmid # 90265) was also previously

described (Caltagarone et al 2015). To generate the R60A mutation in the template of YFP-DAT (no HA tag, Addgene plasmid # 90228) (Sorkina et al 2003), the 1622 bp DAT sequence (beginning with bp 242 in DAT cDNA) in YFP-HA-R60A was replaced by the corresponding sequence from the YFP-DAT construct using PflMI (5' end) and SmaI (3' end) restriction sites. The R60A mutation in YFP-DAT (Addgene plasmid # 90247) was confirmed by sequencing. Lifeact-RFP was provided by Dr. Lichius (Berepiki et al 2010).

2.3.3 Cell culture and transfections

Human HEK293 cells (Invitrogen # R70507) were grown in DMEM with 10% fetal bovine serum (FBS, Hyclone, Logan, UT). Porcine aortic endothelial (PAE) cells were originally obtained from Dr. B. Westermark (University of Uppsala, Sweden) and used in our previous studies (Sorkina et al 2003). PAE cells were grown in F12 medium with 10% FBS. PAE cells stably expressing YFP-HA-DAT were described previously (Sorkina et al 2009).

The cells were transiently transfected with plasmids using Effectene kit (Qiagen, Valencia, CA) according to the manufacturer's protocol. After transfection, HEK293 cells were grown on Poly-D-Lysine (Sigma-Aldrich) coated 18 mm glass coverslips and PAE cells were grown on coverslips without coating. Cells were used for imaging 2 days after transfection.

2.3.4 Fluorescence microscopy

Cells grown on glass coverslips were placed onto the stage of a spinning disk confocal imaging system equipped with an EM-CCD camera and an environmental chamber controlled by SlideBook software (Intelligent Imaging Innovation, Denver, CO). A 63x oil immersion lens was

used (207 nm/pixel). For JHC1-64, cocaine and zinc binding experiments, cells were imaged in Dulbecco's Phosphate Buffered Saline (DPBS) (plus 1 mM $CaCl_2$, 0.5 mM $MgCl_2$ and 5 mM D-glucose) at room temperature (RT). For AMPH treatment experiment, cells were imaged in Krebs Ringer HEPES solution (KRH, with 140 mM NaCl, 5 mM KCl, 2 mM $CaCl_2$, 1 mM $MgCl_2$, 5.5 mM HEPES and 1 mM D-glucose, pH 7.4), at 37 °C and 5% CO_2. A z-stack of 15-20 confocal images at 400 nm z-steps was acquired through 515 nm (YFP) or 561 nm (RFP and JHC1-64) laser channels using a single dichroic. All images were captured using the same exposure time (100 ms) and all other image acquisition parameters were also kept the same. Gamma was set on "1" in all images if not specified.

2.3.5 Image analysis

Images were analyzed using SlideBook software. The use of an EM-CCD camera allows high linearity of fluorescence detection within the full intensity range. Background was subtracted in each image. To count filopodia, a maximum projection image was generated from a 3D image, and a mask was generated to manually select the entire cell. The lengths of filopodia were measured using the line tool in SlideBook software. Filopodia longer than 2 μm were counted in a blind fashion. The cell body was selected manually using the SlideBook mask pencil tool, and the perimeter of the cell was calculated using the statistics module of SlideBook software. The filopodia density was expressed as the number of filopodia per 100 μm of cell perimeter.

To facilitate quantitation of JHC1-64 binding, a segmental mask was generated to select YFP-containing voxels in each individual cell. The mean fluorescence intensities (in arbitrary linear units of fluorescence intensity) of JHC1-64 and YFP were calculated in the mask, and the ratio of JHC1-64 and YFP fluorescence, designated as JHC/YFP, was used to estimate the

apparent density of the JHC1-64:YFP-HA-DAT complexes. YFP intensities were corrected for photobleaching whereas no significant photobleaching of JHC1-64 fluorescence was observed during time-course imaging.

To quantitate the ratio of JHC1-64 to YFP-HA-DAT fluorescence intensities in filopodia versus non-filopodial regions of the plasma membrane (FM, flat membrane), 5 xy-confocal planes from the z-stack that encompasses most of the peripheral filopodia and cell-bottom plasma membrane were used for quantification. Peripheral filopodia were selected manually using the SlideBook mask pencil tool in each z-plane (Mask 1). A mask containing all YFP-containing voxels in the cell was also generated using automated segmentation (Mask 2). The overlapping voxels of Masks 1 and 2 were then selected to generate Mask 3 (filopodia) to minimize the error of the manual selection of YFP-positive voxels. Ten or more representative small regions of FM in the periphery of the cells were manually selected to generate FM Mask 4. This mask typically included fluorescence of both bottom and top cell surface due to a limited z-axis resolution. Mean fluorescence intensities (in arbitrary linear units of fluorescence intensity) of JHC1-64 and YFP in Mask 3 and Mask 4 were then calculated in each cell, and the JHC/YFP ratio was used to estimate the relative density of JHC1-64:YFP-HA-DAT complexes in filopodia (Mask3) and non-filopodial plasma membrane (Mask4).

To quantitate the relative density of YFP-HA-DAT fluorescence in filopodia and non-filopodial regions of the plasma membrane (FM), filopodia (Mask 3) and FM (Mask 4) masks were generated from 5 xy-confocal planes from full z-stack of images as described above for experiments with JHC1-64. The mean YFP fluorescence intensities of filopodia Mask 3 and FM Mask 4, and their ratio (Filopodia/FM) were calculated in individual cells.

In cells co-expressing YFP- and RFP-tagged DATs, filopodia (Mask 3) and FM (Mask 4) masks were generated as described above, and the ratio of mean YFP and RFP fluorescence intensities in Mask 3 to Mask 4 were calculated for each individual cell to obtain filopodia/FM ratio values for YFP-HA-DATs and RFP-HA-DAT, respectively. Furthermore, the values of YFP filopodia/FM ratio were divided by values of the RFP filopodia/FM ratio in each individual cell to obtain a YFP/RFP value that corresponds to the relative fluorescence of YFP-HA-DAT versus RFP-HA-DAT in filopodia.

2.3.6 Statistical analysis

All data were analyzed using GraphPad Prism 6.0. Data normality of all data sets was confirmed using the D'Agostino-Pearson test. Student t-test was used to compare the statistical differences. For the comparison of the ratios of the same cells before and after JHC1-64/cocaine/zinc binding or AMPH treatment, paired student t-test was used. In other cases, we used unpaired student t-test. In all the figures, bar graphs show the mean value of quantified results, and error bars represent the S.E.M. *$p<0.05$, **$p<0.01$, ***$p<0.001$, ****$p<0.0001$.

2.4 RESULTS

2.4.1 Expression of DAT induces filopodia formation

To better characterize DAT-containing filopodia, we performed time-lapse 3D imaging of live PAE cells stably expressing YFP-HA-DAT at 37 °C. Maximal intensity projection images of the

z-stack are presented in Figure 2.1. Same cells in different time frames (times are in seconds) are shown in the figure. The arrows point to protruding and retracting movements of membrane extensions. The scale bar is 10 μm. Peripheral and dorsal filopodia were highly mobile with rapid lateral, protruding and retracting motions at 37 °C, which distinguishes them from retraction fibers (Figure 2.1). Similar though less dramatic dynamics was detected at room temperature (data not shown).

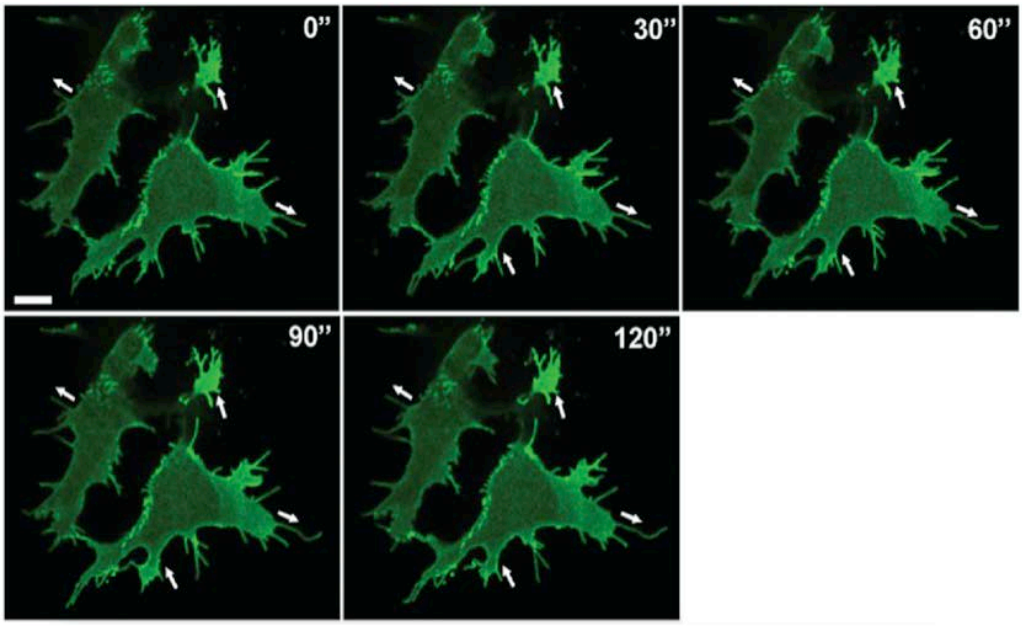

Figure 2.1. DAT-containing filopodia are highly mobile.

From our visual inspection of the images, cells with high expression level of DAT tended to have more DAT-containing filopodia. Therefore, we tested whether wild-type DAT can promote filopodia formation. PAE cells were transfected with Lifeact-RFP to label F-actin, and with YFP-HA-DAT or YFP. Z-stacks of 10 confocal images (400 nm stepsize) of living cells was acquired through 515 (YFP) and 561 (RFP) channels at 37°C. One group of the images is shown in Figure 2.2A. The RFP image is presented with the gamma for the 561 channel set to 0.5 to allow for better visualization of the low Lifeact-RFP signals in filopodia without interference from the bright signal of the cell cortex. The insets show high magnification of the

region marked by the white rectangle to demonstrate enrichment of YFP-HA-DAT in distal filopodia regions compared to Lifeact-RFP. Live-cell 3D imaging of Lifeact-RFP revealed large stress fibers in the cell body and smaller filaments that were detected in filopodia containing YFP-HA-DAT, although Lifeact-RFP did not penetrate into distal parts of these filopodia (Figure 2.2A). Figure 2.2B shows an example of the selection mask used for counting peripheral filopodia. The mask was manually generated by encircling the perimeter of the cell Lifeact-RFP fluorescence. Filopodia extending for more than 2 μm outside of the mask were marked. The perimeter of the cell body was calculated and the number of filopodia was counted using the SlideBook statistics module. In the example presented in Figure 2.2 B, there are 11.6 filopodia per 100 μm of cell perimeter. Figure 2.2C shows an example of PAE cells with transiently expressed YFP and Lifeact-RFP, and the mask selection for counting peripheral filopodia. There are 4.5 filopodia per 100 μm of cell perimeter in this image. Figure 2.2D shows the quantifications of the filopodia density (number per 100 μm of cell perimeter). The statistical difference between cells expressing YFP-HA-DAT and YFP was analyzed using unpaired student t-test. Graph bars represent mean values of filopodia number per cell perimeter from 30 to 40 cells in each experimental variant. The scale bars are 10 μm. Analysis of Lifeact-RFP images revealed a statistically significant increase in the peripheral filopodia membrane density in cells expressing YFP-HA-DAT over control cells (expressing YFP and Lifeact-RFP) as measured by the number of filopodia per unit of the cell perimeter (Figure 2.2D).

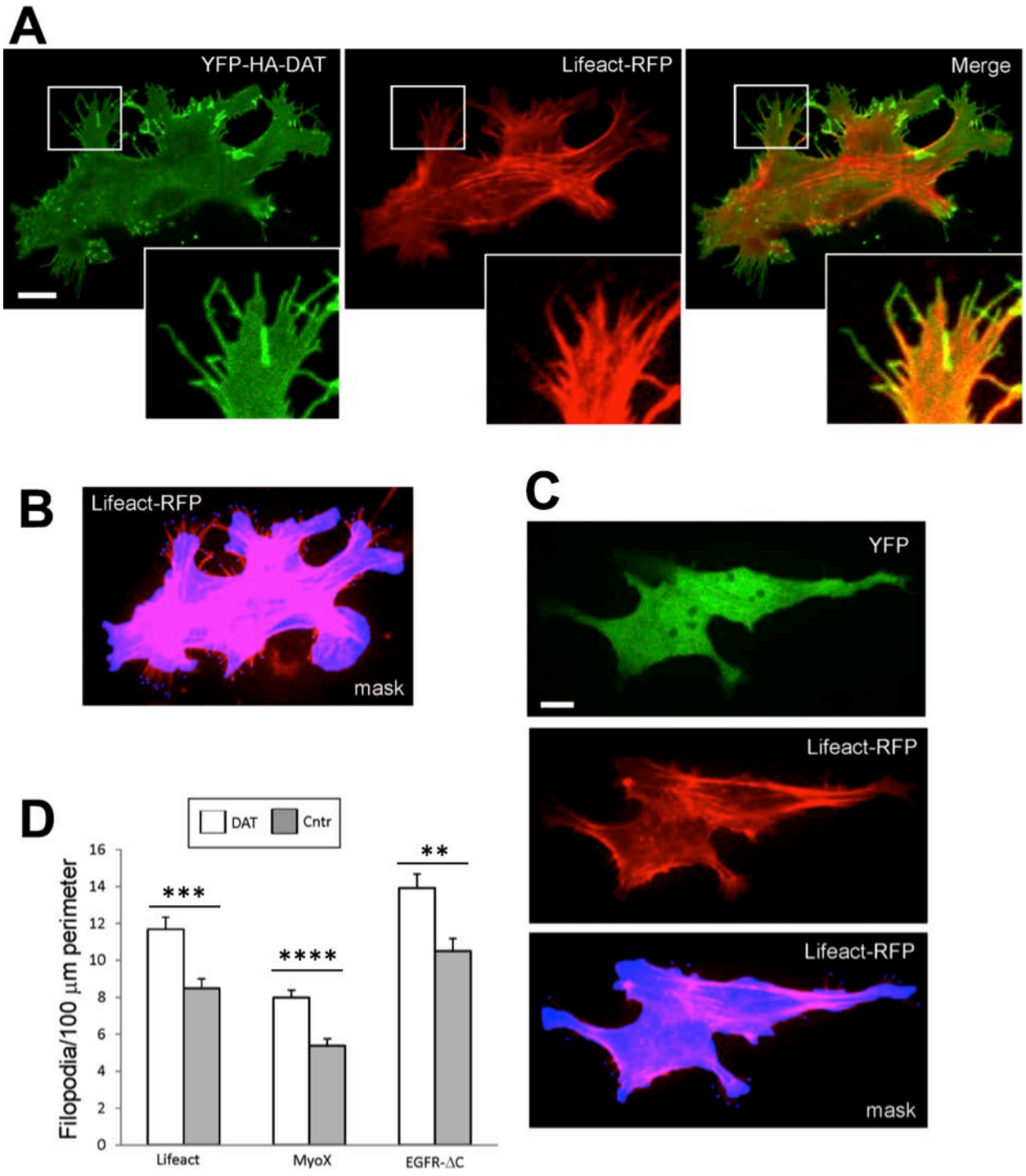

Figure 2.2. DAT induces filopodia formation.

PAE cells expressing YFP-HA-DAT or YFP were fixed and stained with MyoX. Numbers of MyoX positive filopodia tips were counted. The analysis also demonstrated a high number of filopodia in cells expressing YFP-HA-DAT (Figure 2.2D). Finally, PAE cells were

co-transfected with EGFR-ΔC ΔC (model transmembrane homogeneously distributed in the plasma membrane) and YFP-HA-DAT or YFP. In these experiments, an increased density of EGFR-ΔC labeled filopodia was observed in YFP-HA-DAT expressing cells as compared to control (YFP) cells (Figure 2.2D).

In all three approaches, the number of peripheral filopodia per length of the perimeter of the cell was calculated. Dorsal filopodia were difficult to count, especially in fixed cells, because of their overlap with the strong fluorescence of actin, MyoX and EGFR-ΔC staining throughout the perinuclear area of the cell. However, it is likely that the numbers of DAT-enriched filopodia were underestimated because Lifeact-RFP and EGFR-ΔC did not penetrate to the entire length of DAT-enriched filopodia, and may therefore, be undetectable in short filopodia. Nevertheless, all three approaches to detect and count filopodia indicated that DAT can induce and/or maintain filopodia in both transiently and stably DAT-expressing cells.

2.4.2 DAT mutants W63A and R60A do not concentrate in filopodia

Demonstration of DAT accumulation in filopodia prompted the investigation of the mechanism of DAT filopodia targeting. We have previously observed that DAT mutants with disrupted substrate uptake activity appear not to concentrate in membrane protrusions (Sorkina et al 2009). To directly compare the localization of wild-type and mutant DATs, RFP-HA-DAT was transiently co-expressed with W63A or R60A mutants of YFP-HA-DAT in PAE cells. Cells were imaged through 561 (RFP) and 515 (YFP) filter channels. Maximal projection images of 3D images are presented in Figure 2.3A and C. The insets show high magnification of the region marked by the white rectangle to demonstrate the enrichment of RFP-HA-DAT in distal

filopodia regions as compared to DAT mutants. The scale bars are 10 μm. Both DATs were highly co-localized in all areas of the cell including in filopodia (Figure 2.3A, C).

In each image, the RFP/YFP fluorescence ratio in filopodia and planner flat membrane (flat membrane, FM, where we observed a diffuse distribution of DAT) was quantified. The statistical difference between the ratios of filopodia and FM was analyzed using paired student t-test. The quantification of RFP/YFP ratios from 30 to 35 cells are shown in Figure2.3B and D. Interestingly, the ratio of RFP to YFP fluorescence intensities (RFP/YFP) in filopodia was substantially higher than in other regions of the cell (Figure 2.3B, D). The difference in scale between Figure 2.3B and Figure 2.3D is big, this is probably because the instability of transient expression of RFP-HA-DAT and the mutants. In fact, distal parts of many RFP-HA-DAT containing filopodia did not contain detectable amounts of W63A or R60A mutants regardless of the expression levels of wild-type and mutant DATs. The extent of the differential distribution of wild-type versus mutant DAT observed in co-expression experiments was probably underestimated because of wild-type/mutant DAT hetero-oligomerization (Sorkina et al 2003, Torres et al 2003). These two non-filopodial targeting mutants R60A and W63A were highly useful for further studying the mechanisms of DAT filopodia targeting.

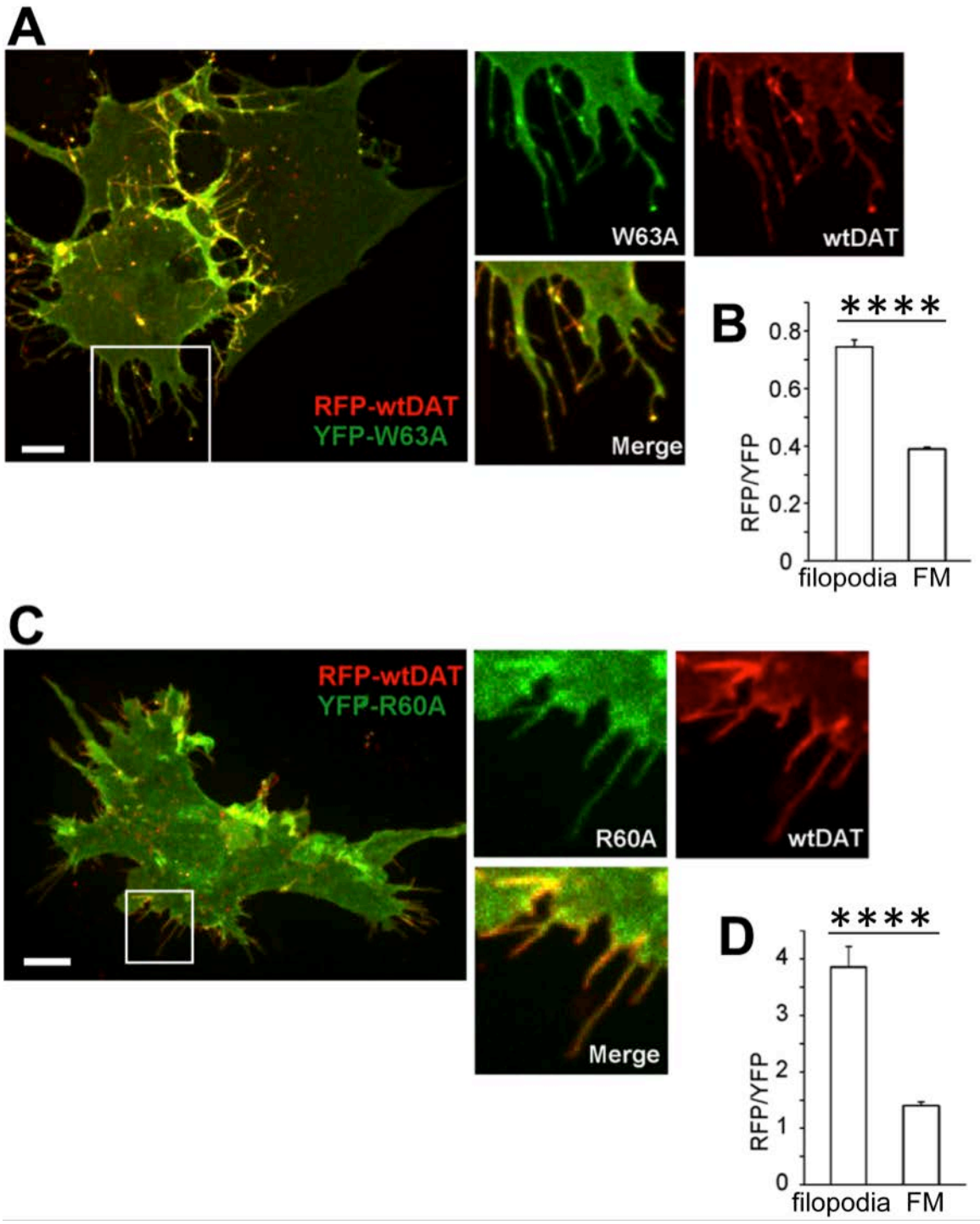

Figure 2.3. DAT mutants are not enriched in filopodia.

2.4.3 Fluorescent cocaine analog JHC1-64 preferentially binds to filopodia-located DAT and its R60A mutant

To quantitatively compare the distribution of the wild-type (wt) DAT and the mutants in the plasma membrane, we used JHC1-64 (the chemical structure is shown in Figure 2.4A), a membrane-impermeable fluorescent cocaine analog, to detect surface YFP-HA-DAT (Cha et al 2005). It was previously shown that JHC1-64 does not alter the membrane mobility and trafficking properties of DAT (Eriksen et al 2009). Transient expression of wt YFP-HA-DAT and its mutants was used to avoid clonal variations of stably expressing cells, and differences in expression levels of wt and mutant DATs in these clones.

HEK293 cells transiently expressing wt YFP-HA-DAT, or its mutants (R60A or W63A) were incubated with 100 nM JHC1-64 for 30 min at room temperature (RT). Live-cell imaging was performed at RT to minimize the motility of highly dynamic filopodia during 3D image acquisition. Images were acquired through 515 nm (YFP, *green*) and 561 nm (JHC1-64, *red*) filter channels. Maximal projections of 5 z-planes are shown in Figure 2.4B. The arrows point to examples of peripheral filopodia. The scale bars are 10 μm. JHC1-64 bound to the R60A mutant, albeit to a lesser extent than to wt YFP-HA-DAT. By contrast, no detectable binding of JHC1-64 to the W63A mutant was observed (Figure 2.4B). YFP-HA-DAT wt and the R60A mutant were treated with 10-200 nM JHC1-64 for 30 min at RT. The ratio of JHC1-64 and YFP fluorescence intensities (designated JHC/YFP) was quantitated for whole cells as described in section **2.3.5**. The statistical difference between the ratios of wt YFP-HA-DAT and the R60A mutant in each dose of JHC1-64 was analyzed using unpaired student t-test (n=3) (Figure 2.4C). A JHC1-64 concentration of 100 nM was found to yield the best signal-to-noise fluorescence ratio in cells expressing wt YFP-HA-DAT or the R60A mutant.

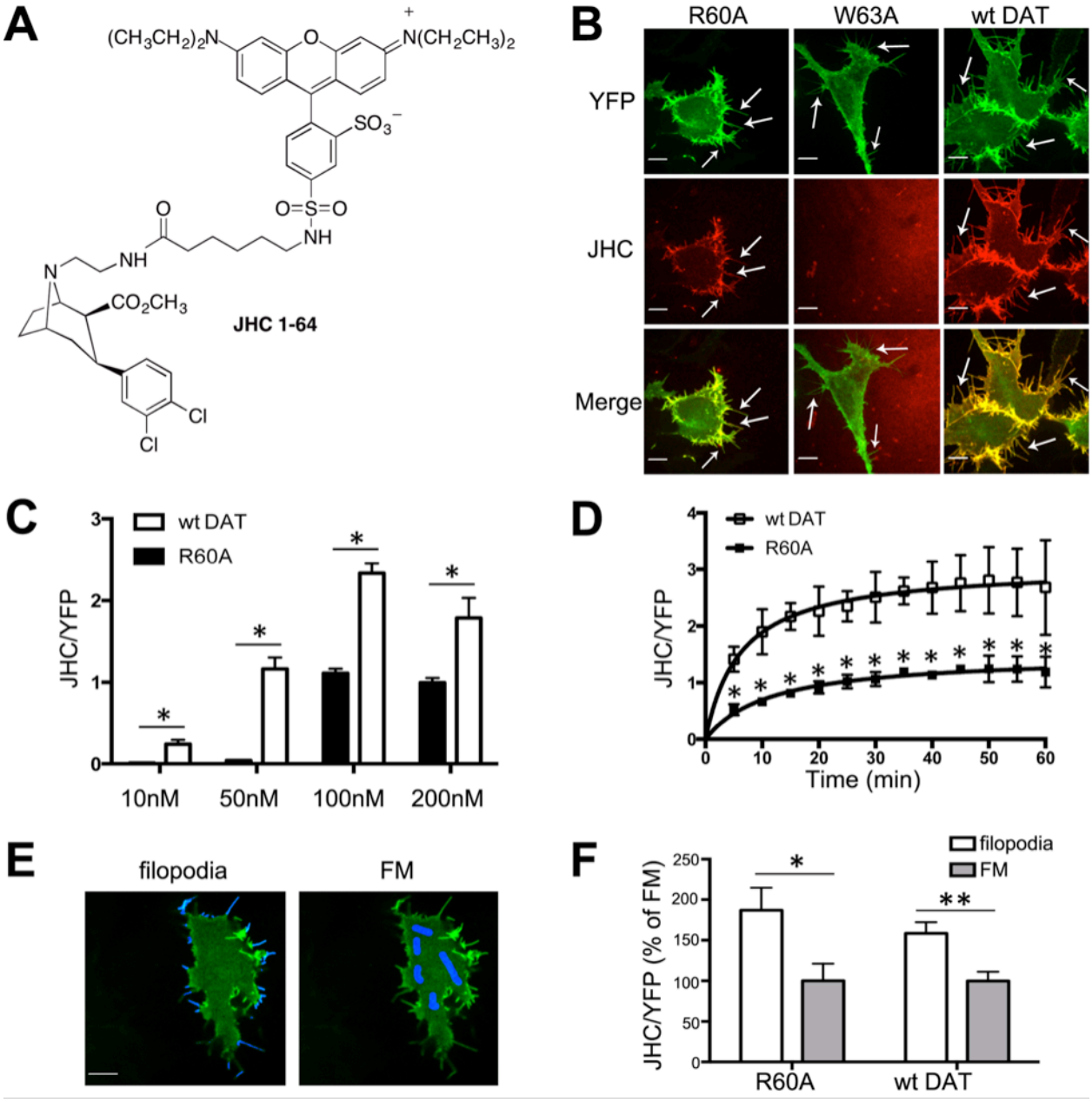

Figure: 2.4. Preferential binding of JHC1-64 to wt DAT and its R60A mutant in filopodia and cell edges of HEK293 cells.

HEK293 cells with transiently expressed YFP-HA-DAT or YPP-HA-R60A were treated with 100 nM JHC1-64, and the time dependence of the JHC/YFP ratio was determined by time-lapse imaging of YFP and JHC1-64 at RT. The statistical difference between the ratios of wt YFP-HA-DAT and the R60A mutant in each time point was analyzed using unpaired student t-test (n=10). As shown in Figure 2.4D, quantification of the JHC1-64/YFP ratio during the time-

course of JHC1-64 (100 nM) binding to wt YFP-HA-DAT and the R60A mutant using single-cell imaging showed that binding to either DAT approached a maximum after 20-30 min at RT, and that binding to the R60A mutant was 2-times less efficient than that to wt YFP-HA-DAT. Binding of JHC1-64 at 37 °C was much faster compared to that at RT (maximum binding to wt YFP-HA-DAT was reached at 1 min), while the pattern of JHC1-64 localization was identical to that observed at RT. No significant dissociation of JHC1-64 was observed after washing out JHC1-64 for at least 1 hour at 37 °C, suggesting that the JHC1-64 dissociation rate constant is low (data not shown).

Visual inspection of JHC1-64 localization revealed a striking preference of JHC1-64 to decorate filopodia and cell edges, areas of increased membrane curvature (Figure 2.4B). Accumulation of both JHC1-64 and YFP-HA-DAT (indicative of the formation of JHC1-64:YFP-HA-DAT complexes) was most pronounced in filopodia emanating near cell-cell contacts. The ratio of the fluorescence intensities of JHC1-64 and YFP-HA-DAT, designated as JHC/YFP, was adopted as a measure of the JHC1-64 binding fraction (see section **2.3.5**). To compare the JHC/YFP ratio in the filopodia to that in regions of the planar plasma membrane (FM, flat membrane), peripheral filopodia and FM masks were generated in each cell. Figure 2.4E shows an examples of the segmentation masks for quantification of the mean fluorescence intensities of peripheral filopodia (l*eft*) and non-filopodial membrane (FM; *right*) regions from YFP images obtained in the experiments represented in Figure 2.4B. JHC/YFP ratio values were quantified in the peripheral filopodia because DAT density in dorsal filopodia is technically difficult to measure due to limited z-axis resolution.

To quantitatively analyze whether there is more JHC1-64 binding in filopodia than FM, HEK293 cells expressing YFP-HA-DAT wt or R60A were imaged after incubation with 100 nM

JHC1-64 for 30 min at RT. The JHC/YFP ratio in filopodia and FM masks was quantitated in individual cells. Each ratio of cell expressing wt YFP-HA-DAT or the R60A mutant was divided by the mean value of the ratios in the FM mask of wt YFP-HA-DAT or the R60A mutant, respectively. The statistical difference between the ratios of filopodia and FM masks was analyzed using unpaired student t-test (n=10). The quantification results are shown in Figure 2.4F. This analysis revealed that the JHC1-64 binding fraction was at least 2-fold higher in filopodia than in flat membrane regions. The same behavior was observed in cells expressing the R60A mutant. These data suggest that both wt YFP-HA-DAT and its R60A mutant either bind JHC-64 more efficiently in filopodia or move to filopodia after JHC1-64 binding

2.4.4 JHC1-64 and cocaine increase R60A concentration in filopodia

The observation of a high concentration of the JHC1-64-bound R60A mutant in filopodia prompted us to test whether JHC1-64 binding promotes targeting of this mutant to filopodia or whether those mutant transporters already located in the filopodia exhibit a higher propensity to bind JHC1-64.

To this end, HEK293 cells transiently expressing YFP-HA-DAT wt or R60A were incubated with 100 nM JHC1-64 for 30 min at RT. Live-cell imaging was performed through 515 nm (YFP, *green*) and 561 nm (JHC1-64, *red*) filter channels. Maximal z-projections of 5 consecutive x-y confocal planes are shown in Figure 2.5A. The scale bars are 10 μm. The insets representing high magnification images of the regions marked by the white rectangle in Figure 2.5A are shown in Figure 2.5B. The arrows point to representative filopodia. The Filopodia/FM ratios of mean intensities of the YFP fluorescence were calculated as described in section **2.3.5**. The statistical difference between the ratios of individual cells before and after JHC1-64 binding

is analyzed using paired student t-test (n=10) and is shown in Figure 2.5C. These experiments demonstrated that binding of JHC1-64 increased the filopodia/FM ratio of the YFP fluorescence intensity in cells expressing the R60A mutant by 50%, suggesting an elevated targeting of R60A mutant to filopodia in the presence of JHC1-64 (Figure 2.5). The distribution of wt YFP-HA-DAT in filopodia was not significantly affected by JHC1-64 (Figure 2.5). Similar filopodia targeting effect of JHC1-64 on R60A (increase in the filopodia/FM ratio by ~30%) was observed in PAE cells (data not shown).

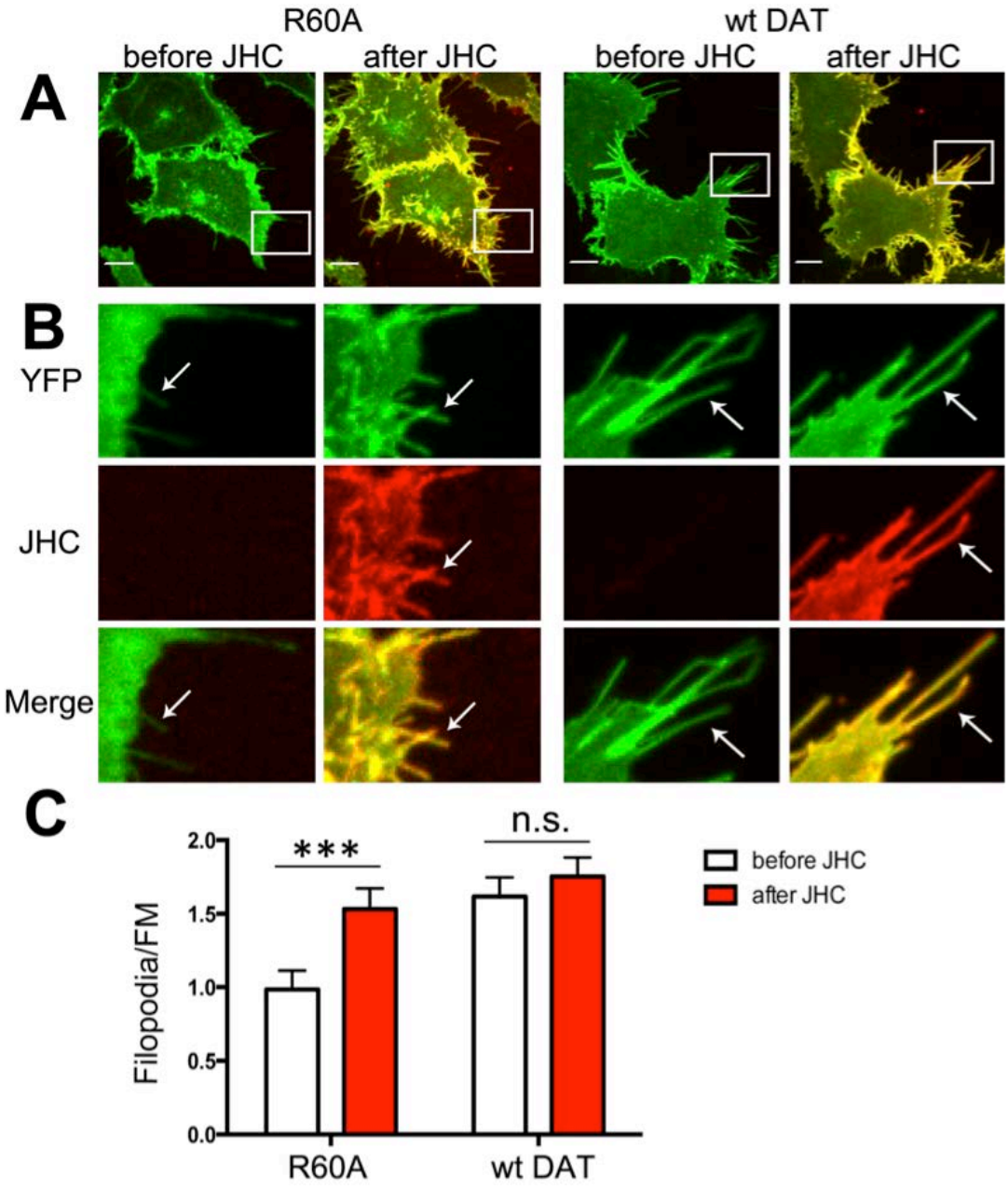

Figure 2.5. Binding of JHC1-64 increases the concentration of R60A in filopodia of HEK293 cells.

We further tested whether unlabeled cocaine, that has slightly lower binding affinity than JHC1-64 for DAT but is available for use in high concentrations allowing a maximum occupancy of surface DATs, would also cause the re-distribution of the R60A mutant toward filopodia. Cells transiently expressing wt YFP-HA-DAT, or its R60A and W63A mutants were incubated with 10 μM cocaine for 30 min at RT. Live-cell imaging was performed through the

515 nm (YFP, *green*) filter channel. Maximal z-projections of 5 consecutive x-y confocal planes are shown in Figure 2.6A. Figure 2.6B show the insets representing high magnification images of the regions marked by the white rectangle in Figure 2.6A. And the arrows point to representative filopodia. Consistent with the effects of JHC1-64 (Figure 2.5C), the filopodia/FM ratio in HEK293 cells expressing the R60A mutant increased by 60 % after cell incubation with cocaine, whereas the subcellular distribution of wt YFP-HA-DAT did not change (n=10) (Figure 2.6C). Similar results were observed in PAE cells where the filopodia/FM ratio of the R60A mutant increased by 70% after cocaine treatment (data not shown). Cocaine treatment did not result in increased targeting to filopodia of the W63A mutant that does not bind JHC1-64, confirming that elevated filopodial targeting of R60A was mediated by cocaine through its binding to this mutant transporter (Figure 2.6C).

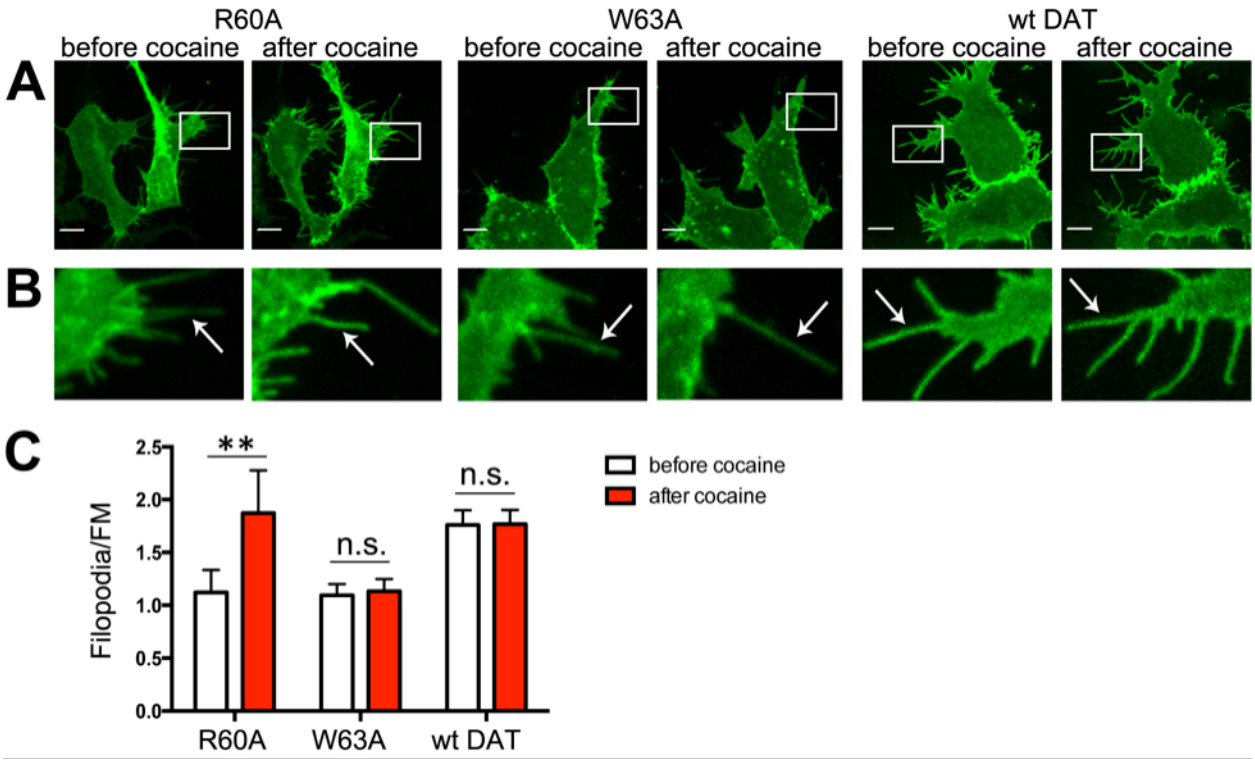

Figure 2.6. Binding of cocaine increases the concentration of R60A (but not W63A) in the filopodia of HEK293 cells.

We further examined the effect of cocaine on the filopodia targeting of DAT mutants using an independent quantitative imaging approach: YFP-HA-DAT or its mutants were co-expressed with wt RFP-HA-DAT in HEK293 cells, and the cells were imaged through 515 nm (YFP, *green*) and 561 nm (RFP, *red*) filter channels before and after cocaine treatment. This approach enabled direct comparison of the local densities and localization of wt (referred to YFP-HA-DAT and RFP-HA-DAT) and mutant DATs (YFP-HA-R60A and YFP-HA-W63A) in filopodia and FM regions in single cells imaged before and after cocaine incubation.

HEK293 cells co-expressing RFP-HA-DAT with YFP-HA-DAT, YFP-HA-R60A or YFP-HA-W63A were imaged before and after cocaine treatment (30 min at RT). Maximal z-projections of 5 consecutive x-y confocal planes are shown in Figure 2.7A. Insets representing high magnification images of the regions marked by the white rectangles in Figure 2.7A are shown in Figure 2.7B. Overall, YFP-tagged DATs were co-localized with RFP-HA-DAT in the images.

The filopodia/FM ratios of YFP and RFP fluorescence intensities in cells co-expressing RFP-HA-DAT with YFP-HA-R60A (Figure 2.7C), YFP-HA-W63A (Figure 2.7D) or wt YFP-HA-DAT (Figure 2.7E) were calculated as described in section **2.3.5**. The statistical difference between the ratios of individual cells before and after cocaine binding was analyzed using paired student t-test (n=10). The filopodia/FM ratio of the R60A mutant was increased upon binding of cocaine by ~2-fold (Figure 2.7C), whereas the filopodia/FM ratios of wt YFP-HA-DAT and the W63A mutant were not significantly changed (Figure 2.7D, E). The YFP/RFP ratio in filopodia was calculated and the statistical difference between the ratios of individual cells before and after cocaine binding was analyzed using paired student t-test (n=10). The results suggested that cocaine caused a relatively stronger enrichment of the R60A mutant than wt RFP-HA-DAT in

filopodia, whereas the YFP/RFP ratio in cells expressing YFP-HA-W63A and RFP-HA-DAT was not increased by cocaine (Figure 2.7F), consistent with the inability of W63A mutant to bind cocaine. The data in Figure 2.7 are in agreement with the results presented in Figure 2.5 and Figure 2.6, and altogether these measurements demonstrate that binding of either cocaine or its analog JHC1-64 favors localization of the R60A mutant to filopodia.

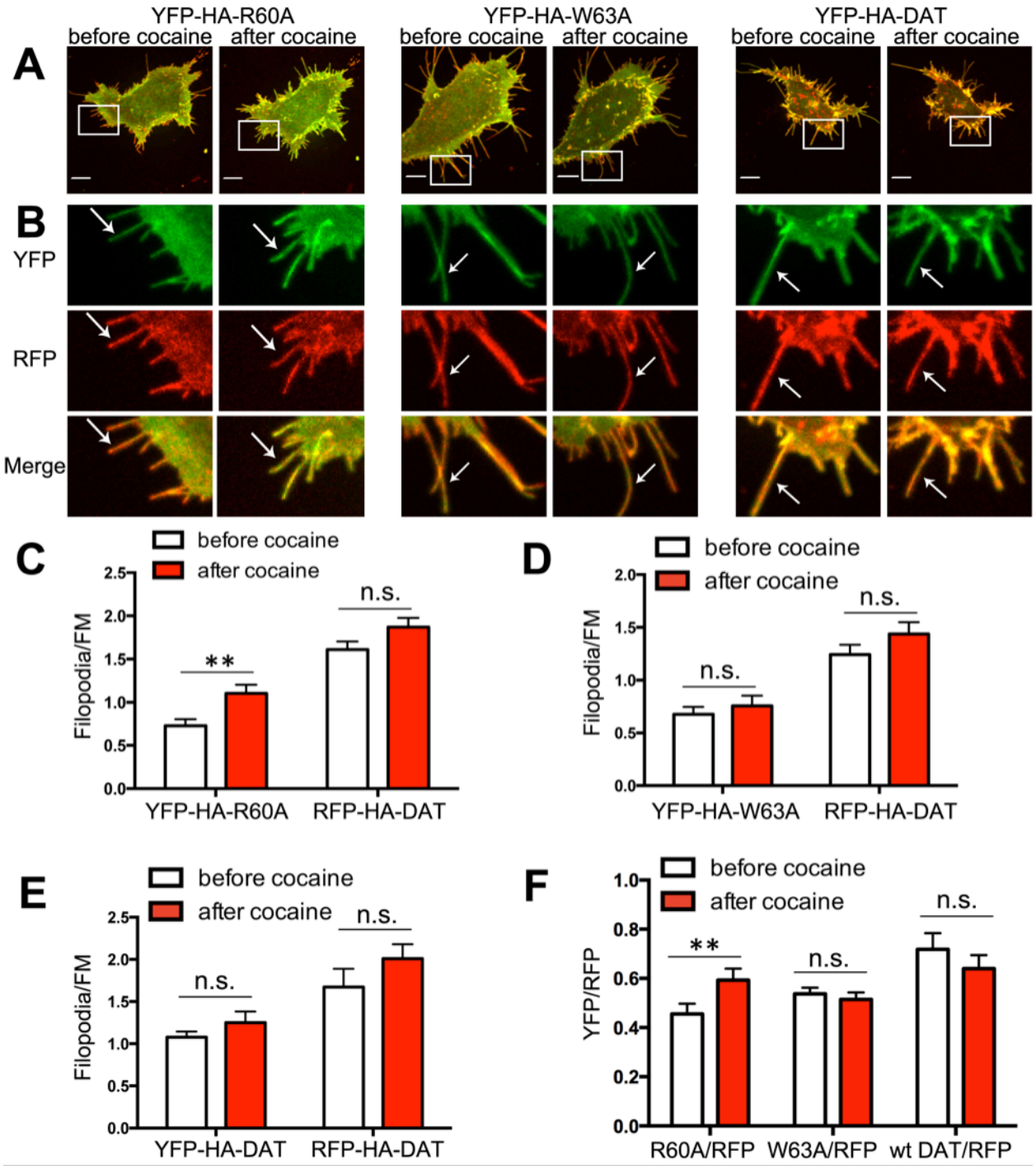

Figure 2.7. Binding of cocaine results in the enrichment of the R60A mutant in the filopodia of HEK293 cells relative to co-expressed wt DAT.

2.4.5 Modeling of the binding of cocaine and JHC1-64 to wt and mutant DAT (performed by Mary Cheng and Ivet Bahar)

To gain a mechanistic understanding of the effect of cocaine or JHC1-64 on the distribution of wt and mutant DATs on the plasma membrane (as demonstrated in Figures 2.4-2.7), a series of MD and docking simulations were performed by Mary Cheng and Ivet Bahar. MD simulations showed that the W63A mutant is stable in the IF state due to weakened interactions between the TM1a, TM5 and TM6b segments, while the weakening of the IC interactions in the R60A mutant was compensated via re-distribution of salt bridges. It suggests that wt DAT and the R60 mutant maintain their access to the OF state, while W63A does not (Figure 2.8A). In wt DAT, the salt-bridge R60-D436 and close interactions between W63 and F332 and Y335 stabilize the substrate/sodium-binding site in the OF state. In the mutant W63A, substitution of W63 by alanine breaks the stabilizing network of molecular interactions, leading to the opening of the IC vestibule. Substitution of R60 by alanine breaks the salt-bridge R60-D436. Yet, alternative IC salt bridges such as R260-E61 maintain the closed state of the IC vestibule. Docking simulations demonstrated that cocaine binds near the S1 site of R60A and the S1 and S2 sites of wt DAT (Figure 2.8B), whereas there is no cocaine binding inside the EC vestibule of W63A (data not shown), suggesting that binding of cocaine can stabilize the R60A mutant (but not the W63A mutant) in the OF state, similar to its action on the wt DAT (Chen et al 2000, Dehnes et al 2014). The predicted binding poses of JHC1-64 to DAT (Figure 2.8C) were comparable to those of cocaine in the OF state of DAT. Notably, JHC1-64 bound to both sites S1 (interacting with D79 at the lower portion of the EC vestibule) and S2 (at the upper portion of the EC vestibule). Like cocaine, JHC1-64 did not show any docking occupancy inside the EC vestibule of W63A (data not shown). On the other hand, JHC1-64 was able to bind deep inside the EC vestibule of the

R60A mutant (Figure 2.8C). These results were consistent with observations made in live-cell imaging experiments (Figure 2.4). Overall, the MD simulations and docking analysis predict that binding of cocaine or JHC1-64 stabilizes the OF conformation of both wt DAT and the R60A mutant.

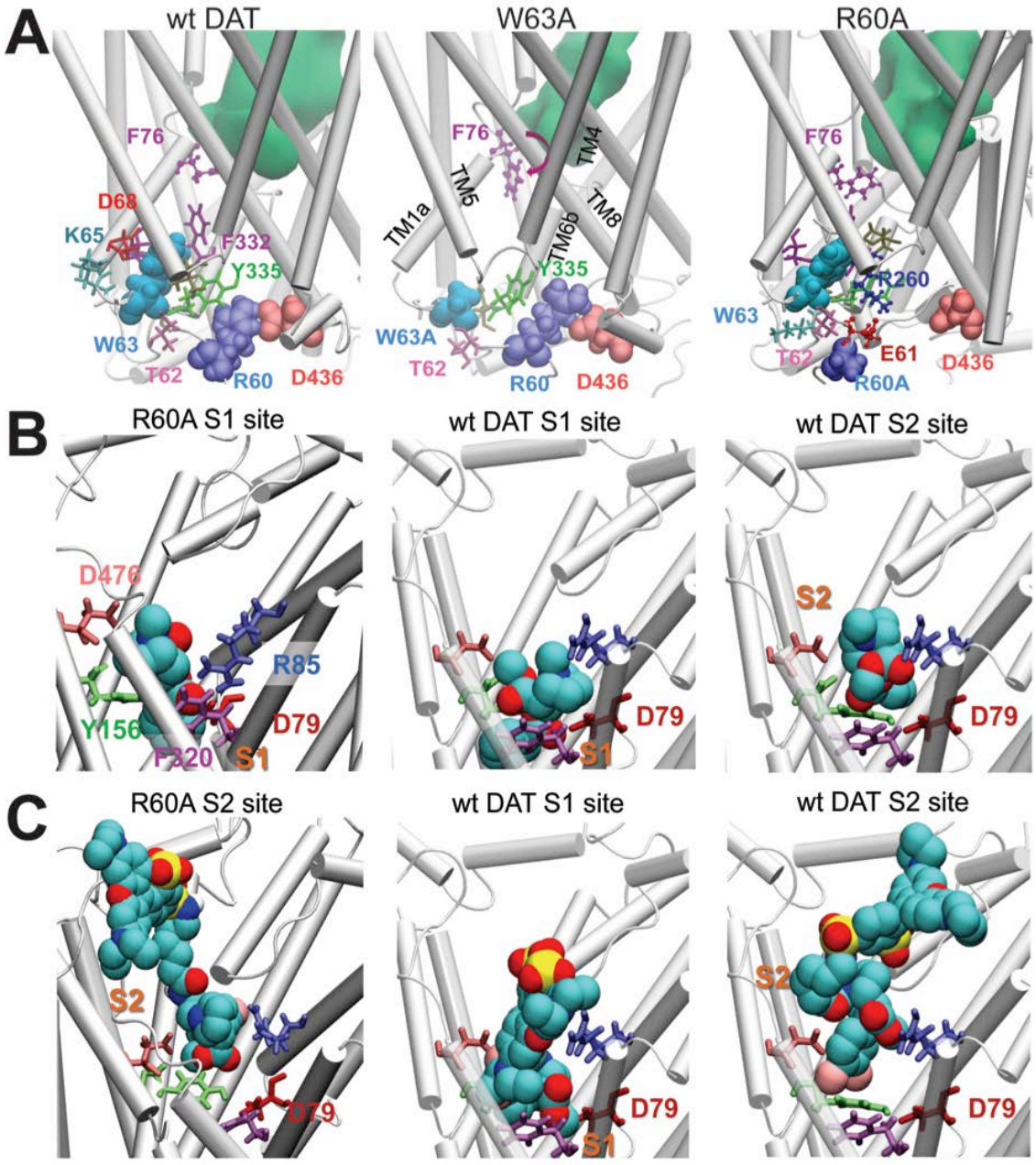

Figure 2.8. Cocaine and its analog bind to and stabilize the outward-facing (OF) state of the wt DAT and the R60A mutant (Mary Cheng, Bahar lab).

2.4.6 Zinc increases the concentration of R60A in filopodia

To test whether the stabilization of the OF state by means other than cocaine binding would drive R60A mutant DAT to filopodia, the effect of zinc on DAT localization was tested. Zinc binding to the EC residues in DAT (e.g. H193, D206, H375 and E396 in the EL2 and EL4 loops) has been reported to shift its conformational equilibrium towards the OF state (Loland et al 2002, Stockner et al 2013). Binding of zinc was shown to partially rescue the uptake activity of the R60A mutant, presumably, by stabilizing the OF conformation of this mutant (Kniazeff et al 2008). Therefore, we examined if zinc increased the concentration of the R60A mutant in filopodia. Because H193 was mutated to tyrosine in YFP-HA-DAT to incorporate the HA tag, these experiments were performed in wt and mutant YFP-DAT lacking the HA tag. HEK293 cells transiently expressing wt YFP-DAT or the YFP-DAT R60A mutant were imaged before and after incubation with 10 μM zinc chloride for 30 min at RT. Images were acquired through the 515 nm (YFP, *green*) filter channel. Maximal z-projections of 5 consecutive x-y confocal planes are shown in Figure 2.9A. The scale bars are 10 μm. Figure 2.9B show the insets represent high magnification images of the regions marked by the white rectangle in Figure 2.9A. The arrows point to examples of peripheral filopodia. The filopodia/FM ratios of YFP fluorescence intensities were quantified, and the statistical difference between the ratios of individual cells before and after zinc binding was analyzed using paired student t-test (n=10) (Figure 2.9C). The filopodia/FM ratio of YFP-R60A fluorescence increased by ~40% after zinc treatment, whereas this ratio did not change for wt YFP-DAT (Figure 2.9). These results provided cocaine-independent evidence that shifting an equilibrium of DAT conformational state towards the OF conformer increases the concentration of R60A in filopodia.

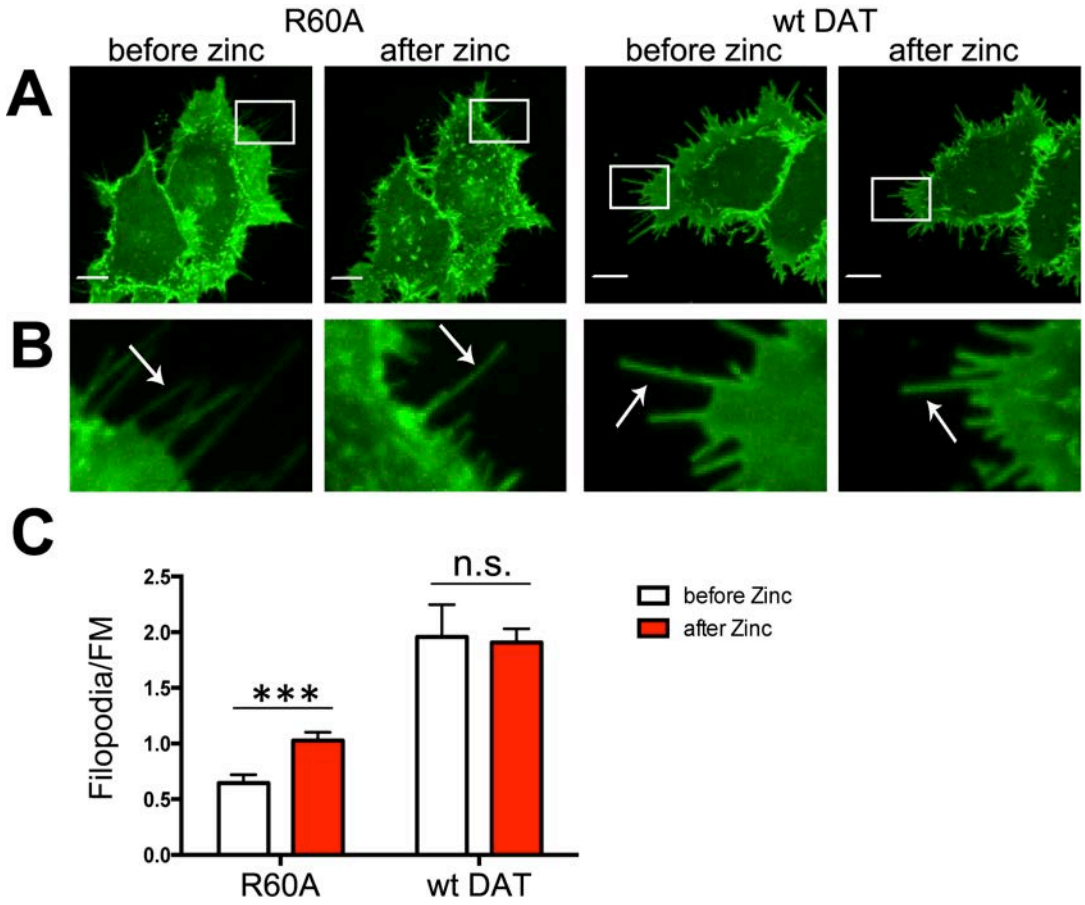

Figure 2.9. Binding of zinc increases the concentration of R60A in filopodia of HEK293 cells.

2.4.7 AMPH reduces DAT density in filopodia

In Figures 2.4-2.7 and 2.10, we demonstrated that stabilizing an OF state of the R60A mutant drives the enrichment of the mutant in the filopodia. To test whether the reverse change, i.e. an alteration in the conformation of wt DAT favoring an IF state, affects transporter redistribution in the plasma membrane in the opposite direction, HEK293 cells expressing YFP-HA-DAT were treated with AMPH. AMPH is transported by DAT into the cell where it activates signaling pathways leading to phosphorylation of the N-terminus of DAT, which in turn results in the reverse substrate transport activity of DAT (efflux) that has been attributed to a shift in the equilibrium distribution of DAT conformation towards its IF state (Cheng et al 2015, Fog et al

2006, Guptaroy et al 2011). To test the binding efficiency of JHC1-64 to DAT after AMPH treatment, HEK293 cells transiently expressing YFP-HA-DAT were treated with AMPH or vehicle (control) at 37 °C for 1 hr, followed by 10 min incubation of 100 nM JHC1-64 at RT. Images were acquired through 515 nm (YFP, green) and 561 nm (JHC1-64, red) filter channels. The ratio of JHC1-64 and YFP fluorescence intensities (JHC/YFP) was calculated for individual cells. The statistical difference between the ratios of cells with AMPH and vehicle treatment was analyzed using unpaired student t-test (n=5). The results showed that cells expressing YFP-HA-DAT that were treated with AMPH for 1 hour at 37 °C did not efficiently bind JHC1-64 as compared with the vehicle-treated cells (Figure 2.10A), indicating that the OF conformation of DAT was indeed disrupted after AMPH treatment.

To test whether AMPH treatment affects the distribution of DAT in filopodia, HEK293 cells transiently expressing YFP-HA-DAT were incubated with 10 μM AMPH or vehicle in KRH at 37°C for 30 min, and live-cell imaging was performed through 515 nm (YFP, *green*) filter channel. Maximal z-projections of 5 consecutive x-y confocal planes are shown in Figure 2.10B. The insets representing high magnification images of the regions marked by the white rectangle in Figure 2.10B are shown in Figure 2.10C. The arrows point to examples of peripheral filopodia. The statistical difference between the filopodia/FM fluorescence intensity ratios of individual cells before and after treatment was analyzed using paired student t-test (n=10) (Figure 2.10D). The fluorescence of YFP-HA-DAT in filopodia was decreased by the 30-min AMPH treatment at 37 °C (Figure 2.10B-D). These results further supported the close relationship between the stabilization of the OF state of DAT and its propensity to target DAT to filopodia.

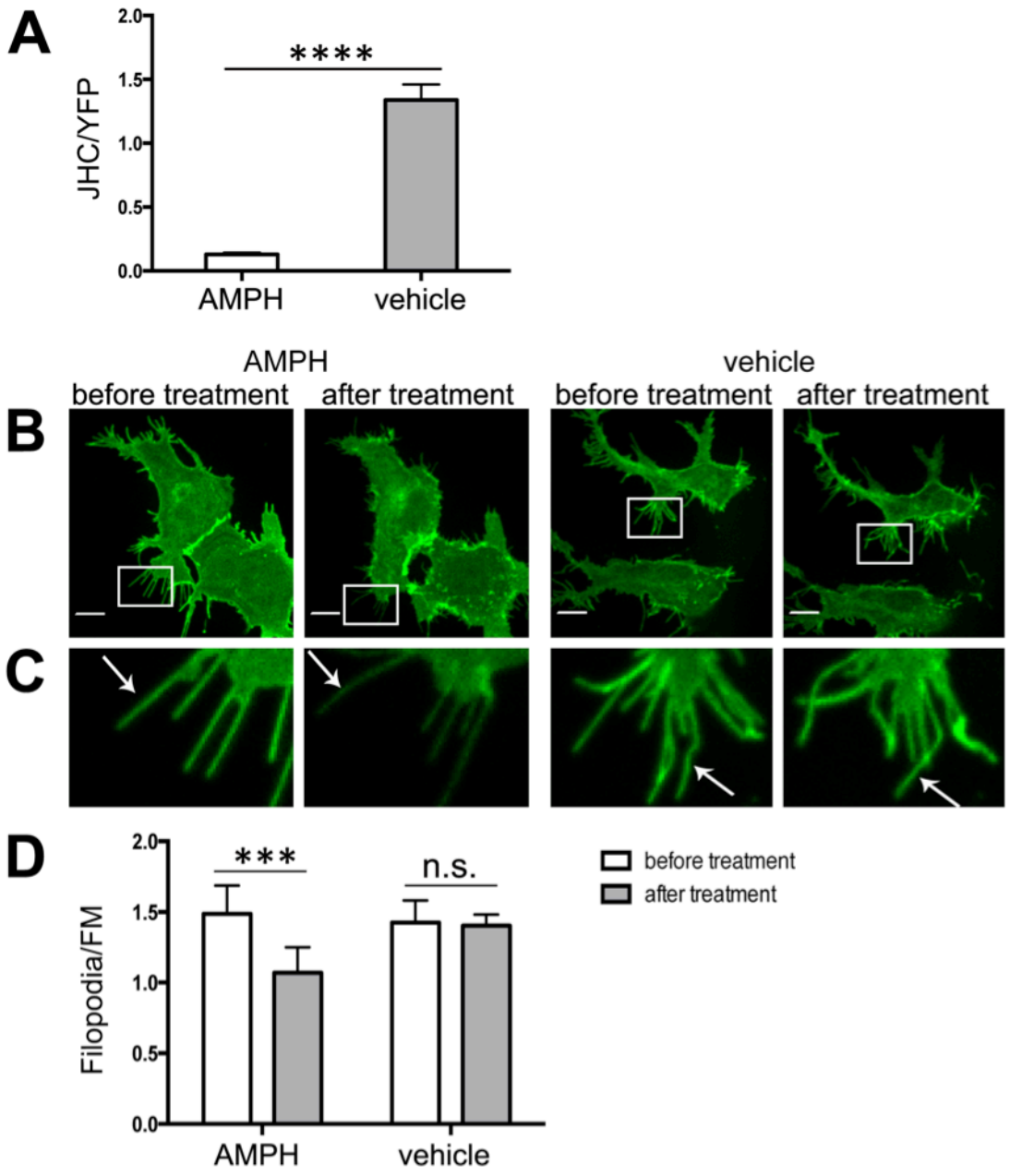

Figure 2.10. AMPH treatment reduces the concentration of wt DAT in the filopodia of HEK293 cells.

2.5 DISCUSSION

To study the mechanism for DAT targeting to filopodia, we utilized several approaches to control the conformational state of DAT molecules and performed quantitative live-cell imaging. We have demonstrated that 1) the OF state of DAT promotes its targeting to filopodia, and 2) heterologously overexpressed DAT may induce filopodia formation.

To study the mechanism of DAT accumulation in filopodia, we used the R60A mutant of DAT as the main experimental model. R60A does not transport substrate and is not concentrated in filopodia (Kniazeff et al 2008, Sorkina et al 2009), but unlike another non-functional DAT mutant, W63A, is capable of binding cocaine and its analogs. The ability of R60A to bind cocaine and its analogs was demonstrated using a fluorescent cocaine analog JHC1-64 (Figure 2.4) and by MD and docking simulations (Figures 2.8). Docking simulations also suggested that cocaine and JHC1-64 binding tends to stabilize the OF state of wt DAT or R60A, but not W63A (Figure 2.8). Importantly, binding of cocaine or its analog to R60A drives this mutant to filopodia, while the same compounds do not affect localization of the W63A mutant (Figures 2.5-2.7). Because there is no evidence that R60A and W63A mutations affect the interaction of DAT with other proteins, we assumed that the effects of these two mutations on substrate binding and filopodia localization are due to destabilized DAT molecule conformation, which is in agreement with previous reports (Chen et al 2001, Kniazeff et al 2008). However, mass-spectrometry studies should be performed to formally eliminate the possibility of altered interactions of R60A and W63A mutants as compared to wt DAT.

The prediction of the role of the OF DAT conformation in filopodia targeting was further supported by the observation of the increased targeting of R60A to filopodia by stabilizing the OF state of R60A by zinc binding (Figure 2.9). The molecular mechanisms of the zinc effect on

DAT conformation are not fully understood, although the hypothesis of "correcting" DAT conformation by zinc is supported by the rescue of the substrate uptake activity of the R60A mutant by zinc (Kniazeff et al 2008).

Interestingly, binding of cocaine or JHC1-64 did not change the distribution of wt DAT between non-filopodial and filopodia domains of the plasma membrane in our experiments (Figures 2.4-2.7). This result is consistent with the original studies where JHC1-64 did not change the surface expression and endocytosis of DAT (Eriksen et al 2009). It is possible that the bulk of the transporter is present in the OF state in the absence of substrates, and therefore, stabilizing the OF state by cocaine or JHC1-64 does not significantly increase the pool of the wt DAT OF conformer. Indeed, wt DAT is significantly enriched in filopodia, cell edges, and nanotubes at steady-state (Caltagarone et al 2015), and the data in Figure 2.4 show that JHC1-64-occupied wt DAT (OF state) is accumulated in these regions of the membrane with high curvature. On the other hand, it has been shown using cell surface biotinylation that cocaine increased the plasma membrane concentration of wt DAT (Kahlig & Galli 2003). Such up-regulation of surface DAT at the cell surface could be due to accumulation of cocaine-occupied DAT in filopodia, which serves in part to protect DAT from endocytosis (Sorkina et al 2009). It is possible that the magnitude of the effects of cocaine on the subcellular distribution of DAT is dependent on total cellular levels of DAT, and that uncovering such effects requires a highly sensitive DAT localization detection assay.

One can predict that cocaine may stabilize DAT at the surface of dopaminergic neurons, and possibly in juxtasynaptic membrane, leading to increased density of synapses in the striatum. However, long-term cocaine administration was shown to reduce the density of DA terminals in the striatum (Lee et al 2011). Such an effect is likely due to the oxidative stress caused by

increased extracellular DA in the presence of cocaine, or a homeostatic mechanism to maintain normal DA level.

Additional evidence in support of the hypothesis of the filopodial localization of the OF conformation of DAT was obtained using cell treatment with AMPH that decreased the density of wt DAT in filopodia (Figure 2.10). The molecular details of the AMPH effect on the DAT conformational state are not fully defined, although AMPH, like DA, is predicted to drive a structural transition toward the IF state of DAT (Cheng & Bahar 2015, Cheng et al 2015, Khelashvili et al 2015, Shan et al 2011). AMPH activates CaMKII, leading to phosphorylation of the N-terminus of DAT, which is proposed to alter DAT conformation in favor of substrate binding to the IC site and its reverse transport (efflux) (Fog et al 2006). Re-distribution of a pool of DAT from filopodia to the non-filopodial membrane by AMPH detected by quantitative image analysis is consistent with the observation of AMPH-induced DAT endocytosis (Saunders et al 2000, Wheeler et al 2015), given the surface-retention function of the filopodia localization of DAT (Sorkina et al 2009). Long-term AMPH administration also reduces DA terminal density, although it is likely due to the dopaminergic degeneration induced by increased extracellular DA levels (Cadet et al 2007).

Based on our previous observations and the findings in the present study, we propose a hypothetical model describing the regulation of DAT localization in the membrane by its molecular conformational state (Figure 2.11A). An atomic structure of DAT in the OF state shows that the TM core of the molecule has a concave shape with the diameter of the cytoplasmic interface of the core smaller than that of the EC interface (Penmatsa et al 2013). Therefore, the OF state of wt DAT and cocaine-bound R60A mutant are stabilized in outward-invaginated (convex-shaped) membranes such as filopodia (Figure 2.11A). When DAT

concentration is high, local membrane crowding by DAT molecules may induce outward bending of the membrane, thus initiating filopodia formation as shown in Figure 2.2. DAT mutants, in which mutations disrupt intramolecular interactions required to stabilize the OF conformation, or wt DAT with phosphorylated N-terminus, do not maintain a concave shape, and therefore have a lower propensity to occupy curved membranes and do not concentrate in filopodia. The OF conformer of wt DAT tends to accumulate in membrane regions with high curvature like filopodia and cell edges due to the convex shape of the OF conformer. AMPH shifts the equilibrium of DAT conformation towards an IF state and thus reduces DAT concentrations in filopodia. Non-functional DAT mutant R60A with disrupted OF conformation is not targeted to curved membranes. Binding of cocaine or zinc to R60A stabilizes its OF state and a convex shape, thus driving R60A to filopodia.

Figure 2.11B shows an illustration of a monomer (*green* ribbons) and a dimer (*orange* and *yellow* ribbons) embedded into filopodia (Provided by Mary Cheng in Bahar lab), indicating that the oligomerization of DAT tends to generate more curvature than monomer. Therefore, the oligomerization of DAT may be an additional factor in targeting DAT to the membrane regions with high curvature, as it could increase the “concaveness” in the DAT multimer. However, it is currently impossible to test the role of oligomerization in DAT filopodia targeting because the mechanism of DAT oligomerization is unknown, and DAT mutants that cannot be oligomerized are unfolded and unable to traffic to the plasma membrane (Sorkina et al 2003).

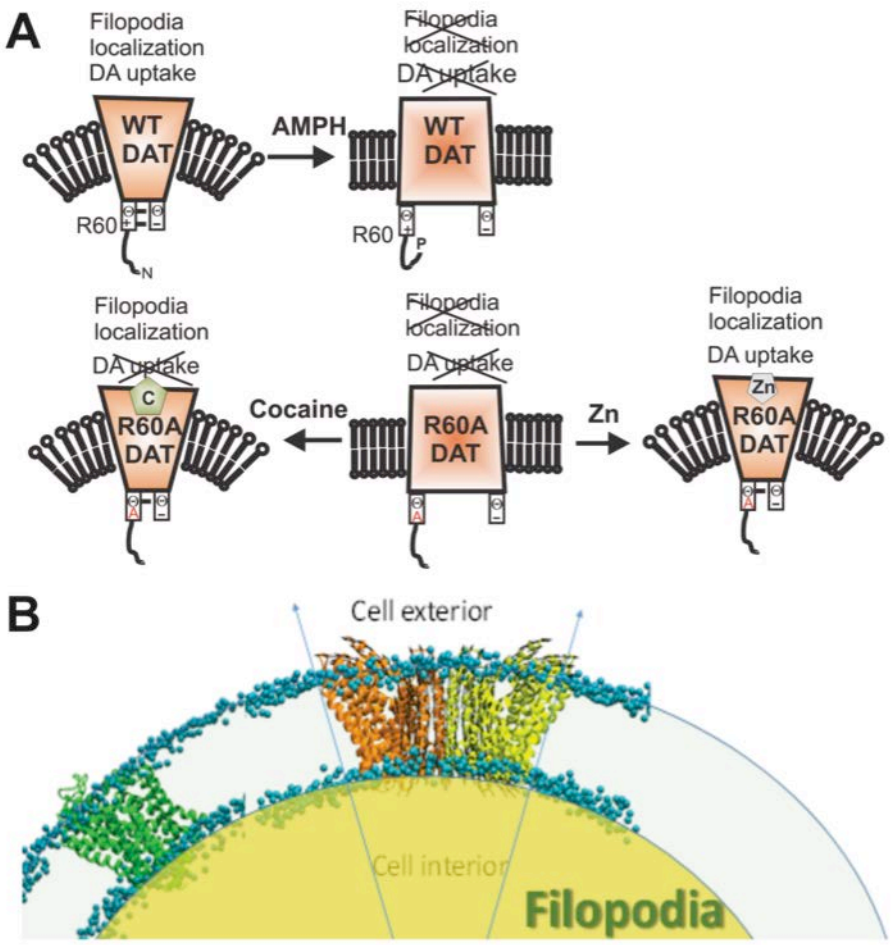

Figure 2.11. Hypothetical model of the regulation of DAT concentration in curved membranes by its conformation.

The increased number of filopodia in cells expressing high levels of YFP-HA-DAT is a surprising finding (Figure 2.2). This finding suggests that DAT may induce filopodia formation and/or maintain filopodia. It has been proposed that membrane bending by I-BAR domain proteins together with actin polymerization that regulated by Rho family small GTPases and I-BAR domain protein binding partners is involved in the initiation of filopodia formation (section **1.5**). We propose that membrane bending induced by transmembrane proteins with concave shapes may contribute to the initiation of filopodia. Similar observation of the filopodia-induced activity of a transmembrane protein, lipoprotein receptor-related protein (LRP), was reported (Chazaud et al 2002). We propose that high local concentrations of concave-shaped DAT may

promote outward membrane bending, which would in turn facilitate the recruitment of I-BAR proteins and their binding partners to negatively-curved membranes, thus allowing stabilization of forming membrane protrusions by growing actin filaments. DAT overexpression does not significantly change the length of filopodia in heterologous expression system in our experiments (data not shown), consistent with the hypothetic role of DAT in initiation but not maintenance of filopodia.

Certainly, targeting or filopodia-initiation capacity of DAT may also involve DAT interactions with actin-associated proteins or lipids enriched in filopodia. DAT and MyoX colocalize at the tips of filopodia, but MyoX knockdown does not fully diminish the ability of DAT to induce filopodia formation in heterologous expression system (Caltagarone et al 2015). Both DAT and MyoX can be detected in the growth cones of cultured dopaminergic neurons (Caltagarone et al 2015). Up to date, other filopodia-specific proteins has not been shown to interact with DAT. DAT interacts with phosphatidylinositol-4,5-bisphosphate (PIP_2), a lipid that is important for the formation of filopodia (section **1.5**). However, deletion of the putative PIP_2 binding site in the N-terminus of DAT (mutant Δ36 N-terminus) did not abolish the enrichment of DAT in filopodia (Sorkina et al 2009). Membrane cholesterol binds DAT and is proposed to stabilize DAT's outward-facing conformation (Hong & Amara 2010, Penmatsa et al 2013). We have used methyl-β-cyclodextrin (MβCD) (5-10 mM, 5-20 min treatment) to deplete membrane cholesterol in HEK293 cells. The MβCD treatment did not affect the concentration of wt YFP-HA-DAT to filopodia (data not shown), however, it may not eliminate cholesterol molecule that is bound to DAT while disrupting lipid rafts. In summary, MyoX may stabilize DAT localization in filopodia, but it is not necessary. Filopodial DAT interacts with lipids such as PIP_2 and cholesterol.

The ability of proteins with domains that have intrinsic convex or concave shapes to sense high-curvature membrane regions, concentrate in these regions, or contribute to membrane bending is well established (Jarsch et al 2016). For example, IRSp53 and MIM (described in section 1.5) initiate membrane bending during the formation of filopodia. Potassium channel KvAP has been demonstrated to be enriched in membrane nanotubes formed from giant unilamellar vesicles *in vitro* (Aimon et al 2014). The chemoreceptor TlpA oligomers of *Bacillus subtilis* are localized to highly curved membranes and this localization is affected when the convex shape of the receptor is disrupted by mutations (Strahl et al 2015). Assembly of ATP synthase dimer rows shapes the highly curved mitochondrial cristae of yeast (Davies et al 2012). The regulation of DAT submembrane distribution by its conformational states and their transitions presented in this study gives the first example of the regulation of the localization of mammalian multi-membrane spanning proteins by membrane curvature.

The concentration of DAT in dopaminergic neurons is difficult to quantify, and therefore, it is unclear whether endogenous DAT can promote membrane protrusions in neurons or it is simply concentrated in filopodia and other curved membranes. The width of mammalian filopodia is about 100-300 nm, which is similar to the width of axon shaft (Block et al 2015, Chéreau et al 2017). Based on our observations in cultured primary dopaminergic neurons using immunofluorescence microscopy, DAT is concentrated in axons, in particular, axonal varicosities, as compared to the somatodendritic region of the neuron (Block et al 2015). In cultured neurons, DAT is shown to be concentrated at the tips of filopodia-like protrusions along axons (Rao et al 2012). Although the multi-scale imaging of DAT knockout mice did not reveal any obvious morphological changes in dopaminergic neurons (Berlanga et al 2011), more detailed comparative imaging analysis of dopaminergic neurons in wt and DAT knockout mice

are necessary in order to determine whether DAT also plays a role in axonal growth, branching and synaptogenesis in developing dopaminergic neurons.

3.0 EFFECTS OF PIP_2 DEPLETION ON DAT LOCALIZATION AND ENDOCYTOSIS

3.1 ABSTRACT

Since DAT functions at the cell surface, endocytosis is a major regulator of DAT DA clearing activity. Other research groups and our laboratory have demonstrated that DAT is slowly constitutively endocytosed via clathrin-mediated endocytosis (CME) and clathrin-independent endocytosis (CIE) pathways, and that protein kinase C (PKC) activation results in accelerated clathrin-mediated endocytosis of DAT. Recently, it has been shown that phosphatidylinositol 4,5-bisphosphate (PIP_2), a phosphoinositide highly enriched in the plasma membrane, directly binds to the N-terminus of DAT through electrostatic interaction. The interaction of DAT with PIP_2 was proposed to regulate DAT activity and density in the plasma membrane, possibly by stabilizing DAT in the plasma membrane. We have combined the approach of inducible, targeted depletion of PIP_2 in the plasma membrane with a quantitative DAT endocytosis assay to directly examine the role of PIP_2 in the regulation of DAT endocytosis. These experiments demonstrated that depletion of PIP_2 did not affect DAT steady-state distribution in the cell, suggesting that DAT-PIP2 interaction does not play a significant role in DAT retention at the cell surface. By contrast, PIP_2 depletion inhibited PKC-dependent DAT endocytosis, consistent with the predominant role of the clathrin pathway in this endocytosis.

3.2 INTRODUCTION

Phosphatidylinositol 4,5-bisphosphate (PIP_2) is a minor phospholipid that is highly enriched in the plasma membrane. PIP_2 levels are controlled by kinases converting it from PI4P and dephophorylated by multiple PI5P phosphatases (Hammond et al 2012). PIP_2 can be hydrolyzed by phospholipase C (PLC) to produce diacylglycerol (DAG) and inositol 1,4,5-trisphosphate (IP_3). DAG stays on the plasma membrane to activate PKC, therefore initiating PKC-stimulated signaling cascades, while IP_3 enters the cytoplasm to activate its receptors. PIP_2 also acts as lipid binding partner to regulate the activity of membrane proteins such as the sodium-calcium exchanger (NCX1) and the ATP-sensitive KATP channel (Kir6.2/SUR2) (Suh & Hille 2005). Through direct binding, PIP_2 promotes the membrane insertion of many transporters and ion channels (Huang 2007). PIP_2 was shown to be necessary for recruitment of AP-2, epsin and dynamin to the plasma membrane, thus having an important role in initiating the assembly, stabilization and maturation of clathrin-coated pits and vesicles (Antonescu et al 2011). In addition, PIP_2 regulates proteins involved in initiating actin filament assembly and reinforcing membrane cytoskeletal linkage, and dissociates barbed end and capping proteins to promote actin polymerization (Zhang et al 2012). Because many CIE pathways are mediated by actin cytoskeleton, these pathways are also PIP_2-dependent.

It has been proposed that PIP_2 binds to amino acid residues 1-20 in the N-terminus of DAT through electrostatic interactions (Hamilton et al 2014). Mutation of both Lys3 and Lys5 to alanine disrupts DAT-PIP_2 interaction, suggesting that the positive charge of the N-terminus is critical for DAT-PIP_2 interaction. Using these mutations, it has been demonstrated that DAT-PIP_2 interaction is necessary for AMPH-induced reverse transport activity (efflux) of DAT (Hamilton et al 2014). Expression of the DAT K3A/K5A mutant in *Drosophila* dopamine

neurons does not affect locomotor activity but impairs AMPH-induced hyper-locomotion *in vivo* (Hamilton et al 2014). Computational modeling analysis predicts that PIP_2 regulates the spontaneous inward opening of DAT, which results in the release of an sodium ion from the sodium binding site of DAT, facilitating the uptake of DA (Khelashvili et al 2015).

Since PIP_2 interacts with the N-terminus of DAT, which is important for retaining/protecting DAT from endocytosis (Sorkina et al 2009), it is logical to test whether the N-terminus interaction with PIP_2 is important for stabilizing the surface level of DAT. In fact, it has been proposed that PIP_2 depletion enhances DAT endocytosis and reduces DA uptake activity (Fagan et al 2015). However, the approach of PIP_2 depletion used in the latter studies was not highly specific, therefore, long-term depletion of PIP_2 may result in pleiotropic cellular changes that are difficult to interpret also, as PIP_2 is involved in many signaling pathways. In the present study, we have optimized the combination of targeted, inducible depletion of PIP_2 in the plasma membrane with quantitative measurement of DAT endocytosis to examine the role of PIP_2 in regulating steady-state and PKC-stimulated traffic of DAT.

3.3 MATERIALS AND METHODS

3.3.1 Cell culture and transfections

HEK293 cells (Invitrogen, #R70507) were grown in DMEM containing 10% FBS. The plasmid HA-DAT with the HA epitope inserted in EL2 of DAT was described previously (Sorkina et al 2006). Lyn11-FRB (FKBP-rapamycin binding domain)-iRFP (Lyn11-FRB-iRFP), Lyn11-FRB-CPF, mRFP-FKBP (FK506 binding protein)-INPP5E (inositol polyphosphate-5-phosphatase E)

(mRFP-FKBP-INPP5E), BFP-FKBP-INPP5E, GFP-tagged PH (Pleckstrin Homology) domain of phospholipase C δ (GFP-PH-PLCδ) and YFP-PH-PLCδ were kindly provided by Dr. G. Hammond (University of Pittsburgh, Pittsburgh, PA). The Effectene method (Qiagen, Valencia, PA) was used for plasmid transfections. Cells were plated on poly-D-lysine-coated glass coverslips one day after transfection and used for experiments on the next day.

3.3.2 Endocytosis assay

The schematic strategy of the endocytosis assay using Fab fragment secondary antibodies is shown in Figure 3.1. HEK293 cells transiently expressing HA-DAT were incubated with mouse anti-HA11 antibodies (1:1000) at 37 °C for 1-2 h. The cells were then stained with anti-mouse antigen-binding (Fab) fragment antibody conjugated with Cy3 (Fab-Cy3) (1:400) at RT for 10 min (conditions of minimal DAT endocytosis), followed by treatment with rapamycin and/or the PKC activator phorbol 12-myristate 13-acetate (PMA) or vehicle in DMEM at 37 °C. Surface DAT with Fab-Cy3 may internalize, and some DAT localized to endosomes may recycle back to the plasma membrane. Cells were then incubated with an excess of anti-mouse Fab-Cy5 antibodies (1:100) at RT for 10 min to label surface DAT. Cells were fixed with freshly prepared 4% paraformaldehyde at RT for 15 min, and mounted in ProLong Gold (Invitrogen).

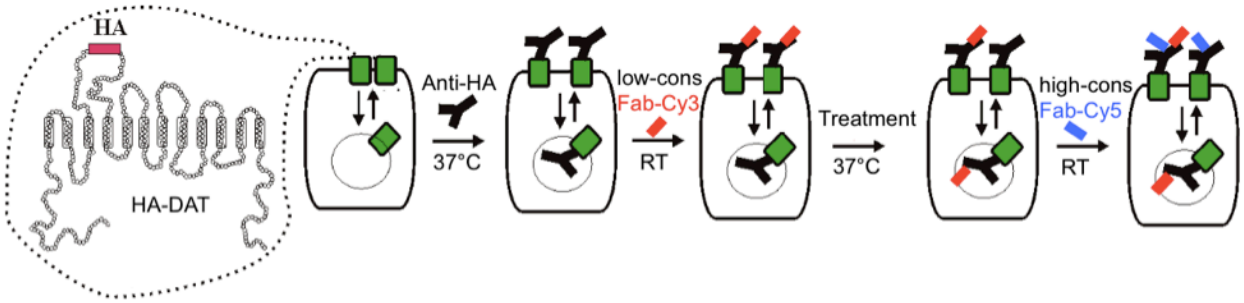

Figure 3.1. Schematic strategy of endocytosis assay.

3.3.3 Fluorescence microscopy and image analysis

The coverslips were placed onto the stage of the spinning disk confocal imaging system controlled by SlideBook software (Intelligent Imaging Innovation, Denver, CO) as described in **2.2.4**. To obtain high-resolution 3D images of the cells, a z-stack of 10-20 confocal images at 400 nm z-stepsize was acquired.

To quantify the relative amount of Cy5 (surface DAT) and Cy3 (internalized DAT) fluorescence in images obtained in the endocytosis assay, background-subtracted 3D images were segmented using the minimal intensities of Cy5 and Cy3 as low thresholds to obtain Mask1 and Mask2 corresponding to the surface and total DAT, respectively. The overlapping portions of Mask1 and Mask2 were used to generate Mask3 to measure Cy3-labeled surface DAT. Mask3 was subtracted from Mask2 to obtain corrected Cy3-labeled internalized DAT in Mask4. The integrated voxel intensity of Mask1 (Cy5) and Mask4 (Cy3) (in arbitrary linear units of fluorescence intensity) were quantitated, and the ratio of Mask4 to Mask1 integrated intensities (Internalized/surface DAT) was calculated in each image.

3.3.4 Statistical analysis

All data were analyzed using GraphPad Prism 6.0. Data normality of all data sets was confirmed using the D'Agostino-Pearson test. The statistical differences among each experimental groups were calculated using two-way ANOVA followed by Bonferroni's multiple comparisons (Figure 3.4B). F (1,36)=4.647, P=0.0379 (for the interaction of rapamycin treatment and PMA treatment in two-way ANOVA). Results are shown as mean ± S.E.M, n=10. *p<0.05, **p<0.01.

3.4 RESULTS

3.4.1 Rapid depletion of PIP_2 in the plasma membrane

Because PIP_2 is involved in multiple essential cellular processes, continuous depletion of PIP_2 from the plasma membrane results in significant general toxicity. A rapamycin-inducible strategy of rapid and organelle-targeted depletion of PIP_2 provides a controllable way to specifically reduce PIP_2 level in the plasma membrane (PM) (Varnai et al 2006). PIP_2 can be dephosphorylated to phosphatidylinositol 4-phosphate (PI4P) by inositol polyphosphate-5-phosphatase E (INPP5E). In the method, schematically depicted in Figure 3.2, cells are transfected with two plasmids, in which: 1) INPP5E is fused to FK506 binding protein (FKBP12) and mRFP (monomeric red fluorescent protein) (or BFP, blue fluorescent protein); and 2) a plasma membrane targeting sequence from Lyn tyrosine kinase (Lyn11) is fused to FKBP-rapamycin binding domain (FRB) and iRFP (near-infrared fluorescent protein) (or CFP, cyan fluorescent protein) (Hammond et al 2012). In addition, the localization of PIP_2 is detected

by fluorescent probes such as GFP (green fluorescent protein) (or YFP) fused to the Pleckstrin Homology (PH) domain of phospholipase C δ (PH-PLCδ) (Hammond et al 2014). As shown in Figure 3.3, before rapamycin treatment, FKBP-INPP5E locates in the cytosol and PH-PLCδ decorates the plasma membrane due to binding to PIP_2. Rapamycin induces the heterodimerization of FRB and FKBP12. Therefore, upon rapamycin treatment, FKBP-INPP5E translocates to the plasma membrane and converts PIP_2 to PI4P, resulting in the relocation of PH-PLCδ from the plasma membrane to the cytosol.

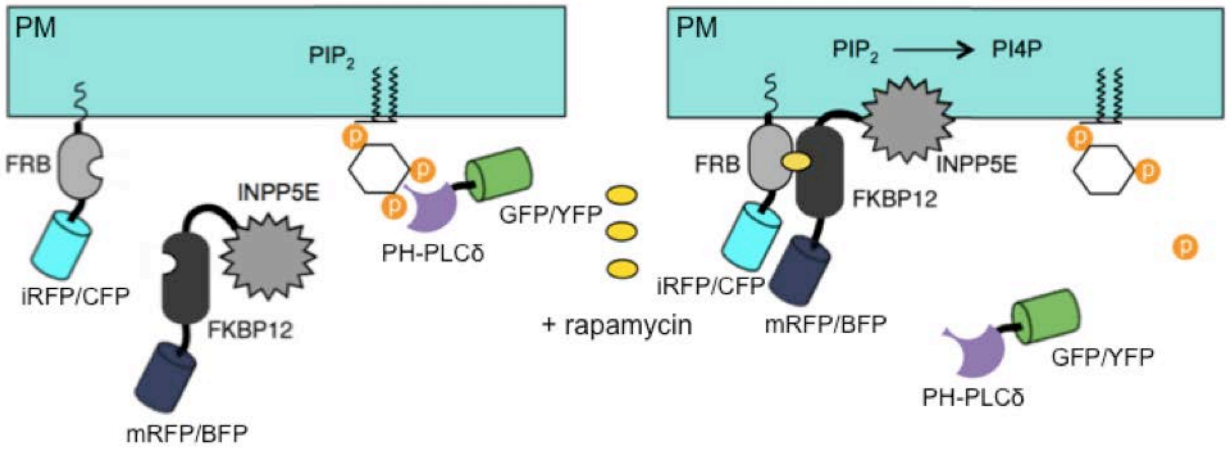

Figure 3.2. Strategy of rapamycin-induced PIP_2 depletion.

To test the this new approach, Lyn11-FRB-iRFP, mRFP-FKBP-INPP5E and GFP-PH-PLCδ were transiently co-expressed in HEK293 cells. Live cells were visualized by confocal microscopy before and after rapamycin (1μM) incubation for 5 min at RT through 488 nm (GFP), 561 nm (mRFP), and 640 nm (iRFP) filter channels. Representative images from one single z-plane are shown in Figure 3.3. The scale bars are 10 μm. After rapamycin treatment, a substantial amount of mRFP-FKBP-INPP5E translocated from the cytosol to the plasma membrane, whereas a bulk of GFP-PH-PLCδ translocated from the plasma membrane to the cytosol, indicating that PIP_2 was depleted from the plasma membrane. The depletion (as measured by membrane-associated sensor protein) was typically not complete after 5 min

rapamycin treatment, likely, because of insufficient mRFP-FKBP-INPP5E recruitment to the membrane. Incubations of 5-30 min with rapamycin resulted in a more efficient PIP_2 depletion, though longer incubations caused visible general toxicity in some cells.

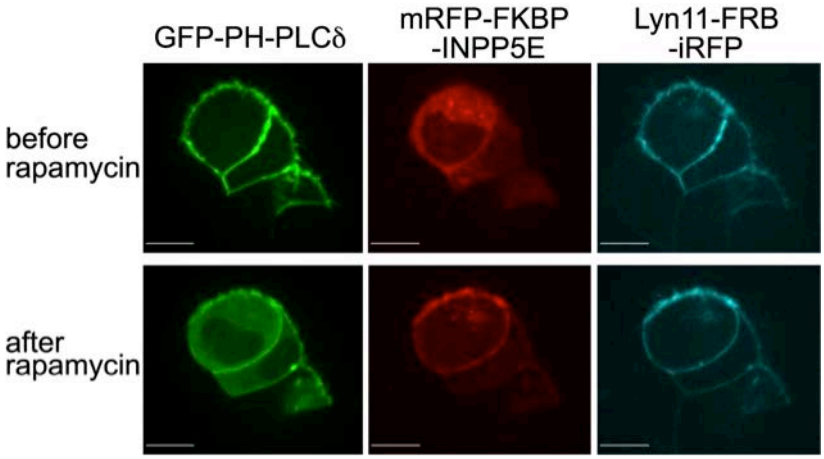

Figure 3.3. Rapamycin-induced PIP_2 depletion from the plasma membrane in HEK293 cells.

3.4.2 Plasma membrane PIP_2 depletion blocks PKC-stimulated DAT endocytosis

Establishing experimental conditions of targeted PIP_2 depletion allowed us to examine the role of PIP_2 in constitutive and PKC-stimulated DAT endocytosis. We performed our endocytosis assay in HEK293 cells with the transient co-transfection of four plasmids: HA-DAT, Lyn11-FRB-CFP, BFP-FKBP-INPP5E and YFP-PH-PLCδ. After labeling surface HA-DAT with the HA11 antibody and sequential incubation with Fab-Cy3 (see section **3.3.2**), the cells were incubated with DMSO (vehicle control) or rapamycin (1 μM) for 5 min at RT. Cells were then incubated with PMA (1 μM) or DMSO for 30 min at 37°C in the same medium, followed by short exposure to Fab-Cy5 (10 min at RT) to label HA-DAT complexes remaining on the cell surface, and fixed. Images were acquired through 515 nm (YFP, *green*), 561 nm (Cy3, *red*) and 640 nm (Cy5, *blue*) filter channels. Cells with cytosolic YFP-PH-PLCδ were identified as cells with PIP_2

depletion and used for quantitation of Cy3/Cy5 ratios. Representative images of single z-planes are shown in Figure 3.4A. The arrows point to examples of DAT endosomes (Cy3, no Cy5). The scale bars are10 μm.

As shown in Figure 3.4A, a few vesicles containing internalized HA-DAT (labeled by Cy3 but not Cy5) were detected in vehicle treated cells (no PMA). The amount of endosomal HA-DAT was significantly increased upon PMA treatment. Cells in which most YFP-PH-PLCδ was translocated from the plasma membrane to the cytosol were selected for quantification of the extent of HA-DAT endocytosis. The quantitation of internalized/surface DAT ratios is shown in Figure 3.4B (n=10). It appears that PIP_2 depletion does not affect the amount of endosomal (Cy3-labeled) HA-DAT in vehicle-treated cells, indicating that PIP_2 depletion does not affect steady-state of internalized DAT. By contrast, PKC-stimulated endocytosis of HA-DAT was inhibited by PIP_2 depletion, as evident by the reduced number of Cy3-labeled HA-DAT vesicles in the presence of rapamycin (Fig. 3,4A), which is confirmed by quantitation (Fig. 3.4B). These experiments demonstrated that PIP_2 depletion inhibits PKC-stimulated but not constitutive DAT trafficking.

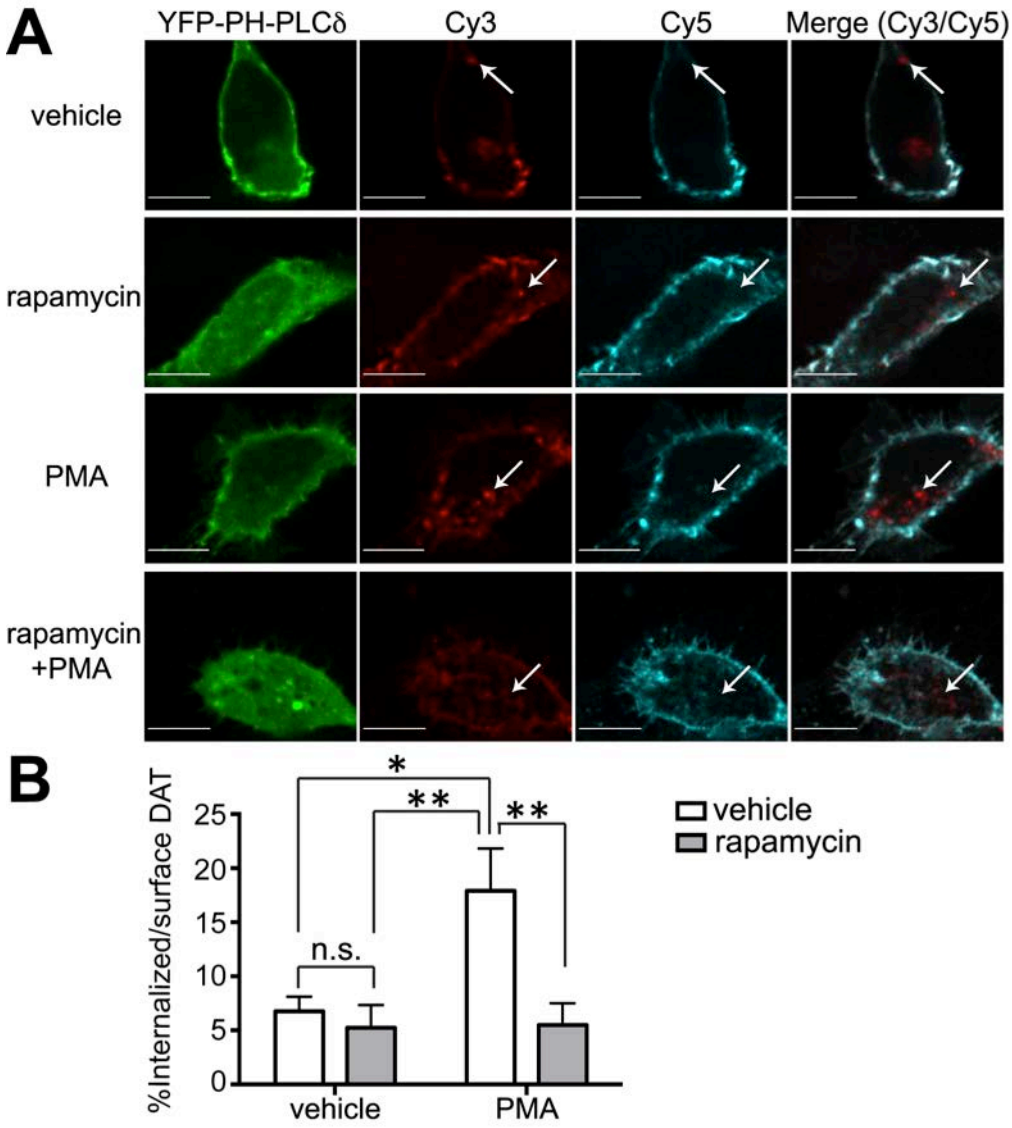

Figure 3.4. PIP_2 depletion inhibits PKC-stimulated DAT endocytosis.

3.5 DISCUSSION

In this study, we have combined rapamycin-induced membrane PIP_2 depletion and optimized endocytosis assay using Fab fragment antibodies, which are capable to enter live cells, to quantitatively study the role of PIP_2 in constitutive versus PKC-stimulated DAT endocytosis.

This method required simultaneous high levels of co-expression four proteins. We have been able to achieve this only in HEK293 cells.

The observation that PIP_2 depletion blocked PKC-stimulated endocytosis of DAT in our experiments provides an important positive control to our approach. Indeed, it has been shown that PKC-induced DAT endocytosis is clathrin-dependent (Daniels & Amara 1999, Sorkina et al 2005, Sorkina et al 2006). Thus, our experiments confirm this notion, and also confirm the role of PIP_2 in CME using DAT as an endocytic cargo. Plasma membrane PIP_2 depletion has been shown to result in significant loss of CCPs and disruption of CME (Zoncu et al 2007). In fact, in our control experiments, PIP_2 depletion substantially inhibited endocytosis of transferrin-TexasRed, a classical marker of CME (Hansen et al 1993) (data not shown).

PIP_2 depletion did not result in increased accumulation of DAT in endosomes in the absence of stimuli, suggesting that this depletion did not increase constitutive endocytosis or decreased constitutive recycling of DAT in HEK293 cells (Figure 3.4). This result is inconsistent with the report where Dr. Melikian and co-workers have proposed that PIP_2 is involved in the retention of DAT at the cell surface (Fagan et al 2015). According to their model that PIP_2 depletion inactivates the kinase activated by Cdc42 kinase (Ack1), which maintains DAT surface level by preventing DAT endocytosis (Shen et al 2011, Wu et al 2015). Cdc42 activates Ack1, that negatively regulates basal DAT endocytic rate (Wu et al 2015).

Our experiments also revealed no statistically significant decrease constitutive DAT endocytosis upon membrane PIP_2 depletion, suggesting that blockade of clathrin-dependent endocytosis by membrane PIP_2 depletion does not affect constitutive DAT endocytosis in HEK293 cells. It seems to be counteractive to our previous conclusion that both constitutive and PKC-stimulated DAT endocytosis are at least partially dependent on clathrin in PAE cells

(Sorkina et al 2005). The latter results were obtained using monensin treatment, which resulted in constitutive accumulation of internalized DAT in endosomes due to the blockade of DAT recycling. However, similar effect of monensin treatment was not statistically significant in HEK293 cells. Therefore, constitutive internalization rates could not be directly measured in these cells, because the Cy3/Cy5 ratio measured in HEK293 cells (Fig. 3.4B) is the sum of recycling and internalization rates.

It has been suggested that constitutive DAT internalization is mediated by a dynamin-independent and clathrin-independent endocytosis pathway in SK-N-MC cells using dynamin/clathrin inhibitors (Gabriel et al 2013). Notably, the clathrin inhibitor pitstop blocks both CME and CIE. It is possible that the mechanisms controlling constitutive DAT endocytosis are different in different cell types (Loder & Melikian 2003). There is a possibility that constitutive DAT endocytosis is not dependent on clathrin in HEK293 cells, or that the reduced clathrin-dependent DAT endocytosis is compensated by clathrin-independent DAT endocytosis induced by PIP_2 depletion.

Understanding the mechanisms controlling DAT trafficking in neurons is the most important problem when studying the role of PIP_2 regulation in DAT endocytosis. However, targeted depletion of PIP_2 is not feasible in dopaminergic neurons at this time. Our results in HEK293 cells indicate that PIP_2 is not involved in the retention of DAT in the plasma membrane, whereas it is possible that PIP_2 regulates DAT endocytosis. Interestingly, knockout of synaptojanin (PIP_2 phosphatase) had strong effects on DAT localization in mouse brain (Cao et al 2017), suggesting that DAT is indeed regulated by PIP_2 mediated trafficking.

4.0 IDENTIFICATION OF PROTEINS INTERACTING WITH DAT IN MOUSE STRIATUM

4.1 ABSTRACT

The function of DAT may be regulated by its interaction with other proteins. To identify DAT interacting proteins, we immunoprecipitated HA-DAT from synaptosomes isolated from mouse striatum and performed quantitative mass spectrometry proteomic analysis of immunoprecipitates. Differential mass-spectrometry (dMS) analysis revealed the specific co-immunoprecipitation of several proteins with DAT, including previously identified DAT interactors and novel putative interactors. We focused our follow-up analysis on one of the putative DAT interactors, Gαo, the α subunit of Go heterotrimeric proteins, because it is coupled to the D2 auto-receptor (D2R), expressed in dopaminergic neurons and a known regulator of DAT. In subsequent experiments we demonstrated that Gαo is partially co-localized with DAT in primary cultured mesencephalic postnatal dopaminergic neurons. Reciprocal co-immunoprecipitation followed by western blotting confirmed the interaction between DAT and Gαo in mouse brain striatum and HEK293 cells in which tagged DAT and Gαo were transiently expressed. These experiments revealed new DAT interactions, which may underlie novel mechanisms of DAT regulation by GPCR signaling.

4.2 INTRODUCTION

As discussed in section **1.4**, despite multiple attempts to define DAT interactome and its functional role, most reported interactions remain poorly characterized and not confirmed by more than one published study. With the development of truly quantitative methods of proteomics analysis of unlabeled samples, such as dMS (Wiener et al 2004), it has become possible to re-visit this research direction and perform careful analysis of proteins interacting with DAT in the mouse brain. This analysis is described below and points on the potential importance of DAT regulation by D2 receptors.

Multiple studies indicate that DAT dynamics are regulated by D2 GPCR signaling. It has been demonstrated that activation of presynaptic D2R (the short form) increases DAT surface expression and function (Gulley & Zahniser 2003). D2R agonists enhance DAT uptake activity by increasing the surface expression of DAT in HEK cells and *Xenopus laevis* oocytes (Bolan et al 2007, Mayfield & Zahniser 2001). Conversely, knockout mice lacking presynaptic D2R exhibit decreased DAT uptake activity (Dickinson et al 1999). Similarly, treatment with D2R antagonist also results in decreased DA clearance rate (Dickinson et al 1999). The Gi/o inhibitor pertussis toxin (PTX) prevents the increase of DAT surface expression and its DA uptake activity that is induced by D2R activation (Bolan et al 2007, Mayfield & Zahniser 2001). The increase in DAT function by presynaptic D2R activation can be utilized to rescue decreased DA uptake in hypoinsulinemia (Sevak et al 2007). However, signal transduction mechanisms involved in D2R regulation of the DAT activity are unclear.

D2R predominantly couples to Go proteins in the human central nervous system (Jiang et al 2001). Upon D2R activation, Gαo, the alpha subunit of Go proteins, is released from the heterotrimeric Go protein complex and binds to its downstream effectors. Gαo is widely

expressed in the CNS. Mice with Gαo knockout display multiple neural abnormalities (Jiang & Bajpayee 2009). Because we have identified Gαo-DAT interaction in mouse striatum, we hypothesize that Gαo directly interacts with DAT, and have begun to investigate the mechanism and functional role of this putative interaction.

4.3 MATERIALS AND METHODS

4.3.1 Reagents

Antibodies were purchased from the following sources: monoclonal mouse anti-HA11 antibody was from Covance (Berkley, CA); monoclonal rat anti-DAT and polyclonal rabbit anti-Gαo antibodies were from EMD Millipore (Billerica, MA); rabbit anti-α-actinin antibody was from Cell Signaling Technology (Danvers, MA); donkey anti-mouse and anti-rabbit antibodies conjugated with Cy5 or Cy3 were from Jackson Immuno Research (West Grove, PA). Yellow fluorescent protein (YFP)- and HA-tagged human DAT (YFP-HA-DAT) was described previously (Sorkina et al 2009). Human Gαo sequence cloned into pcDNA 3.1+ vector was purchased from Invitrogen (Carlsbad, CA). Protein G-Sepharose was purchased from Invitrogen. Paraformaldehyde was purchased from Electron Microscopy Sciences (Hatfield, PA). Cell culture reagents were purchased from Invitrogen. All other chemicals were from Sigma-Aldrich (St. Louis, MO) unless otherwise specified.

4.3.2 Striatal synaptosome preparation and immunoprecipitation (IP)

Twelve 8-week HA-DAT knock-in mice with hemagglutinin epitope inserted into the second loop of DAT (Rao et al 2012) were euthanized and decapitated. Brains were quickly removed and rinsed in ice-cold Gey's balanced salt solution with 10 mM D-glucose. Striatal tissue was collected from the brain and placed in a glass homogenizer with ice-cold 5 mM HEPES (with 0.32 M sucrose, pH 7.4, 1 ml for 45-50 mgs striatal tissue from one brain), followed by homogenization. The homogenate was centrifuged at 1,000 g for 10 min at 4 °C, and the resulting supernatant was transferred to a new tube and centrifuged at 12,500 g for 20 min at 4°C to isolate synaptosomes in the pellet.

Synaptosomes were re-suspended in freshly prepared TGH lysis buffer (1% Triton X-100, 10% glycerol, 25 mM HEPES, 1 mM EDTA, 1 mM EGTA, 1 mM sodium orthovanadate, 10 mM sodium fluoride, 1 mM PMSF, 10 g/ml leupeptine, 10 g/ml aprotinin, 100 M iodacetamide) for 20 min at 4 °C. Lysed synaptosomes were centrifuged at 100,000 g for 20 min at 4 °C. The supernatants were incubated with 10 μg rat anti-DAT antibodies (6 tubes) or 10 μg rat IgG antibodies (6 tubes) for 3 h at 4 °C. The supernatants were further incubated with protein G-Sepharose for 1 h, and centrifuged at 12,500 g for 4 min at 4 °C to precipitate the protein G-Sepharose. The protein G-Sepharose was washed with TGH buffer three times.

Protein-G beads were boiled with 1x NuPAGE® LDS sample buffer containing 100 mM DTT and separated by SDS-PAGE for analysis by mass spectrometry.

4.3.3 Dopaminergic neuronal cultures

Primary mesencephalic postnatal cultures were prepared from HA-DAT knock-in mice. The procedures were developed from our previous experiments (Rao et al 2011). Five to six mice pups aged P0-P3 were euthanized and decapitated. Brains were quickly removed and rinsed in ice-cold Gey's balanced salt solution with freshly added 10 mM D-glucose. Coronal sections were taken and the mesencephalic dopamine region was dissected and placed in ice-cold Gey's balanced salt solution with 10 mM D-glucose. After the dissection, midbrain tissue was placed in papain solution from the Papain Dissociation System Kit (Worthington, Lakewood, NJ). Tissue was dissociated following the kit protocol. Cells were suspended in feeding media made from Basal Medium Eagle with 4% fetal bovine solution (HyClone, Logan, UT), 1× B27 (Thermo Fisher Scientific, Pittsburgh, PA), 12.5 mM D-Glucose, 10 mM HEPES, 1 mM Sodium Pyruvate, 2 mM L-Glutamine, 40 Units/ml Penicillin and 100 µg/ml Streptomycin. About 150,000 cells were plated onto 18 mm diameter glass coverslips coated with poly-D-lysine and laminin (neuVitro, Vancouver, WA) in 1 ml feeding media. Neurons were cultured in an incubator containing 5% CO_2. 0.5 ml of feeding media was added to each coverslip to replace half the medium every other day.

4.3.4 Fluorescence microscopy

At days *in vitro* (DIV) 6-10, neurons were washed with CMPBS (DPBS plus 1 mM $CaCl_2$, 0.5 mM $MgCl_2$ and 5 mM D-glucose) and fixed with freshly made 4% paraformaldehyde (PFA) in CMPBS for 15 min at room temperature. Neurons were permeabilized with 0.1% Triton X-100 in CMPBS with 0.5% bovine serum albumin (BSA) for 5 min. Neurons were washed in CMPBS

with 0.5% BSA, and incubated with primary mouse anti-HA11 antibody (1:1000) and rabbit anti-Gαo antibody (1:500) for 1 h at room temperature, followed by 3X washes with CMPBS containing 0.5% BSA. Neurons were then incubated with secondary Cy3 anti-mouse and Cy5 anti-rabbit antibodies for 1 h, followed by 3X washes with CMPBS containing 0.5% BSA. The coverslips were mounted in ProLong Gold (Invitrogen) and dried overnight for use.

Neurons were imaged through 561 nm (Cy3) and 640 nm (Cy5) filter channels using our spinning disk confocal imaging system controlled by SlideBook software. A z-stack of 20 confocal images at 400 nm z-step size was acquired under the 63× oil immersion objective lens with a 50-100 ms exposure time.

4.3.5 Cell culture and transfections

HEK293T cells were purchased from American Type Cell Culture Collections (Manassas, VA). Cells were grown in DMEM containing 10% FBS. The cells were transiently transfected with YFP-HA-DAT and Gαo using Effectene kits (Qiagen, Valencia, CA) following the kit protocol. Cells were plated in 100 mm dishes to grow, and used 2 days after transfection.

4.3.6 Cross-linking enhanced immunoprecipitation (IP) and western blotting

HEK293 cells were incubated with 1 mM dithiobis(succinimidyl propionate) (DSP, Thermo Fisher Scientific, Pittsburgh, PA) in HBSS buffer (with 1.26 mM $CaCl_2$, 0.5 mM $MgCl_2$, 0.4 mM $MgSO_4$, 5 mM D-Glucose) for 10 min at 37 °C. Cross-linking was terminated with 20 mM Tris-HCl, pH 7.0 at RT for 5 min (Zhang et al 2007). Cells were washed three times in ice-cold PBS, and lysed in freshly prepared TGH lysis buffer (1% Triton X-100, 10% glycerol, 25 mM HEPES,

1 mM EDTA, 1 mM EGTA, 1 mM sodium orthovanadate, 10 mM sodium fluoride, 1 mM PMSF, 10μg/ml leupeptine, 10 μg/ml aprotinin, 100 μM iodacetamide) for 20 min at 4 °C.

For mouse brain immunoprecipitation, tissue was collected from the brain striatum and was lysed in freshly prepared TGH lysis buffer.

Cell/tissue lysates were rotated at 4 °C for 1 h and centrifuged at 100,000 g for 20 min at 4 °C. The supernatants were incubated with antibodies and kept rotating overnight at 4 °C. Protein G-Sepharose was added to the supernatants the following day. After a one-hour incubation, Protein G-Sepharose was precipitated and washed three times with TGH buffer (1% Triton X-100, 10% glycerol and 25 mM HEPES). For cells with DSP treatment, the protein G-Sepharose was washed once with TGH buffer containing 500 mM sodium chloride, and then washed twice with regular TGH buffer.

Ten-percent aliquots of cell/tissue lysates and immunoprecipitates were denatured in sample buffer at 95°C, resolved by 10% SDS-PAGE and transferred to nitrocellulose. Blots were probed with primary antibodies at 4 °C overnight. Secondary antibodies conjugated to far-red fluorescent dyes (IRDye-680 and 800) were applied the following day. Signal was detected using an Odyssey Li-COR system.

4.4 RESULTS

4.4.1 Gαo is a putative DAT interacting partner identified by MS

To identify DAT interactors, we performed high-resolution MS analysis of the proteins pulled down from mouse striatum synaptosomes using antibodies against DAT or the same amount of

control non-specific antibodies. Dr. Xuemei Zeng from BioMS center performed the MS experiments. A total of 137 897 molecular features, including 5016 features for 1264 peptides from 363 proteins, were quantified using liquid chromatography mass spectrometry (LC-MS). Statistical analysis yielded seven putative DAT interactors, with at least half of their identified peptides being significantly more abundant in DAT IP samples than in control samples (Unpaired student's t test p value < 0.05), including Gαo (Gao1), plasma membrane calcium-transporting ATPase (PMCA, Atp2b1), reticulon (Rtn1), excitatory amino acid transporter (EAAT, Slc1a2), mitochondrial glutamate carrier (GC, Slc25a22), synaptic vesicle glycoprotein 2A (SV2A, Sv2a), and synaptogyrin-3 (Syngr3). The relative intensities of DAT (Slc6a3) and seven putative DAT interactors in IP samples pulled down using DAT antibodies (*red*) and non-specific antibodies (*green*) are shown in Figure 4.1.

Among seven putative DAT interacting proteins identified from MS analysis, the synaptic vesicle protein synaptogyrin-3 has been shown to interact with the recombinant peptide corresponding to the N-terminus of DAT, and when overexpressed, to up-regulate DAT activity (Egaña et al 2009). MS analysis is a primary method for searching for novel interactions and the results need to be further confirmed using other methods such as co-immunoprecipitation. SV2A is another synaptic vesicle protein that regulates neurotransmitter release, although its precise role in neurotransmitter release is unknown. Disrupted expression of SV2C leads to reduced DA release in dorsal striatum without changing DAT levels (Dunn et al 2017). PMCA and EAAT are presynaptic membrane transporters, and thus potentially capable of cis-interaction with DAT in the membrane. Reticulon predominantly resides in the ER and shapes the membrane curvature of the tubular ER (Voeltz et al 2006). GC catalyzes the entrance of glutamate into the mitochondrial matrix (LaNoue & Schoolwerth 1979). The interaction of these two proteins with DAT in intact

cells is unlikely because DAT is not present in the ER in axonal domains of neurons in the striatum and because DAT is not located in mitochondria.

For the reasons described above, we focused on the role of DAT-Gαo interactions. As described in sections **1.1** and **4.2**, Go proteins are coupled to D2 auto-receptors, and Go/i inhibitor PTX blocks the elevated DAT activity induced by D2R activation. Therefore, Gαo may play an important role in the regulation of DAT activity by D2R. Besides, Gαo has also been identified as a DAT interactor in our previous, qualitative MS analyses of DAT interacting proteins (data not shown).

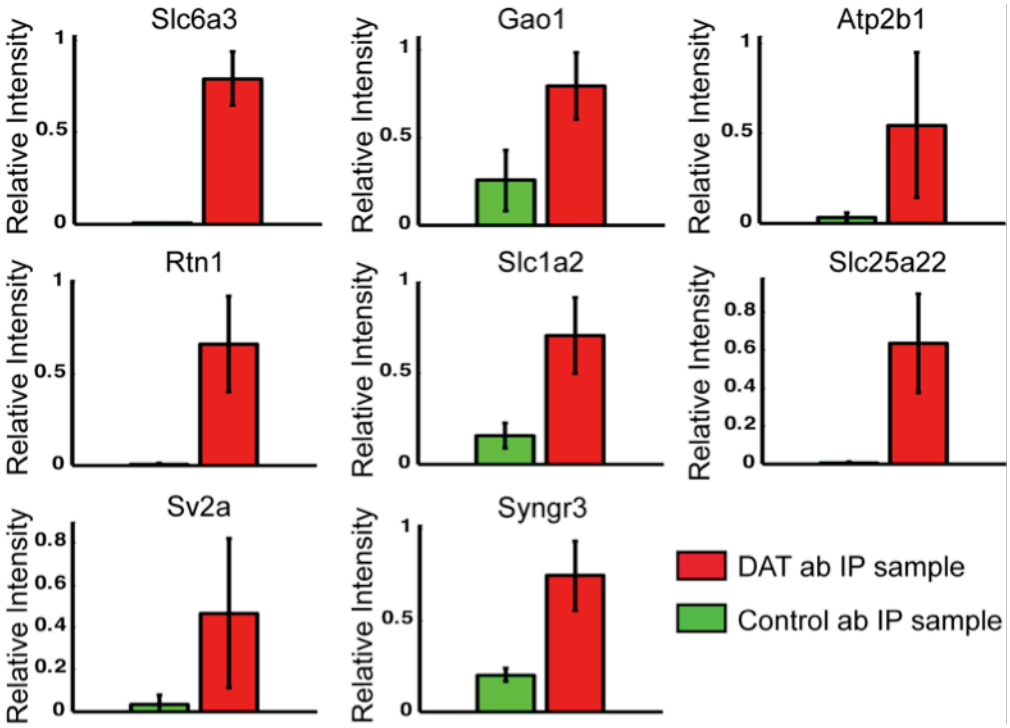

Figure 4.1. Relative abundance of putative DAT interactors (Xuemei Zeng, Yates lab).

4.4.2 Validation of DAT and Gαo interaction

To confirm the interaction between Gαo and DAT in the brain, we performed reciprocal co-IP experiments. The midbrain and striatum from one HA-DAT knock-in and wild-type mouse were

lysed and incubated with 10 μg HA11 antibody. Midbrain contains the cell body of dopaminergic neurons, while stratum contain the most axonal projections of dopaminergic neurons. IP and western blotting were carried out as described in section **4.3.6**. Transferred proteins were probed with rat anti-DAT and rabbit anti-Gαo antibodies, followed by goat anti-rat and goat anti-rabbit secondary antibodies conjugated with far-red fluorescent 680 and 800 dyes, respectively. Gαo was immunoprecipitated with HA-DAT from the striatum of the HA-DAT knock-in mouse (fourth lanes from the left), but not that of the wild-type mouse (second lanes) (Figure 4.2A). The amounts of Gαo in lysates were similar, while the amount of Gαo in specific IP (the forth lane) is significantly larger than that in the second lane (non-specific IP).

To test if DAT is co-immunoprecipitated with Gαo, the brains from two 8-week old wild-type mice were dissected, and the midbrain and striatum tissue were lysed. Lysates were incubated with either rabbit anti-Gαo (2 μg) or non-specific rabbit IgG antibodies (2 μg). IP and western blotting were carried out similar to that of Figure 4.2A. DAT was co-immunoprecipitated with Gαo but not with control IgG in the striatum (Figure 4.2B). We were not able to detect co-immunoprecipitation of DAT and Gαo in the midbrain because the amount of DAT in the midbrain is significantly lower than in the striatum.

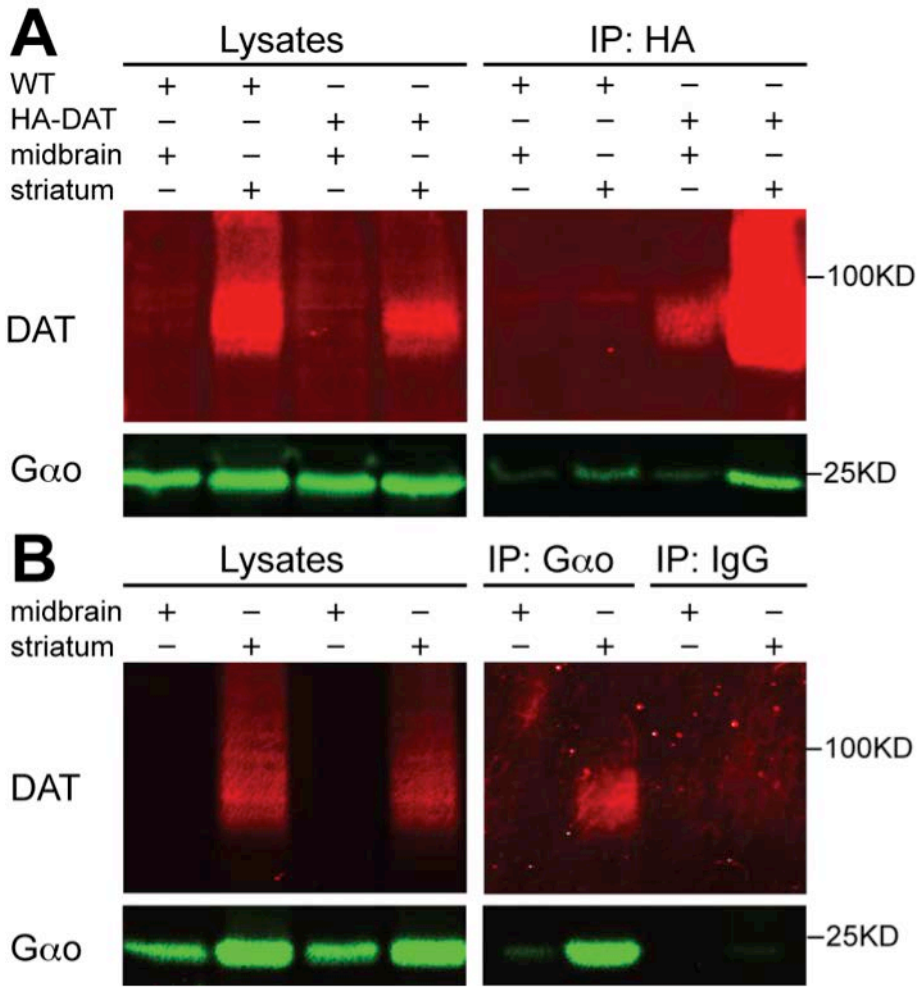

Figure 4.2. DAT and Gαo interact with each other in mouse brain striatum.

To examine the localization of Gαo in dopaminergic neurons, immunofluorescence (IF) staining was performed in primary mesencephalic neurons cultured for 6-10 days *in vitro* from P0-P3 HA-DAT knock-in mice. Neurons were fixed and stained as described in **4.3.4**. Neurons were imaged through 561 nm (Cy3) and 640 nm (Cy5) filter channels. Both HA-DAT (*red*) and Gαo (*green*) are expressed in dopaminergic neuron axons and soma (Figure 4.3A) and dendrites (Figure 4.3B). White arrows point to colocalization of DAT and Gαo. The scale bars are 10 μm. As shown in Figure 4.3, Gαo was readily detected in dopaminergic neurons that were also positive for HA-DAT as well as in other neurons and glial cells in the preparation. In the axonal processes and somatodendritic compartments, Gαo and DAT displayed similar localization

patterns and were partially co-localized. Collectively, co-immunoprecipitation and IF experiments confirmed Gαo and DAT interaction in the perinatal brain.

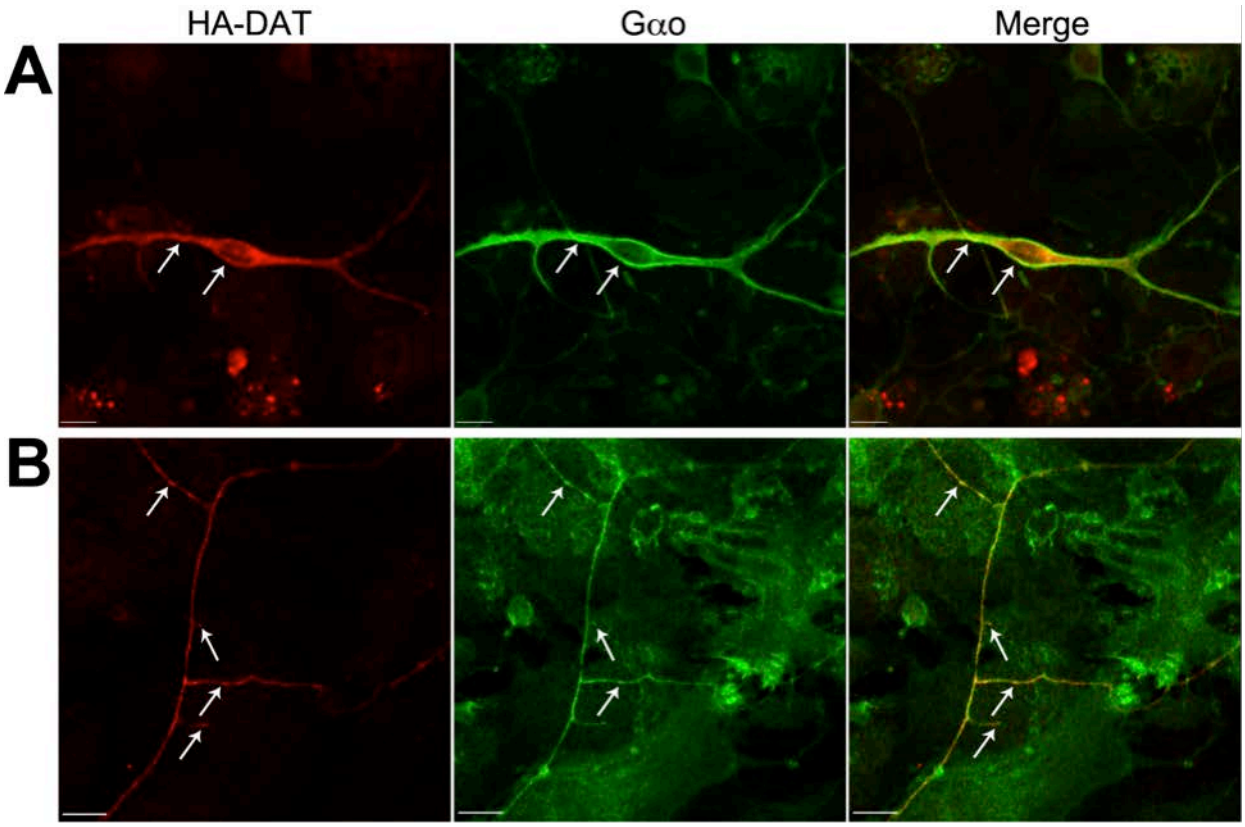

Figure 4.3. Both DAT and Gαo are expressed in the membrane of dopaminergic neurons.

4.4.3 Interaction of recombinant DAT and Gαo in heterologous cells

In order to further study the mechanisms of DAT-Gαo interaction, we performed immunoprecipitation experiments in HEK293 cells transfected with YFP-HA-DAT and Gαo. Cells transfected with only YFP-HA-DAT or Gαo were used as controls. At the third day after transfection, cells were lysed and incubated with the HA11 antibody. In another control group, cells expressing YFP-HA-DAT and Gαo were incubated with HA11 antibodies in the presence of the excess of the blocking HA11 peptide. To increase efficiency of co-precipitation and

reduce non-specific binding, we developed a method that uses reversible cross-linking with DSP to covalently trap interacting proteins before immunoprecipitation followed by washing of Protein G-Sepharose precipitates with high sodium chloride to minimize non-specific co-precipitations. IP and western blotting were carried out as described in section **4.3.6**. Transferred proteins were probed with primary rat anti-DAT, rabbit anti-Gαo and rabbit anti-α-actinin antibodies, followed by goat anti-rat and goat anti-rabbit secondary antibodies conjugated with far-red fluorescent 680 and 800 dyes, respectively.

As shown in Figure 4.4, Gαo was immunoprecipitated by HA11 antibodies in HEK cells expressing both YFP-HA-DAT and Gαo (first lanes from the left). HA11 peptides competed out binding of YFP-HA-DAT to HA11 antibodies, thus minimizing co-immunoprecipitation of Gαo (second lanes). Gαo co-IP was also reduced in cells expressing only Gαo (fourth lanes) compared to the specific immunoprecipitates, despite essentially similar inputs. The experiments presented in Fig4.4 were repeated twice with the similar outcomes. These data demonstrate that recombinant DAT and Gαo interact in HEK293 cells.

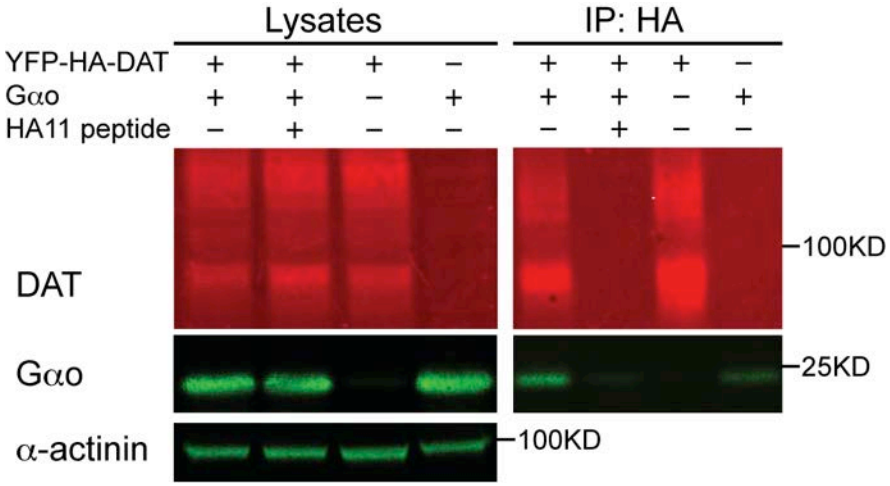

Figure 4.4. Gαo binds to DAT in HEK293 cells.

To determine what part of the DAT molecule is involved in the Gαo interaction, we performed immunoprecipitation experiments in HEK293 cells in which Gαo was co-expressed

with wt YFP-HA-DAT or its mutants. YFP-HA-DAT with the deletion of the N-terminal amino acids 1-65 (YFP-HA-DAT ΔNT) caused a marked reduction in Gαo co-IP (Figure 4.5). The effects of DAT N-terminal deletion on DAT-Gαo interaction have been examined three times, and representative data are shown in Figure 4.5. HEK293 cells were transfected with Gαo and YFP-HA-DAT wt or YFP-HA-DAT ΔNT. After culturing for 3 days, cells were lysed and immunoprecipitated by mouse anti-HA11 antibody. In the first lanes, HA11 peptide was added as a control. IP and western blotting were carried out as described in section **4.3.6**. Transferred proteins were probed with primary rabbit anti-Gαo and rabbit anti-α-actinin antibodies, followed by goat anti-rabbit secondary antibody conjugated with far-red fluorescent 800 dye. After the UV inactivation fluorescent dyes, transferred proteins were then probed with primary mouse anti-HA11 antibody, followed by goat anti-mouse secondary antibody conjugated with far-red fluorescent 800 dye.

As shown in Figure 4.5, the HA11 peptide eliminated YFP-HA-DAT and Gαo signals (first lanes). The amount of Gαo co-immunoprecipitated with wt DAT (second lanes) is significantly higher than the amount in control IPs (third lanes). The Gαo bands in the lysates part are similar, while the Gαo IP band in the third lane is less bright than in the second lane, suggesting that deletion of DAT N-terminus partially inhibits DAT-Gαo interaction. Other mutants (YFP-HA-DAT with partially deleted N-terminus, YFP-HA-DAT with C-terminus deletion, and EGFR-linked DAT C-terminus) did not show the reduction in Gαo binding (data not shown). This analysis is highly preliminary and more experiments are necessary to define the mechanisms of DAT-Goa interaction. However, these co-IP experiments further confirm that the interaction between DAT and Gαo is likely direct, and that the N-terminal tail may be involved.

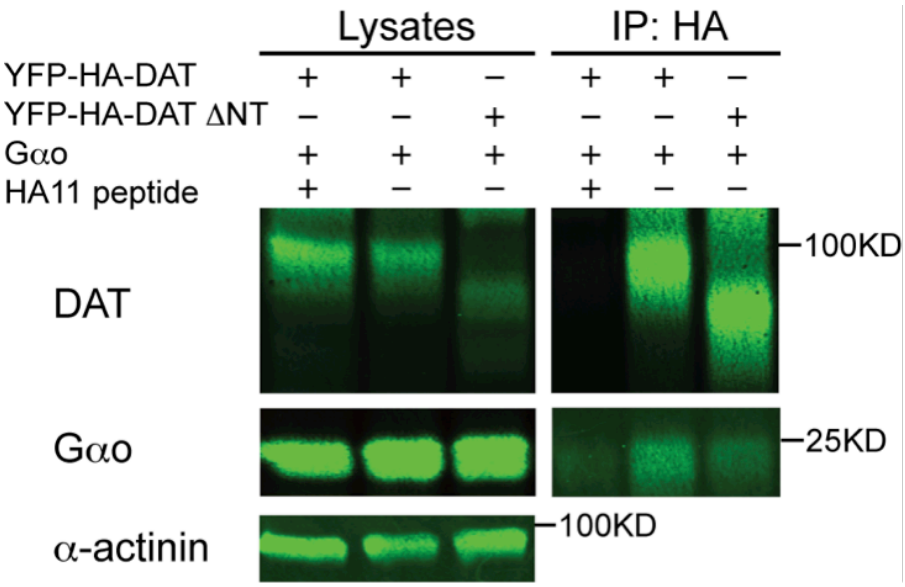

Figure 4.5. The N-terminus of DAT is involved in interaction with Gαo.

4.5 DISCUSSION

In this study we performed MS analysis of the proteins co-immunoprecipitated with DAT from striatal synaptosomes. The identification of synaptogyrin-3 in DAT immunoprecipitates validates our analysis as DAT:synaptogyrin-3 interaction has been previously reported by the Torres group (Egaña et al 2009). On the other hand, detection of mitochondrial glutamate carrier (GC, Slc25a22), which is a intramitochondrial transporter and cannot physically associate with DAT in intact cells, as a specific ($P<0.05$) DAT interactor suggests that the results of MS interactome analysis must be carefully validated using alternative methods (Figure 4.1). Certainly, co-immunopreciptation, such as with Slc22A or reticulon, may be due to the interaction of DAT with these proteins after solubilization rather than in intact cells.

Lack of comprehensive follow-up studies could be responsible for an inconsistent literature on DAT interactome. For example, interaction of DAT with HIC5 and RIN1 was

demonstrated only in single studies (Carneiro et al 2002, Navaroli et al 2011). The mechanisms of these interactions have not been characterized, e.g. sequence motifs in DAT have not been mapped, and there were no follow-up structure-function studies. Likewise, our laboratory demonstrated the role of NEDD4-2 in DAT ubiquitination in several studies (Sorkina et al 2006, Vina-Vilaseca & Sorkin 2010) but direct interaction between NEDD4-2 and DAT and its mechanism in regulating DAT ubiquitination have not been elucidated.

We focused on a newly identified DAT interactor, Gαo, given the potential functional importance of this interaction. Gαo is known to be expressed in the CNS and is coupled to GPCRs expressed in DA neurons (Jiang & Bajpayee 2009). In dopaminergic neurons, dopamine D2 auto-receptors (D2SRs) are coupled to Go proteins. Previously published studies provide a strong rationale for focusing on the interaction. It has been demonstrated that the activation of D2 auto-receptor modulates the surface expression and function of DAT (Mayfield & Zahniser 2001). DA treatment of *Xenopus laevis* oocytes expressing both DAT and D2SR up-regulates the surface expression and DA uptake activity of DAT. The increased DAT uptake activity upon D2SR activation is indeed blocked by PTX treatment in *Xenopus* oocytes. The PTX ADP-ribosyltransferase ADP-ribosylates Gαo/i, resulting in the Go/i proteins being uncoupled from the associated receptors such as D2R (Mangmool & Kurose 2011). D2 agonist quinpirole rapidly increases DAT surface expression in HEK293/EM4 cells expressing both D2SR and DAT, and this effect is also blocked by PTX, again suggesting that the up-regulation of DAT function through D2SR activation is dependent on the activation of Gαo/i (Bolan et al 2007). The PTX-sensitive up-regulated effect of D2SR activation on DAT has also been demonstrated in striatal synaptosomes (Thompson & Certain 2005). Although D2R has been shown to couple to both

Gαo and Gαi proteins in heterologous cells (Gazi et al 2003), studies in Gαo-deficient mice suggest that most D2 receptors are predominantly coupled to Gαo in the CNS (Jiang et al 2001).

In this study, we confirmed the interaction between DAT and Gαo in mouse brain striatum through reciprocal co-immunoprecipitation (Figure 4.2). Immunofluorescence staining of cultured primary mouse dopaminergic neurons showed that both DAT and Gαo were expressed in the membrane of dopaminergic neurons (Figure 4.3). We also observed the co-immunoprecipitation of overexpressed recombinant Gαo and YFP-HA-DAT in HEK293 cells (that express negligible levels of endogenous Gαo) with the help of DSP-mediated crosslinking (Figure 4.4). The mutant of YFP-HA-DAT with deleted N-terminus co-immunporecipitated less amount of Gαo than wild-type YFP-HA-DAT, indicating that the N-terminus of DAT may be involved in DAT-Gαo interaction (Figure 4.5).

The main known function of active Gα subunits is to activate or inhibit the activity of adenylyl cyclase, thus regulating the cellular level of cAMP. Besides modulating adenylyl cyclase, active Gα subunits may bind to and regulate the activity of calcium, potassium, and sodium channels independent of cAMP level changes (Jiang & Bajpayee 2009). The detailed mechanisms for these Gαo effects have not been fully elucidated. However, there is direct physical interaction between Gαo and the α subunit of voltage-gated sodium channels, suggesting that Gαo may regulate the activity of downstream effectors through direct interaction (Anis et al 1999). Therefore, we hypothesize that the increase in DAT activity induced by D2SR activation in dopaminergic neurons can be mediated by direct Gαo interaction with DAT, and that DAT is a novel example of Goa effectors. Of note, it has also been shown that D2R directly binds to the N-terminus of DAT (Lee et al 2007). The co-expression of DAT and D2R results in increased DAT surface expression and activity, which is independent of the activation of D2R,

indicating that the direct DAT-D2R interaction may regulate DAT trafficking. However, D2R was not detected in our DAT immunoprecipitation experiments (data not shown). Therefore, whether DAT-D2R complex exists and whether such complex is important for regulation of DAT localization and activity remains to be further investigated.

Dr. Torres and co-workers have demonstrated that Gβγ subunits directly interact with DAT and down-regulate the activity of DAT in both heterologous cells and brain tissue (Garcia-Olivares et al 2013). It is possible that a Gβγ-induced decrease in DAT activity occurs upon the activation of GPCRs other than D2SR. Of note, Gβγ subunits have not been detected by MS or western blotting in our DAT immunoprecipitation experiments.

Based on the previously demonstrated regulation of DAT by D2SR, and our demonstration of the physical interaction between DAT and Gαo, we propose a hypothetical model for Gαo mediated regulation of DAT activity by D2R (Figure 4.6). DA is released upon the fusion of DA vesicles with the presynaptic cell surface membrane. The binding of DA activates presynaptic D2 auto-receptors (D2SR). Gαo and Gβγ subunits are then released from heterotrimeric Go proteins that bound to D2SR. Gαo binds to DAT N-terminus that is important for maintaining surface DAT level by preventing constitutive endocytosis of DAT (Sorkina et al 2009). Gαo binding to the N-terminus of DAT may be part of this retention mechanism, thus ensuring increased surface DAT levels and/or increased DAT uptake activity. Gβγ subunits may bind DAT and inhibit DAT activity, but this effect would be compensated by the function of Gαo. PTX treatment prevents DAT-Gαo interaction when D2SR is activated through uncoupling the D2SRs and Go proteins. Certainly, this model is highly speculative and all events proposed in Figure 4.6 must be tested experimentally in dopaminergic neuronal models.

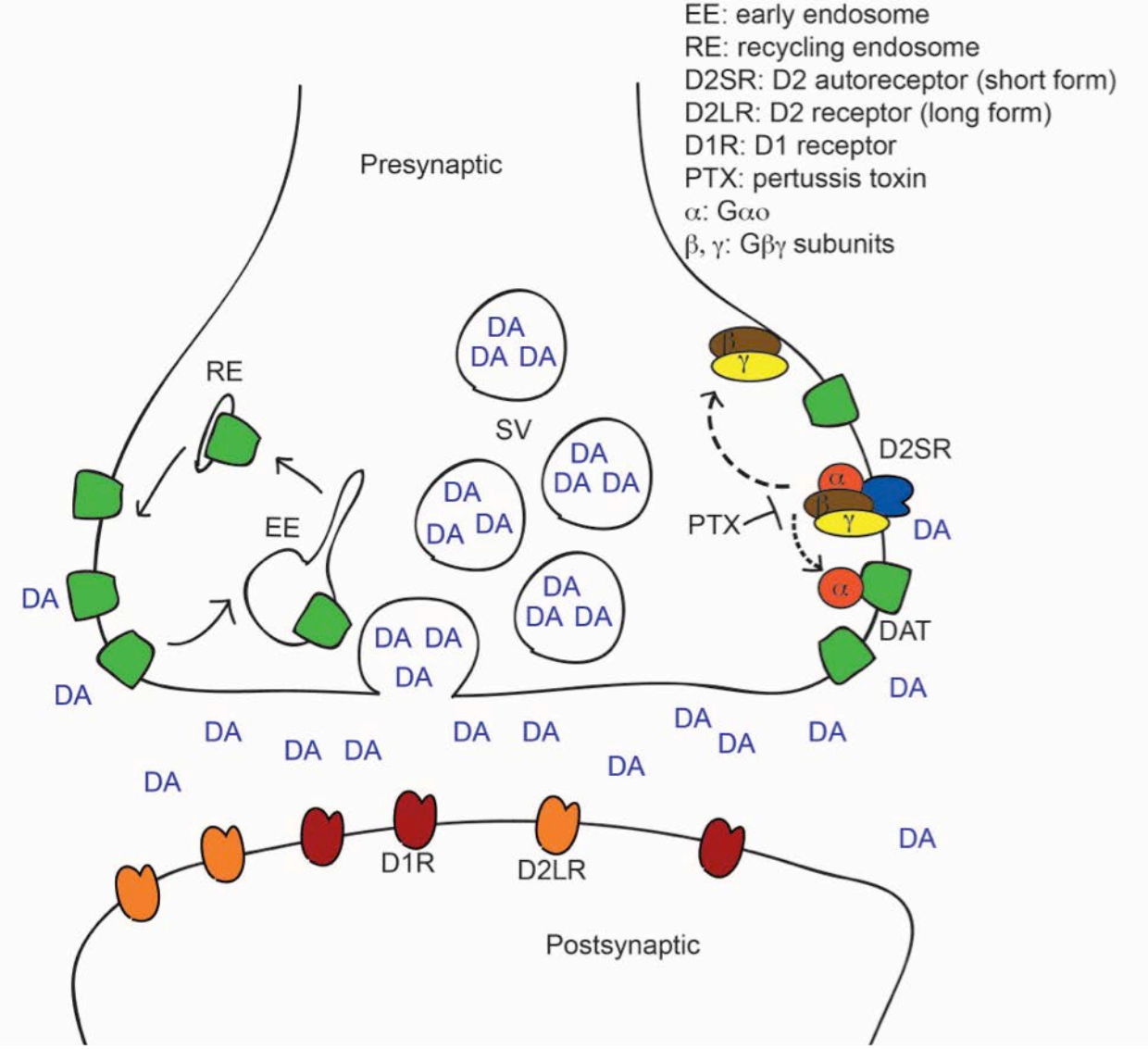

Figure 4.6. Hypothetical model for Go protein mediated regulation of DAT by D2R.

5.0 DISSERTATION SUMMARY

5.1 OVERALL DISCUSSION AND CONCLUSIONS

The overall goal of the dissertation is to further understand the mechanisms regulating DAT subcellular localization and trafficking. The research has been performed in three directions.

The first project dealing with defining the mechanisms of filopodia targeting of DAT was the main focus of my thesis. These data described in Chapter **2** and two publications (Caltagarone et al 2015, Ma et al 2017) demonstrated for the first time that DAT molecule conformation is an important regulator of its subcellular localization. Although most mechanistic approaches to extend these studies in dopaminergic neurons have not been technically feasible, these studies provide a hypothetical model for the role of DAT conformation in the mechanisms responsible for DAT targeting to axonal domains of dopaminergic neurons.

The second and third directions were highly exploratory. In the PIP_2 project (chapter **3**), we for the first time directly and specifically tested the role of PIP_2 in DAT localization and trafficking. We developed a new approach where we combined the controllable membrane PIP_2 depletion and a modified endocytosis assay using Fab fragment antibodies to study the effects of PIP_2 depletion and DAT trafficking. We have demonstrated that PIP_2 depletion blocks PKC-stimulated clathrin-dependent DAT endocytosis but does not change the steady-state of internalized DAT. PIP_2 is essential for the formation of filopodia, as it provides a stage area for

the accumulation of filopodia assembly proteins such as IRSp53, MIM, profilin, and Ena/VASP. During our observation of rapamycin-induced membrane PIP_2 depletion in HEK293 cells expressing YFP-HA-DAT, short-term membrane PIP_2 depletion (5 min) did not affect the number of filopodia with YFP-HA-DAT, while long-term membrane PIP_2 depletion (30 min) reduced the number of filopodia in HEK293 cells, resulting in many round cells (data not shown). Therefore, we propose that PIP_2 is also important for the maintenance of filopodia enriched with DAT. The interaction between DAT and PIP_2 may also play a role in DAT-induced/facilitated filopodia formation. However, since long-term global membrane PIP_2 depletion eliminates the formation of all filopodia, it is hard to test the role of DAT-PIP_2 interaction in DAT-induced filopodia formation.

In our proteomics experiments, we identified a novel interactor of DAT, Gαo. The MS analysis also confirmed the interaction between DAT and synaptogyrin-3, which has been shown by other research groups (Egaña et al 2009). These findings expand the knowledge of the DAT interactome. The expression of Gαo in the tips of the neurites of PC12 cells is increased after NGF treatment, indicating that Gαo may be involved in the extension of neurites during NGF-induced differentiation (Andreopoulos et al 1995). This observation, together with the fact that DAT is localized to filopodia, suggests that DAT-Gαo interaction may appear in the neurites/growth cones neurons. The active Gαo subunits in the growth cones of dopaminergic neurons may be resulted from the activation of presynaptic D2 auto-receptor (D2SR).

DAT-Gαo interaction may be required for the elevated DAT uptake activity induced by D2SR activation. So far, it is generally believed that D2SR activation increases the activity of DAT through stabilizing the surface expression of DAT (Bolan et al 2007, Mayfield & Zahniser 2001). Therefore, we propose that DAT-Gαo interaction stabilizes the expression of DAT in the

membrane and protects DAT from endocytosis that may be caused by drugs of abuse and other pathophysiological conditions. Since that OF conformation helps to stabilize the localization of DAT in filopodia, where a large fraction of DAT is immobile (Rao et al 2012), this conformation may also protect DAT from endocytosis.

While these three research projects were carried out as independent directions, experimental findings indicate that the three processes, filopodial targeting of DAT, the role of PIP_2 in DAT trafficking and interaction between DAT and Gαo, may all be interconnected and involved in the regulation of DAT biology in neurons. Our hypothetical model of DAT regulation by the three above processes is summarized in Figure 5.1. In dopaminergic neurons, DAT is expressed in the plasma membrane of the cell body and axons. DAT undergoes constitutive endocytosis mostly in the cell body and only a little in the axon terminal. DAT is associated with PIP_2 in the plasma membrane. The interaction between DAT and PIP_2 may be involved in the filopodia formation that requires PIP_2. DAT-PIP_2 interaction may also regulate DAT trafficking in the cell body of dopaminergic neurons. DAT colocalizes with MyoX, which is also important for the formation of filopodia. The role of DAT in the tips of the filopodia of the growth cones needs to be understood. However, we have demonstrated that the mechanism for DAT entering filopodia is probably the intrinsic outward-facing conformation, which is independent of MyoX or the DAT-PIP_2 interaction. It is possible that the DAT-Gαo interaction occurs in the tips of filopodia, as there is evidence that Gαo functions in the development of neurites/growth cones (Andreopoulos et al 1995). We propose that the main function of the DAT-Gαo interaction is to mediate elevated DAT surface expression level induced by the activation of D2SR in the presynaptic area. The coupling of D2SR and Go proteins can be disrupted by PTX, resulting in no effects of D2SR activation on DAT. The DAT-Gαo interaction

may stabilize DAT surface level and prevent DAT from endocytosisThe localization of DAT in filopodia can be regulated by the OF conformation and DAT-PIP_2 interaction, and the DAT-Gαo interaction may also appear in filopodia.

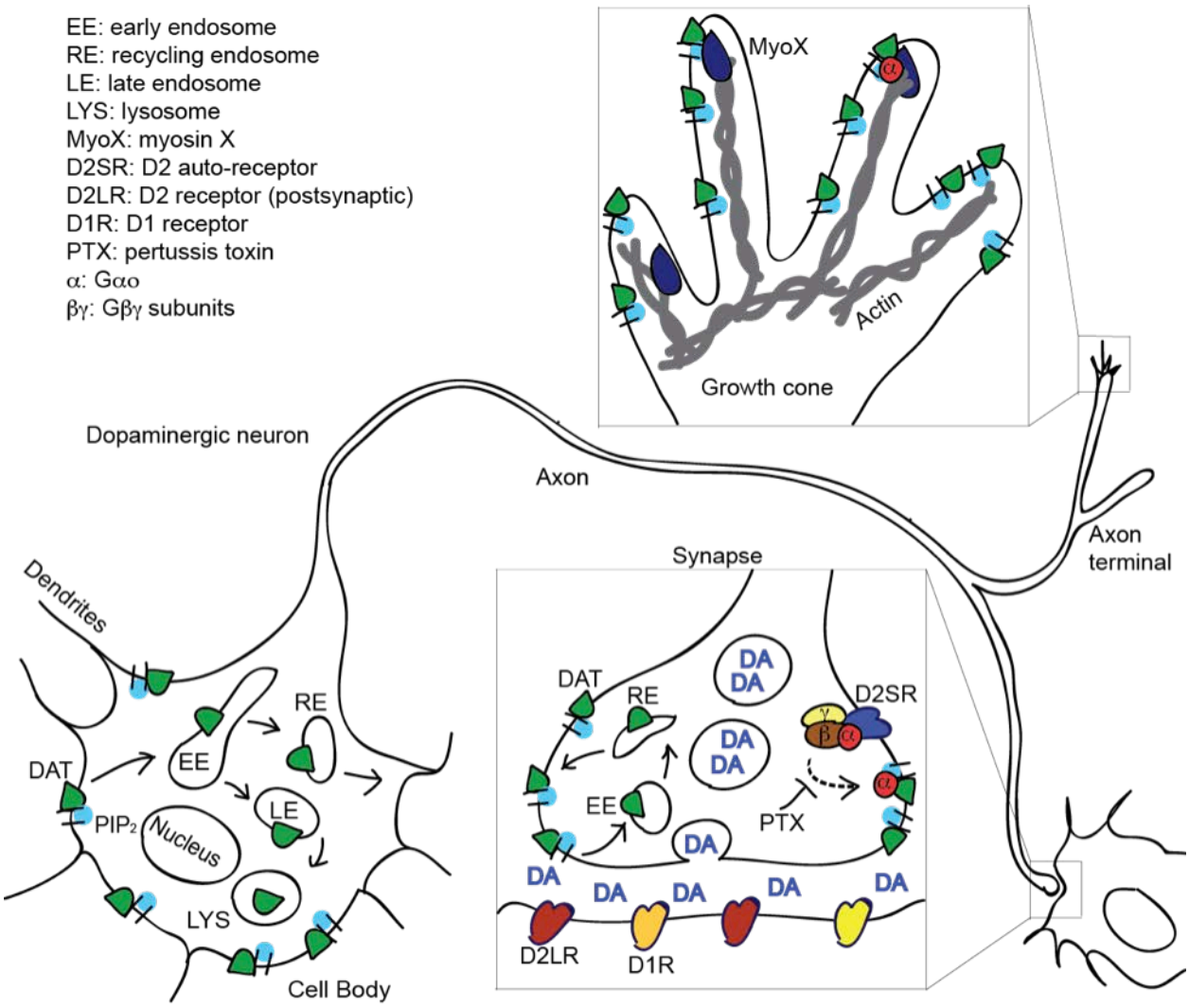

Figure 5.1. The schematic review of the dissertation.

5.2 FUTURE RESEARCH DIRECTIONS

5.2.1 The role of the OF conformation in the distribution of DAT in the cell membrane

In live-cell studies, it is very difficult to rule out all possible alternative or additional mechanisms for the targeting of DAT to filopodia, and in vitro biochemical studies must be performed to fully test our hypotheses. Membrane tube pulling method using giant plasma membrane vesicles (GPMVs) is a recently developed method to study the distribution of transmembrane proteins in curved membranes without interference of other cellular processes and cytoskeletal interactions (Aimon et al 2014). We will generate GPMVs from cells expressing YFP-DAT and its mutants with different conformations, and pull membrane tubes from the GPMVs. The GPMVs with membrane pulling can be imaged using our sensitive confocal microscope. If wt YFP-DAT but not R60A and W63A mutants are concentrated in the tubule domain of GPMVs, it supports our hypothesis that the localization of DAT in filopodia is driven by the intrinsic molecular conformation. If the results of *in vitro* experiments demonstrate that DAT is not accumulate in the membrane pulling of the GPMVs, we will continue our proteomics efforts in identifying DAT interactions that might be responsible for its accumulation in filopodia.

The DAT mutation W84L has been proposed to be stabilized in the OF conformation (Jones et al 2012). This mutant can be compared to the W63A mutant, which exhibits the IF conformation, in future experiments to examine the regulatory role the OF conformation in DAT localization. We will express YFP-HA-W84L in HEK cells and test if the localization of this mutant in filopodia can be affected by AMPH treatment. AMPH treatment disrupts the OF conformation of wt DAT. If AMPH treatment does not reduce the concentration of YFP-HA-

W84L in filopodia, it means that the OF conformation of these mutants cannot be disrupted by AMPH, further suggesting the importance of OF conformation in DAT filopodia localization.

Further, we will also express the wt YFP-HA-DAT and the W84L, W63A mutants in cultured dopaminergic neurons derived from DAT KO mouse. We will use the approach of adeno-associated virus (AAV)-mediated delivery of the constructs under the tyrosine hydroxylase (TH) promoter into primary cultures of dopaminergic neurons. We will compare localization of wt and mutant DAT between axonal and somatodendritic domains to test our hypothesis that the OF state is important for DAT enrichment in axons. The morphology of dopaminergic neurons expressing wt DAT and the mutants will be also quantitatively analyzed. If the dopaminergic neurons expressing the W84L mutant demonstrate elevated numbers of filopodia and/or synapses, and/or enhanced axonal branching than those neurons expressing wt YFP-HA-DAT or the W63A mutant, this will suggest that DAT in its OF state may be directly involved in the development of dopaminergic neurons and their morphological organization.

5.2.2 The mechanism of DAT trafficking upon PIP_2 depletion

One caveat of PIP_2 depletion approach is that the depletion of total membrane PIP_2 affects a multitude of DAT-related and unrelated processes. Therefore, I suggest developing a new approach. We will generate a chimeric protein in which the FRB construct is inserted before the N-terminus of HA-DAT (FRB-HA-DAT). This protein will be co-expressed with BFP-FKBP-INPP5E and YFP-PH-PLC in HEK293 cells. The idea is that rapamycin-induced recruitment of the phosphatase to DAT will deplete PIP_2 locally, in the proximity of DAT. We will then test the effect of rapamycin-induced local membrane PIP_2 depletion on DAT localization and endocytosis. The specific deletion of membrane PIP_2 near DAT as oppose to global PIP_2

depletion will help to distinguish the specific role of PIP_2 in DAT trafficking from the role of PIP_2 in general trafficking processes. Cargo-specific targeting of PIP_2 phosphatases has not been performed, and this project is expected to require considerable troubleshooting. If the local depletion of membrane PIP_2 increases or decreases the internalized/surface ratio of DAT, it means that PIP_2 regulates DAT internalization, endocytic trafficking, or recycling.

5.2.3 The role of Gαo in regulating DAT function

To reveal the function of the DAT-Gαo interaction, we will firstly identify Gαo binding motif in DAT and generate corresponding mutants. YFP-HA-DAT or its mutants incapable of binding Goa and CFP-Gαo will be co-expressed in HEK293 cells. Fluorescence-activated cell sorting (FACS) analysis will be used to collect cells expressing both YFP-HA-DAT and CFP-Gαo, followed by biotinylation and DA uptake assay. If the cells expressing both YFP-HA-DAT and CFP-Gαo exhibit more surface DAT and DA uptake activity in the assays than cells that express YFP-HA-DAT and control CFP, it suggests that the DAT-Gαo interaction increases DAT surface expression and activity in HEK293 cells. The direct physical interaction between DAT and Gαo will be confirmed using co-immunoprecipitation experiments.

We will also examine the role of Gαo in regulating DAT function in dopaminergic neurons. We will develop the approach of adeno-associated virus (AAV)-mediated delivery of Gαo shRNA and GFP expressed under the TH promoter into dopaminergic neurons. GFP positive dopaminergic neurons (with Gαo knockdown) will be evaluated for endocytosis assay and single-cell substrate uptake assay uisng 4-(4-(dimethylamino)steryl)-*N*-methylpyridinium (ASP+) as described in (Inyushin et al 2013). ASP+ is a fluorescent substrate of DAT that can be used to test the uptake activity of DAT using quantitative confocal microscopy. If there is more

DAT endocytosis and less ASP+ uptake in dopaminergic neurons with Gαo knockdown, it would suggest that Gαo helps to stabilize DAT surface expression and reduce DAT endocytosis. Since active Gαo inhibits adenylyl cyclase, thus inhibiting the production of cAMP from ATP, we will also use adenylyl cyclase inhibitor to reduce cAMP level in dopaminergic neurons with Gαo knockdown. If the adenylyl cyclase inhibitor cannot rescue the effects of Gαo knockdown on DAT endocytosis and activity, it suggests that the capacity of Gαo to inhibit adenylyl cyclase is not involved in Gαo-regulated DAT function, which is consistent with our hypothesis that Gαo regulates DAT function through direct physical interaction.

In the future, we will also generate HA-DAT knock-in mice with Gαo knockout by crossing Gαo knockout mice with the HA-DAT knock-in mice in our laboratory. Therefore, we will be able to perform DAT endocytosis assay in the cultured primary dopaminergic neurons prepared from these mice. If the internalized/surface ratio of DAT in the neurons with Gαo knockout is higher than that of the control neurons, it means that the expression of Gαo reduces constitutive DAT endocytosis. The adenylyl cyclase inhibitor will also be used to examine if the role of Gαo in regulating DAT endocytosis is dependent on cAMP changes. We will also test if Gαo knockout increase surface DAT level using biotinylation in brain slices. If mice with Gαo knockout exhibit increased surface DAT level compared to the control mice, it supports our hypothesis that Gαo stabilizes surface DAT expression.

BIBLIOGRAPHY

Ahmed S, Goh WI, Bu W. 2010. I-BAR domains, IRSp53 and filopodium formation. *Seminars in Cell & Developmental Biology* 21: 350-356

Aimon S, Callan-Jones A, Berthaud A, Pinot M, Toombes GES, Bassereau P. 2014. Membrane Shape Modulates Transmembrane Protein Distribution. *Dev Cell* 28: 212-218

Amara SG, Kuhar MJ. 1993. Neurotransmitter Transporters: Recent Progress. *Annual Review of Neuroscience* 16: 73-93

Andreopoulos S, Li PP, Warsh JJ. 1995. Developmental Expression of G-Alpha(O) and G-Alpha(S) Isoforms in Pc12 Cells - Relationship to Neurite Outgrowth. *Dev Brain Res* 88: 30-36

Anis Y, Nürnberg B, Visochek L, Reiss N, Naor Z, Cohen-Armon M. 1999. Activation of Go-proteins by Membrane Depolarization Traced by in Situ Photoaffinity Labeling of Gαo-proteins with [α32P]GTP-azidoanilide. *Journal of Biological Chemistry* 274: 7431-7440

Antonescu CN, Aguet F, Danuser G, Schmid SL. 2011. Phosphatidylinositol-(4,5)-bisphosphate regulates clathrin-coated pit initiation, stabilization, and size. *Mol Biol Cell* 22: 2588-2600

Aramaki S, Mayanagi K, Aoyama K, Yasunaga T. 2014. Revealing the intracellular ultrastructure of filopodia with cryo-electron tomography. *Microscopy* 63: i33-i34

Bello EP, Mateo Y, Gelman DM, Noain D, Shin JH, et al. 2011. Cocaine supersensitivity and enhanced motivation for reward in mice lacking dopamine D-2 autoreceptors. *Nature Neuroscience* 14: 1033-U128

Ben-Jonathan N, Hnasko R. 2001. Dopamine as a Prolactin (PRL) Inhibitor. *Endocrine Reviews* 22: 724-763

Berepiki A, Lichius A, Shoji J-Y, Tilsner J, Read ND. 2010. F-Actin Dynamics in Neurospora crassa. *Eukaryotic Cell* 9: 547-557

Berlanga ML, Price DL, Phung BS, Giuly R, Terada M, et al. 2011. Multiscale Imaging Characterization of Dopamine Transporter Knockout Mice Reveals Regional Alterations in Spine Density of Medium Spiny Neurons. *Brain Res* 1390: 41-49

Beuming T, Kniazeff J, Bergmann ML, Shi L, Gracia L, et al. 2008. The binding sites for cocaine and dopamine in the dopamine transporter overlap. *Nature neuroscience* 11: 780-789

Binda F, Dipace C, Bowton E, Doughty SE, Lute BJ, et al. 2008. Syntaxin1A Interaction with the Dopamine Transporter Promotes Amphetamine-Induced Dopamine Efflux. *Mol Pharmacol* 74: 1101-1108

Bjerggaard C, Fog JU, Hastrup H, Madsen K, Loland CJ, et al. 2004. Surface Targeting of the Dopamine Transporter Involves Discrete Epitopes in the Distal C Terminus But Does Not

Require Canonical PDZ Domain Interactions. *The Journal of Neuroscience* 24: 7024-7036

Björklund A, Dunnett SB. 2007. Dopamine neuron systems in the brain: an update. *Trends Neurosci* 30: 194-202

Block ER, Nuttle J, Balcita-Pedicino JJ, Caltagarone J, Watkins SC, et al. 2015. Brain Region-Specific Trafficking of the Dopamine Transporter. *J Neurosci* 35: 12845-12858

Bohil AB, Robertson BW, Cheney RE. 2006. Myosin-X is a molecular motor that functions in filopodia formation. *Proceedings of the National Academy of Sciences of the United States of America* 103: 12411-12416

Bolan EA, Kivell B, Jaligam V, Oz M, Jayanthi LD, et al. 2007. D-2 receptors regulate dopamine transporter function via an extracellular signal-regulated kinases 1 and 2-dependent and phosphoinositide 3 kinase-independent mechanism. *Mol Pharmacol* 71: 1222-1232

Boucrot E, Ferreira APA, Almeida-Souza L, Debard S, Vallis Y, et al. 2015. Endophilin marks and controls a clathrin-independent endocytic pathway. *Nature* 517: 460-465

Cadet JL, Krasnova IN, Jayanthi S, Lyles J. 2007. Neurotoxicity of substituted amphetamines: Molecular and cellular mechanisms. *Neurotox Res* 11: 183-202

Caltagarone J, Ma SQ, Sorkin A. 2015. Dopamine transporter is enriched in filopodia and induces filopodia formation. *Mol Cell Neurosci* 68: 120-130

Cao M, Wu Y, Ashrafi G, McCartney AJ, Wheeler H, et al. 2017. Parkinson Sac Domain Mutation in Synaptojanin 1 Impairs Clathrin Uncoating at Synapses and Triggers Dystrophic Changes in Dopaminergic Axons. *Neuron* 93: 882-896.e5

Carneiro AM, Ingram SL, Beaulieu J-M, Sweeney A, Amara SG, et al. 2002. The Multiple LIM Domain-Containing Adaptor Protein Hic-5 Synaptically Colocalizes and Interacts with the Dopamine Transporter. *The Journal of Neuroscience* 22: 7045-7054

Cha JH, Zou M-F, Adkins EM, Rasmussen SGF, Loland CJ, et al. 2005. Rhodamine-Labeled 2β-Carbomethoxy-3β-(3,4-dichlorophenyl)tropane Analogues as High-Affinity Fluorescent Probes for the Dopamine Transporter. *Journal of Medicinal Chemistry* 48: 7513-7516

Chazaud B, Ricoux R, Christov C, Plonquet A, Gherardi RK, Barlovatz-Meimon G. 2002. Promigratory Effect of Plasminogen Activator Inhibitor-1 on Invasive Breast Cancer Cell Populations. *The American Journal of Pathology* 160: 237-246

Chen N, Ferrer JV, Javitch JA, Justice JB. 2000. Transport-dependent Accessibility of a Cytoplasmic Loop Cysteine in the Human Dopamine Transporter. *Journal of Biological Chemistry* 275: 1608-1614

Chen NH, Vaughan RA, Reith MEA. 2001. The role of conserved tryptophan and acidic residues in the human dopamine transporter as characterized by site-directed mutagenesis. *J Neurochem* 77: 1116-1127

Chen R, Furman CA, Zhang MJ, Kim MN, Gereau RW, et al. 2009. Protein Kinase C beta Is a Critical Regulator of Dopamine Transporter Trafficking and Regulates the Behavioral Response to Amphetamine in Mice. *J Pharmacol Exp Ther* 328: 912-920

Cheng MH, Bahar I. 2014. Complete Mapping of Substrate Translocation Highlights the Role of LeuT N-terminal Segment in Regulating Transport Cycle. *PLOS Computational Biology* 10: e1003879

Cheng MH, Bahar I. 2015. Molecular Mechanism of Dopamine Transport by Human Dopamine Transporter. *Structure* 23: 2171-2181

Cheng MHY, Block E, Hu FZ, Cobanoglu MC, Sorkin A, Bahar I. 2015. Insights into the modulation of dopamine transporter function by amphetamine, orphenadrine, and cocaine binding. *Front Neurol* 6

Chéreau R, Saraceno GE, Angibaud J, Cattaert D, Nägerl UV. 2017. Superresolution imaging reveals activity-dependent plasticity of axon morphology linked to changes in action potential conduction velocity. *Proceedings of the National Academy of Sciences* 114: 1401-1406

Chi LM, Reith MEA. 2003. Substrate-induced trafficking of the dopamine transporter in heterologously expressing cells and in rat striatal synaptosomal preparations. *J Pharmacol Exp Ther* 307: 729-736

Christine CW, Aminoff MJ. 2004. Clinical differentiation of parkinsonian syndromes: Prognostic and therapeutic relevance. *The American Journal of Medicine* 117: 412-419

Ciliax BJ, Drash GW, Staley JK, Haber S, Mobley CJ, et al. 1999. Immunocytochemical localization of the dopamine transporter in human brain. *The Journal of Comparative Neurology* 409: 38-56

Daniels GM, Amara SG. 1999. Regulated trafficking of the human dopamine transporter - Clathrin-mediated internalization and lysosomal degradation in response to phorbol esters. *Journal of Biological Chemistry* 274: 35794-35801

Davies KM, Anselmi C, Wittig I, Faraldo-Gómez JD, Kühlbrandt W. 2012. Structure of the yeast F(1)F(o)-ATP synthase dimer and its role in shaping the mitochondrial cristae. *Proceedings of the National Academy of Sciences of the United States of America* 109: 13602-13607

Dehnes Y, Shan JF, Beuming T, Shi L, Weinstein H, Javitch JA. 2014. Conformational changes in dopamine transporter intracellular regions upon cocaine binding and dopamine translocation. *Neurochem Int* 73: 4-15

Dickinson SD, Sabeti J, Larson GA, Giardina K, Rubinstein M, et al. 1999. Dopamine D2 Receptor-Deficient Mice Exhibit Decreased Dopamine Transporter Function but No Changes in Dopamine Release in Dorsal Striatum. *J Neurochem* 72: 148-156

Diego S, Sara S, Maria Luisa S, Francesco P. 2012. COMT as a Drug Target for Cognitive Functions and Dysfunctions. *CNS & Neurological Disorders - Drug Targets* 11: 209-221

Dunn AR, Stout KA, Ozawa M, Lohr KM, Hoffman CA, et al. 2017. Synaptic vesicle glycoprotein 2C (SV2C) modulates dopamine release and is disrupted in Parkinson disease. *Proceedings of the National Academy of Sciences* 114: E2253-E2262

Egaña LA, Cuevas RA, Baust TB, Parra LA, Leak RK, et al. 2009. Physical and Functional Interaction between the Dopamine Transporter and the Synaptic Vesicle protein Synaptogyrin-3. *The Journal of neuroscience : the official journal of the Society for Neuroscience* 29: 4592-4604

Eriksen J, Bjorn-Yoshimoto WE, Jorgensen TN, Newman AH, Gether U. 2010. Postendocytic Sorting of Constitutively Internalized Dopamine Transporter in Cell Lines and Dopaminergic Neurons. *Journal of Biological Chemistry* 285: 27289-27301

Eriksen J, Bjørn-Yoshimoto WE, Jørgensen TN, Newman AH, Gether U. 2010. Postendocytic Sorting of Constitutively Internalized Dopamine Transporter in Cell Lines and Dopaminergic Neurons. *Journal of Biological Chemistry* 285: 27289-27301

Eriksen J, Jorgensen TN, Gether U. 2010. Regulation of dopamine transporter function by protein-protein interactions: new discoveries and methodological challenges. *J Neurochem* 113: 27-41

Eriksen J, Jørgensen TN, Gether U. 2010. Regulation of dopamine transporter function by protein-protein interactions: new discoveries and methodological challenges. *J Neurochem* 113: 27-41

Eriksen J, Rasmussen SGF, Rasmussen TN, Vaegter CB, Cha JH, et al. 2009. Visualization of Dopamine Transporter Trafficking in Live Neurons by Use of Fluorescent Cocaine Analogs. *J Neurosci* 29: 6794-6808

Fagan R, Hofmaier T, Sitte H, Melikian H. 2015. PIP2 Stabilizes Dopamine Transporter Surface Expression. *The FASEB Journal* 29

Fog JU, Khoshbouei H, Holy M, Owens WA, Vaegter CB, et al. 2006. Calmodulin Kinase II Interacts with the Dopamine Transporter C Terminus to Regulate Amphetamine-Induced Reverse Transport. *Neuron* 51: 417-429

Ford CP. 2014. The Role of D2-Autoreceptors in Regulating Dopamine Neuron Activity and Transmission. *Neuroscience* 282: 13-22

Foster JD, Adkins SD, Lever JR, Vaughan RA. 2008. Phorbol ester induced trafficking-independent regulation and enhanced phosphorylation of the dopamine transporter associated with membrane rafts and cholesterol. *J Neurochem* 105: 1683-1699

Gabriel LR, Wu SJ, Kearney P, Bellve KD, Standley C, et al. 2013. Dopamine Transporter Endocytic Trafficking in Striatal Dopaminergic Neurons: Differential Dependence on Dynamin and the Actin Cytoskeleton. *J Neurosci* 33: 17836-17846

Gallo G. 2011. The cytoskeletal and signaling mechanisms of axon collateral branching. *Developmental Neurobiology* 71: 201-220

Garcia-Olivares J, Torres-Salazar D, Owens WA, Baust T, Siderovski DP, et al. 2013. Inhibition of Dopamine Transporter Activity by G Protein beta gamma Subunits. *Plos One* 8

Gazi L, Nickolls SA, Strange PG. 2003. Functional coupling of the human dopamine D(2) receptor with Gα(i1), Gα(i2), Gα(i3) and Gα(o) G proteins: evidence for agonist regulation of G protein selectivity. *British Journal of Pharmacology* 138: 775-786

Gether U, Andersen PH, Larsson OM, Schousboe A. 2006. Neurotransmitter transporters: molecular function of important drug targets. *Trends in Pharmacological Sciences* 27: 375-383

Girault J, Greengard P. 2004. The neurobiology of dopamine signaling. *Arch Neurol-Chicago* 61: 641-644

Giros B, Jaber M, Jones SR, Wightman RM, Caron MG. 1996. Hyperlocomotion and indifference to cocaine and amphetamine in mice lacking the dopamine transporter. *Nature* 379: 606-612

Grosshans BL, Ortiz D, Novick P. 2006. Rabs and their effectors: Achieving specificity in membrane traffic. *Proceedings of the National Academy of Sciences of the United States of America* 103: 11821-11827

Gulley JM, Zahniser NR. 2003. Rapid regulation of dopamine transporter function by substrates, blockers and presynaptic receptor ligands. *European Journal of Pharmacology* 479: 139-152

Guptaroy B, Fraser R, Desai A, Zhang MJ, Gnegy ME. 2011. Site-Directed Mutations near Transmembrane Domain 1 Alter Conformation and Function of Norepinephrine and Dopamine Transporters. *Mol Pharmacol* 79: 520-532

Hamilton P, Belovich A, Khelashvili G, Saunders C, Erreger K, et al. 2014. Phosphatidylinositol (4,5)-bisphosphate regulates psychostimulant behaviors through its interaction with the dopamine transporter. *Faseb Journal* 28

Hamilton PJ, Belovich AN, Khelashvili G, Saunders C, Erreger K, et al. 2014. PIP2 regulates psychostimulant behaviors through its interaction with a membrane protein. *Nat Chem Biol* 10: 582-589

Hammond GRV, Fischer MJ, Anderson KE, Holdich J, Koteci A, et al. 2012. PI4P And PI(4,5)P(2) Are Essential But Independent Lipid Determinants Of Membrane Identity. *Science (New York, N.Y.)* 337: 727-730

Hammond GRV, Machner MP, Balla T. 2014. A novel probe for phosphatidylinositol 4-phosphate reveals multiple pools beyond the Golgi. *Journal of Cell Biology* 205: 113-126

Hansen SH, Sandvig K, van Deurs B. 1993. Molecules internalized by clathrin-independent endocytosis are delivered to endosomes containing transferrin receptors. *The Journal of Cell Biology* 123: 89-97

Heckman CA, Plummer HK. 2013. Filopodia as sensors. *Cellular Signalling* 25: 2298-2311

Hersch SM, Yi H, Heilman CJ, Edwards RH, Levey AI. 1997. Subcellular localization and molecular topology of the dopamine transporter in the striatum and substantia nigra. *J Comp Neurol* 388: 211-227

Hoffman BJ, Hansson SR, Mezey É, Palkovits M. 1998. Localization and Dynamic Regulation of Biogenic Amine Transporters in the Mammalian Central Nervous System. *Frontiers in Neuroendocrinology* 19: 187-231

Hong WC, Amara SG. 2010. Membrane Cholesterol Modulates the Outward Facing Conformation of the Dopamine Transporter and Alters Cocaine Binding. *The Journal of Biological Chemistry* 285: 32616-32626

Hong WC, Amara SG. 2013. Differential targeting of the dopamine transporter to recycling or degradative pathways during amphetamine- or PKC-regulated endocytosis in dopamine neurons. *Faseb Journal* 27: 2995-3007

Huang C-L. 2007. *Complex roles of PIP2 in the regulation of ion channels and transporters*. F1761-F1765 pp.

Huang YH, Lin Y, Mu P, Lee BR, Brown TE, et al. 2009. In vivo Cocaine Experience Generates Silent Synapses. *Neuron* 63: 40-47

Inyushin MU, Arencibia-Albite F, de la Cruz A, Vázquez-Torres R, Colon K, et al. 2013. New method to visualize neurons with DAT in slices of rat VTA using fluorescent substrate for DAT, ASP+. *Journal of neuroscience and neuroengineering* 2: 98-103

Ishikawa M, Otaka M, Huang Y, Neumann PA, Winters BD, et al. 2013. Dopamine triggers Heterosynaptic Plasticity. *The Journal of neuroscience : the official journal of the Society for Neuroscience* 33: 6759-6765

Jarsch IK, Daste F, Gallop JL. 2016. Membrane curvature in cell biology: An integration of molecular mechanisms. *The Journal of Cell Biology* 214: 375-387

Jiang M, Spicher K, Boulay G, Wang Y, Birnbaumer L. 2001. Most central nervous system D2 dopamine receptors are coupled to their effectors by Go. *Proceedings of the National Academy of Sciences of the United States of America* 98: 3577-3582

Jiang MS, Bajpayee NS. 2009. Molecular Mechanisms of Go Signaling. *Neurosignals* 17: 23-41

Johnson LA, Furman CA, Zhang MJ, Guptaroy B, Gnegy ME. 2005. Rapid delivery of the dopamine transporter to the plasmalemmal membrane upon amphetamine stimulation. *Neuropharmacology* 49: 750-758

Johnson LA, Guptaroy B, Lund D, Shamban S, Gnegy ME. 2005. Regulation of amphetamine-stimulated dopamine efflux by protein kinase C beta. *Journal of Biological Chemistry* 280: 10914-10919

Jones KT, Zhen J, Reith MEA. 2012. Importance of cholesterol in dopamine transporter function. *J Neurochem* 123: 700-715

Kabouridis PS, Janzen J, Magee AL, Ley SC. 2000. Cholesterol depletion disrupts lipid rafts and modulates the activity of multiple signaling pathways in T lymphocytes. *Eur J Immunol* 30: 954-963

Kahlig KM, Galli A. 2003. Regulation of dopamine transporter function and plasma membrane expression by dopamine, amphetamine, and cocaine. *European Journal of Pharmacology* 479: 153-158

Khan ZU, Mrzljak L, Gutierrez A, de la Calle A, Goldman-Rakic PS. 1998. Prominence of the dopamine D2 short isoform in dopaminergic pathways. *Proceedings of the National Academy of Sciences of the United States of America* 95: 7731-7736

Khelashvili G, Doktorova M, Sahai MA, Johner N, Shi L, Weinstein H. 2015. Computational modeling of the N-terminus of the human dopamine transporter and its interaction with PIP2-containing membranes. *Proteins* 83: 952-969

Khelashvili G, Stanley N, Sahai MA, Medina J, LeVine MV, et al. 2015. Spontaneous Inward Opening of the Dopamine Transporter Is Triggered by PIP2-Regulated Dynamics of the N-Terminus. *Acs Chem Neurosci* 6: 1825-1837

Kirchhausen T, Owen D, Harrison SC. 2014. Molecular Structure, Function, and Dynamics of Clathrin-Mediated Membrane Traffic. *Csh Perspect Biol* 6: a016725

Klumperman J, Raposo G. 2014. The Complex Ultrastructure of the Endolysosomal System. *Csh Perspect Biol* 6: a016857

Kniazeff J, Shi L, Loland CJ, Javitch JA, Weinstein H, Gether U. 2008. An intracellular interaction network regulates conformational transitions in the dopamine transporter. *Journal of Biological Chemistry* 283: 17691-17701

Lai FP, Szczodrak M, Block J, Faix J, Breitsprecher D, et al. 2008. Arp2/3 complex interactions and actin network turnover in lamellipodia. *The EMBO Journal* 27: 982-992

LaNoue KF, Schoolwerth AC. 1979. Metabolite Transport in Mitochondria. *Annu Rev Biochem* 48: 871-922

Lee FJS, Liu F, Pristupa ZB, Niznik HB. 2001. Direct binding and functional coupling of α-synuclein to the dopamine transporters accelerate dopamine-induced apoptosis. *The FASEB Journal* 15: 916-926

Lee FJS, Pei L, Moszczynska A, Vukusic B, Fletcher PJ, Liu F. 2007. Dopamine transporter cell surface localization facilitated by a direct interaction with the dopamine D2 receptor. *The EMBO Journal* 26: 2127-2136

Lee J, Parish CL, Tomas D, Horne MK. 2011. Chronic cocaine administration reduces striatal dopamine terminal density and striatal dopamine release which leads to drug-seeking behaviour. *Neuroscience* 174: 143-150

Lee K-H, Kim M-Y, Kim D-H, Lee Y-S. 2004. Syntaxin 1A and Receptor for Activated C Kinase Interact with the N-Terminal Region of Human Dopamine Transporter. *Neurochem Res* 29: 1405-1409

Li L-B, Chen N, Ramamoorthy S, Chi L, Cui X-N, et al. 2004. The Role of N-Glycosylation in Function and Surface Trafficking of the Human Dopamine Transporter. *Journal of Biological Chemistry* 279: 21012-21020

Loder MK, Melikian HE. 2003. The dopamine transporter constitutively internalizes and recycles in a protein kinase C-regulated manner in stably transfected PC12 cell lines. *Journal of Biological Chemistry* 278: 22168-22174

Loland CJ, Grånäs C, Javitch JA, Gether U. 2004. Identification of Intracellular Residues in the Dopamine Transporter Critical for Regulation of Transporter Conformation and Cocaine Binding. *Journal of Biological Chemistry* 279: 3228-3238

Loland CJ, Norregaard L, Litman T, Gether U. 2002. Generation of an activating Zn(2+) switch in the dopamine transporter: Mutation of an intracellular tyrosine constitutively alters the conformational equilibrium of the transport cycle. *Proceedings of the National Academy of Sciences of the United States of America* 99: 1683-1688

Ma S, Cheng MH, Guthrie DA, Newman AH, Bahar I, Sorkin A. 2017. Targeting of dopamine transporter to filopodia requires an outward-facing conformation of the transporter. *Scientific Reports* 7: 5399

Mangmool S, Kurose H. 2011. G(i/o) Protein-Dependent and -Independent Actions of Pertussis Toxin (PTX). *Toxins* 3: 884-899

Marazziti D, Mandillo S, Di Pietro C, Golini E, Matteoni R, Tocchini-Valentini GP. 2007. GPR37 associates with the dopamine transporter to modulate dopamine uptake and behavioral responses to dopaminergic drugs. *Proceedings of the National Academy of Sciences of the United States of America* 104: 9846-9851

Mattila PK, Lappalainen P. 2008. Filopodia: molecular architecture and cellular functions. *Nat Rev Mol Cell Biol* 9: 446-454

Mattila PK, Pykäläinen A, Saarikangas J, Paavilainen VO, Vihinen H, et al. 2007. Missing-in-metastasis and IRSp53 deform PI(4,5)P2-rich membranes by an inverse BAR domain–like mechanism. *The Journal of Cell Biology* 176: 953-964

Mayfield RD, Zahniser NR. 2001. Dopamine D-2 receptor regulation of the dopamine transporter expressed in Xenopus laevis oocytes is voltage-independent. *Mol Pharmacol* 59: 113-121

Mayor S, Parton RG, Donaldson JG. 2014. Clathrin-Independent Pathways of Endocytosis. *Csh Perspect Biol* 6: a016758

Melikian HE, Buckley KM. 1999. Membrane trafficking regulates the activity of the human dopamine transporter. *J Neurosci* 19: 7699-7710

Miranda M, Sorkina T, Grammatopoulos TN, Zawada WM, Sorkin A. 2004. Multiple molecular determinants in the carboxyl terminus regulate dopamine transporter export from endoplasmic reticulum. *Journal of Biological Chemistry* 279: 30760-30770

Miranda M, Wu CC, Sorkina T, Korstjens DR, Sorkin A. 2005. Enhanced ubiquitylation and accelerated degradation of the dopamine transporter mediated by protein kinase C. *Journal of Biological Chemistry* 280: 35617-35624

Navaroli DM, Stevens ZH, Uzelac Z, Gabriel L, King MJ, et al. 2011. The Plasma Membrane-Associated GTPase Rin Interacts with the Dopamine Transporter and Is Required for Protein Kinase C-Regulated Dopamine Transporter Trafficking. *J Neurosci* 31: 13758-13770

Nieoullon A. 2002. Dopamine and the regulation of cognition and attention. *Progress in Neurobiology* 67: 53-83

Nirenberg M, Vaughan R, Uhl G, Kuhar M, Pickel V. 1996. The dopamine transporter is localized to dendritic and axonal plasma membranes of nigrostriatal dopaminergic neurons. *The Journal of Neuroscience* 16: 436-447

Pacheco A, Gallo G. 2016. Actin filament-microtubule interactions in axon initiation and branching. *Brain Res Bull* 126: 300-310

Penmatsa A, Wang KH, Gouaux E. 2013. X-ray structure of dopamine transporter elucidates antidepressant mechanism. *Nature* 503: 85-+

Pertz O. 2011. Filopodia: Nanodevices that sense nanotopographic ECM cues to orient neurite outgrowth. *Communicative & Integrative Biology* 4: 436-439

Pizzo AB, Karam CS, Zhang Y, Yano H, Freyberg RJ, et al. 2013. The membrane raft protein Flotillin-1 is essential in dopamine neurons for amphetamine-induced behavior in Drosophila. *Mol Psychiatr* 18: 824-833

Rao A, Richards TL, Simmons D, Zahniser NR, Sorkin A. 2012. Epitope-tagged dopamine transporter knock-in mice reveal rapid endocytic trafficking and filopodia targeting of the transporter in dopaminergic axons. *The FASEB Journal* 26: 1921-1933

Rao A, Simmons D, Sorkin A. 2011. Differential subcellular distribution of endosomal compartments and the dopamine transporter in dopaminergic neurons. *Mol Cell Neurosci* 46: 148-158

Rastedt DE, Vaughan RA, Foster JD. 2017. Palmitoylation mechanisms in dopamine transporter regulation. *Journal of Chemical Neuroanatomy*

Richardson BD, Saha K, Krout D, Cabrera E, Felts B, et al. 2016. Membrane potential shapes regulation of dopamine transporter trafficking at the plasma membrane. *Nat Commun* 7: 10423

Romero S, Le Clainche C, Didry D, Egile C, Pantaloni D, Carlier M-F. 2004. Formin Is a Processive Motor that Requires Profilin to Accelerate Actin Assembly and Associated ATP Hydrolysis. *Cell* 119: 419-429

Sato O, Jung HS, Komatsu S, Tsukasaki Y, Watanabe TM, et al. 2017. Activated full-length myosin-X moves processively on filopodia with large steps toward diverse two-dimensional directions. *Scientific Reports* 7: 44237

Saunders C, Ferrer JV, Shi L, Chen J, Merrill G, et al. 2000. Amphetamine-induced loss of human dopamine transporter activity: An internalization-dependent and cocaine-sensitive mechanism. *Proceedings of the National Academy of Sciences of the United States of America* 97: 6850-6855

Saunders C, Ferrer JV, Shi L, Chen JY, Merrill G, et al. 2000. Amphetamine-induced loss of human dopamine transporter activity: An internalization-dependent and cocaine-sensitive mechanism. *Proceedings of the National Academy of Sciences of the United States of America* 97: 6850-6855

Scarr E, Gibbons A, Neo J, Udawela M, Dean B. 2013. *Cholinergic connectivity: It's implications for psychiatric disorders*. 55 pp.

Schultz W. 2002. Getting formal with dopamine and reward. *Neuron* 36: 241-263

Scita G, Confalonieri S, Lappalainen P, Suetsugu S. 2008. IRSp53: crossing the road of membrane and actin dynamics in the formation of membrane protrusions. *Trends in Cell Biology* 18: 52-60

Seaman MNJ. 2008. Endosome protein sorting: motifs and machinery. *Cell Mol Life Sci* 65: 2842-2858

Seeman P. 2010. Historical Overview: Introduction to the Dopamine Receptors In *The Dopamine Receptors*, ed. KA Neve, pp. 1-21. Totowa, NJ: Humana Press

Sevak RJ, Owens WA, Koek W, Galli A, Daws LC, France CP. 2007. Evidence for D2 receptor mediation of amphetamine-induced normalization of locomotion and dopamine transporter function in hypoinsulinemic rats. *J Neurochem* 101: 151-159

Shan JF, Javitch JA, Shi L, Weinstein H. 2011. The Substrate-Driven Transition to an Inward-Facing Conformation in the Functional Mechanism of the Dopamine Transporter. *Plos One* 6

Shen H, Ferguson SM, Dephoure N, Park R, Yang Y, et al. 2011. Constitutive activated Cdc42-associated kinase (Ack) phosphorylation at arrested endocytic clathrin-coated pits of cells that lack dynamin. *Mol Biol Cell* 22: 493-502

Skare P, Karlsson R. 2002. Evidence for two interaction regions for phosphatidylinositol(4,5)-bisphosphate on mammalian profilin I. *Febs Lett* 522: 119-124

Sonders MS, Zhu S-J, Zahniser NR, Kavanaugh MP, Amara SG. 1997. Multiple Ionic Conductances of the Human Dopamine Transporter: The Actions of Dopamine and Psychostimulants. *The Journal of Neuroscience* 17: 960-974

Sorkin A, Puthenveedu MA. 2013. Clathrin-Mediated Endocytosis In *Vesicle Trafficking in Cancer*, ed. Y Yarden, G Tarcic, pp. 1-31. New York, NY: Springer New York

Sorkina T, Caltagarone J, Sorkin A. 2013. Flotillins Regulate Membrane Mobility of the Dopamine Transporter but Are Not Required for Its Protein Kinase C Dependent Endocytosis. *Traffic* 14: 709-724

Sorkina T, Doolen S, Galperin E, Zahniser NR, Sorkin A. 2003. Oligomerization of dopamine transporters visualized in living cells by fluorescence resonance energy transfer microscopy. *Journal of Biological Chemistry* 278: 28274-28283

Sorkina T, Hoover BR, Zahniser NR, Sorkin A. 2005. Constitutive and protein kinase C-induced internalization of the dopamine transporter is mediated by a clathrin-dependent mechanism. *Traffic* 6: 157-170

Sorkina T, Miranda M, Dionne KR, Hoover BR, Zahniser NR, Sorkin A. 2006. RNA interference screen reveals an essential role of Nedd4-2 in dopamine transporter ubiquitination and endocytosis. *J Neurosci* 26: 8195-8205

Sorkina T, Miranda M, Dionne KR, Hoover BR, Zahniser NR, Sorkin A. 2006. RNA Interference Screen Reveals an Essential Role of Nedd4–2 in Dopamine Transporter Ubiquitination and Endocytosis. *The Journal of Neuroscience* 26: 8195-8205

Sorkina T, Richards TL, Rao A, Zahniser NR, Sorkin A. 2009. Negative Regulation of Dopamine Transporter Endocytosis by Membrane-Proximal N-Terminal Residues. *J Neurosci* 29: 1361-1374

Steffensen SC, Svingos AL, Pickel VM, Henriksen SJ. 1998. Electrophysiological Characterization of GABAergic Neurons in the Ventral Tegmental Area. *The Journal of Neuroscience* 18: 8003-8015

Stockner T, Montgomery TR, Kudlacek O, Weissensteiner R, Ecker GF, et al. 2013. Mutational Analysis of the High-Affinity Zinc Binding Site Validates a Refined Human Dopamine Transporter Homology Model. *PLOS Computational Biology* 9: e1002909

Strahl H, Ronneau S, Gonzalez BS, Klutsch D, Schaffner-Barbero C, Hamoen LW. 2015. Transmembrane protein sorting driven by membrane curvature. *Nat Commun* 6

Suh B-C, Hille B. 2005. Regulation of ion channels by phosphatidylinositol 4,5-bisphosphate. *Current Opinion in Neurobiology* 15: 370-378

Sulzer D. 2011. How Addictive Drugs Disrupt Presynaptic Dopamine Neurotransmission. *Neuron* 69: 628-649

Thompson TL, Certain ME. 2005. Estrogen mediated inhibition of dopamine transport in the striatum: Regulation by G alpha(i/o). *European Journal of Pharmacology* 511: 121-126

Tokuo H, Mabuchi K, Ikebe M. 2007. The motor activity of myosin-X promotes actin fiber convergence at the cell periphery to initiate filopodia formation. *The Journal of Cell Biology* 179: 229-238

Torres GE. 2006. The dopamine transporter proteome. *J Neurochem* 97: 3-10

Torres GE, Carneiro A, Seamans K, Fiorentini C, Sweeney A, et al. 2003. Oligomerization and Trafficking of the Human Dopamine Transporter: MUTATIONAL ANALYSIS IDENTIFIES CRITICAL DOMAINS IMPORTANT FOR THE FUNCTIONAL EXPRESSION OF THE TRANSPORTER. *Journal of Biological Chemistry* 278: 2731-2739

Torres GE, Yao WD, Mohn AR, Quan H, Kim KM, et al. 2001. Functional interaction between monoamine plasma membrane transporters and the synaptic PDZ domain-containing protein PICK1. *Neuron* 30: 121-134

Turiault M, Parnaudeau S, Milet A, Parlato R, Rouzeau JD, et al. 2007. Analysis of dopamine transporter gene expression pattern - generation of DAT-iCre transgenic mice. *Febs J* 274: 3568-3577

Varnai P, Thyagarajan B, Rohacs T, Balla T. 2006. Rapidly inducible changes in phosphatidylinositol 4,5-bisphosphate levels influence multiple regulatory functions of the lipid in intact living cells. *Journal of Cell Biology* 175: 377-382

Vina-Vilaseca A, Sorkin A. 2010. Lysine 63-linked Polyubiquitination of the Dopamine Transporter Requires WW3 and WW4 Domains of Nedd4-2 and UBE2D Ubiquitin-conjugating Enzymes. *Journal of Biological Chemistry* 285: 7645-7656

Voeltz GK, Prinz WA, Shibata Y, Rist JM, Rapoport TA. 2006. A Class of Membrane Proteins Shaping the Tubular Endoplasmic Reticulum. *Cell* 124: 573-586

Volkow ND, Fowler JS, Wang GJ, Baler R, Telang F. 2009. Imaging dopamine's role in drug abuse and addiction. *Neuropharmacology* 56: 3-8

Wang KH, Penmatsa A, Gouaux E. 2015. Neurotransmitter and psychostimulant recognition by the dopamine transporter. *Nature* 521: 322-+

Wersinger C, Sidhu A. 2003. Attenuation of dopamine transporter activity by α-synuclein. *Neurosci Lett* 340: 189-192

Wheeler DS, Underhill SM, Stolz DB, Murdoch GH, Thiels E, et al. 2015. Amphetamine activates Rho GTPase signaling to mediate dopamine transporter internalization and acute behavioral effects of amphetamine. *Proceedings of the National Academy of Sciences of the United States of America* 112: E7138-E7147

Wiener MC, Sachs JR, Deyanova EG, Yates NA. 2004. Differential Mass Spectrometry: A Label-Free LC−MS Method for Finding Significant Differences in Complex Peptide and Protein Mixtures. *Analytical Chemistry* 76: 6085-6096

Wu S, Bellve KD, Fogarty KE, Melikian HE. 2015. Ack1 is a dopamine transporter endocytic brake that rescues a trafficking-dysregulated ADHD coding variant. *Proceedings of the National Academy of Sciences of the United States of America* 112: 15480-15485

Yamashiro DJ, Maxfield FR. 1987. Acidification of morphologically distinct endosomes in mutant and wild- type Chinese hamster ovary cells. *The Journal of Cell Biology* 105: 2723-2733

Yamashita A, Singh SK, Kawate T, Jin Y, Gouaux E. 2005. Crystal structure of a bacterial homologue of Na+/Cl--dependent neurotransmitter transporters. *Nature* 437: 215-223

Zahniser NR, Sorkin A. 2009. Trafficking of dopamine transporters in psychostimulant actions. *Seminars in Cell & Developmental Biology* 20: 411-417

Zhang L, Mao YS, Janmey PA, Yin HL. 2012. Phosphatidylinositol 4, 5 Bisphosphate and the Actin Cytoskeleton In *Phosphoinositides II: The Diverse Biological Functions*, ed. T Balla, M Wymann, JD York, pp. 177-215. Dordrecht: Springer Netherlands

Zhang L, Rayner S, Katoku-Kikyo N, Romanova L, Kikyo N. 2007. Successful co-immunoprecipitation of Oct4 and Nanog using cross-linking. *Biochem Bioph Res Co* 361: 611-614

Zhang YW, Turk BE, Rudnick G. 2016. Control of serotonin transporter phosphorylation by conformational state. *Proceedings of the National Academy of Sciences of the United States of America* 113: E2776-E2783

Zhu S, Zhao C, Wu Y, Yang Q, Shao A, et al. 2015. Identification of a Vav2-dependent mechanism for GDNF/Ret control of mesolimbic DAT trafficking. *Nat Neurosci* 18: 1084-1093

Zoncu R, Perera RM, Sebastian R, Nakatsu F, Chen H, et al. 2007. Loss of endocytic clathrin-coated pits upon acute depletion of phosphatidylinositol 4,5-bisphosphate. *Proceedings of the National Academy of Sciences* 104: 3793-3798